8-2019

The Influence of Measurement Scale and Uncertainty on Interpretations of River Migration

Mitchell R. Donovan
Utah State University

THE INFLUENCE OF MEASUREMENT SCALE AND UNCERTAINTY ON INTERPRETATIONS OF RIVER MIGRATION

by

Mitchell R. Donovan

A dissertation submitted in partial fulfillment
of the requirements for the degree

of

DOCTOR OF PHILOSOPHY

in

Watershed Science

Approved:

_____	_____
Patrick Belmont, Ph.D. Major Professor	Sarah Null, Ph.D. Committee Member
_____	_____
Peter Wilcock, Ph.D. Committee Member	Joel Pederson, Ph.D. Committee Member
_____	_____
David Tarboton, Ph.D. Committee Member	Richard S. Inouye, Ph.D. Vice Provost for Graduate Studies

UTAH STATE UNIVERSITY
Logan, Utah

2019

ABSTRACT

The influence of measurement scale and uncertainty on interpretations of river migration

by

Mitchell R. Donovan, Doctorate of Philosophy

Utah State University, 2019

Major Professor: Dr. Patrick Belmont
Department: Watershed Sciences

Measuring temporal and spatial variation in river migration enables us to better understand mechanisms driving one of the most ubiquitous and effective modes of reworking Earth's surface. Studies of river migration span multiple orders of spatial and temporal magnitude- from a single meander bend to geologic-scale evolution of rivers. Uncertainty is inherent but often overlooked in measuring river channel evolution and few consider how spatial and temporal measurement scales bias measurements. Ignoring such uncertainties may confound measurements, obscure patterns of river behavior, and lead to false conclusions regarding processes of river change. In three studies, we describe (1) how to quantify and account for uncertainty in measuring channel adjustments, (2) whether temporal measurement scale impact inferences about river response to agricultural management, and (3) if spatial measurement scale can bias apparent mechanistic relations between meander migration and curvature. We explore 76 years of geomorphic change along the Root River in response to shifting hydrology and

land management, recorded in decadal sets of imagery. The changing conditions and extensive imagery provide an excellent natural experiment to explore our objectives. In Chapter 2 we developed the first comprehensive framework for quantifying and accounting for uncertainty in channel erosion derived measurements from aerial imagery. We review and test best practices for quantifying uncertainty, provide context for applying each practice, and introduce new methods for handling measurements below the threshold of uncertainty. Although this framework is developed for river planform adjustments, it is applicable to many moving boundary measurements. Chapter 3 explores how migration rate measurements from aerial images may be biased by the time interval between measurements. Migration rates measured over longer time intervals systematically underestimate 'true' rates because reversals in migration direction underestimate net migration distance between images. Migration measurements must encompass short-term rate variability in order to accurately demonstrate fluvial change and estimate long-term sediment remobilization and flux for sediment budgets. These results inform our data selection for Chapter 4, wherein we demonstrate how spatial measurement scale can influence apparent relations among factors impacting channel migration. Using measurement scales that capture longitudinal variability in shear stresses helped discern a phase lag between curvature and migration signals.

(169 pages)

PUBLIC ABSTRACT

The influence of measurement scale and uncertainty on interpretations of river migration

Mitchell R. Donovan

Environmental scientists increasingly use remotely-sensed images to measure how rivers develop over time and respond to upstream changes in environmental drivers such as land use, urbanization, deforestation and agricultural practices. These measurements are subject to uncertainty that can bias conclusions. The first step towards accurate interpretation of river channel change is properly quantifying and accounting for uncertainty involved in measuring changes in river morphology. In Chapter 2 we develop a comprehensive framework for quantifying uncertainty in measurements of river change derived from aerial images. The framework builds upon previous uncertainty research by describing best practices and context-specific strategies, comparing each approach and outlining how to best handle measurements that fall below the minimum level of detection. We use this framework in subsequent chapters to reduce the impact of erroneous measurements. Chapter 3 evaluates how the time interval between aerial images influences the rates at which river channels appear to laterally migrate across their floodplains. Multiple lines of evidence indicate that river migration measurements obtained over longer time intervals (20+ years) will underestimate the 'true' rate because the river channel is more likely to have reversed the direction of migration, which erases part of the record of gross erosion as seen from aerial images. If the images don't capture channel reversals and periodic episodes of fast erosion, the river appears to have migrated a shorter distance (which corresponds to a slower rate) than reality. Obtaining multiple

measurements over shorter time intervals (< 5 years) and limiting direct comparisons to similar time intervals can reduce bias when inferring how river migration rates may have changed over time. Chapter 4 explores the physical processes governing the relationship between river curvature and the rate of river migration along a series of meander bends. We used fine-scale empirical measurements and geospatial analyses to confirm theory and models indicating that migration and curvature exhibit a monotonic relationship. The results will improve models seeking to emulate river meander migration patterns.

ACKNOWLEDGMENTS

The research was supported by the Quinney Foundation, National Science Foundation (NSF ENG 1209445), Minnesota Department of Agriculture, Utah Agricultural Experiment Station, and Utah State University.

I would like to extend a personal thank you to Patrick Belmont for his ongoing support and guidance throughout the last four years. Throughout my four years, he has exemplified respect and consideration while still being a great scientific critic. I would also like to thank my committee members, Drs. Peter Wilcock, Sarah Null, Joel Pederson, and David Tarboton, for their input and assistance at each step of the way. Equally important, I want to acknowledge the critical thoughts and ideas put forth by current and past QCNR students, without which, this work would not have been possible.

And an additional thanks goes out to my mentors at UMBC- Andy Miller, Matthew Baker, and Allen Gellis- who each mentored me in the ways of scientific inquiry and never settling for mediocrity. Lastly, I give special thanks to my family and friends for their encouragement, moral support, and patience as I meandered along through the many years of graduate school. Each of you are part of the foundation that my life sits upon, without which, I would quickly fall apart.

Mitchell R. Donovan

CONTENTS

Page

LIST OF TABLES

LIST OF FIGURES

Figure Page

CHAPTER 1

INTRODUCTION

River channels are among the most dynamic landforms on Earth's surface, sweeping laterally across valley bottoms- often in subtle and sometimes catastrophic-ways over event-, decadal-, and millennial timescales. Measuring temporal and spatial variation in river migration enables us to better understand mechanisms driving this ubiquitous and impactful feature of Earth's surface. Remotely-sensed imagery is increasingly used to measure changes in river planform in response to changes in environmental drivers such as landuse, urbanization, deforestation, dam building or removal (Gurnell et al., 1994; Gaeuman et al., 2005; Constantine et al., 2014; Donovan et al., 2015, 2016), develop predictive understanding of channel and floodplain evolution (Lauer and Parker, 2008; Crosato, 2009; Braudrick et al., 2009; Parker et al., 2011), providing constraints for sediment budgets (Trimble, 1983; Reid and Dunne, 2005; Belmont et al., 2011; Stout et al., 2014) and improving bank erosion models (Larsen et al., 2006; Motta et al., 2012). River meander migration also provides intriguing opportunities to test theories regarding basic principles and properties of physics (Hickin and Nanson, 1984; Furbish, 1988; Constantine et al., 2009; Crosato, 2009; Parker et al., 2011). The complexity inherent in modelling meander migration is reflected in studies spanning multiple orders of spatial and temporal magnitude- from individual meander bends (Dietrich et al., 1979; Kasvi et al., 2017), to evolution of floodplains and valleys (Belmont, 2011; Gran et al., 2013; Schwenk et al., 2015), to development of a stratigraphic record spanning eons (Miall, 2006).

Accurately measuring river channel change from remotely-sensed imagery is also

essential for estimating risk to infrastructure (Wente, 2000; Allan, 2004), mapping flood risk (Slater et al., 2015; Call et al., 2017), quantifying sediment loading, and improving success of stream restoration/reclamation and riparian/watershed management. The potential accuracy and precision of meander migration analyses have improved as the result of increased availability of historical and contemporary landscape-scale data (e.g., aerial photographs and high-resolution topography, HRT) for short (<1 year) and long (> 50 years) timescales. Availability of such data has supported a new wave of quantitative approaches that have advanced our understanding of fluvial patterns, processes and trends (Lindsay and Ashmore, 2002; Ghoshal et al., 2010; Donovan et al., 2015; Passalacqua et al., 2015), while also illuminating new challenges and gaps in our understanding of river morphology (Allan, 2004; Lawler, 1993). While we focus on channel migration measured from aerial images, our insights are applicable to changes measured using other platforms, such as repeat topographic surveys, lidar, digitized images, and/or orthoimages.

A critical challenge arising in quantifying fluvial change from aerial imagery is documenting and accounting for measurement uncertainty (Unwin, 1995; Edwards and Lowell, 1996; Kiiveri, 1997). Despite an abundance of remotely-sensed data and new capabilities enabled by continually evolving software packages, studies of fluvial change based upon remote sensing lack a robust and consistent methodology for quantifying and accounting for uncertainty (Kiiveri, 1997; Schook et al., 2017; Werbylo et al., 2017). Several studies have provided recent advances to our understanding of uncertainty in measurements of channel width and lateral migration from remotely sensed imagery (Mount et al., 2003; Mount and Louis, 2005; Hughes et al., 2006; Lea and Legleiter,

2016; Werbylo et al., 2017). Methods for measurement of river migration rates lags considerably behind other measurements of topographic change for which rigorous, repeatable and generalizable uncertainty methods have been developed and are routinely applied by researchers (Brasington et al., 2003; Wheaton et al., 2010; Passalacqua et al., 2015; Schaffrath et al., 2015; Bangen et al., 2016; Vericat et al., 2017; Anderson, 2018).

The first goal of this dissertation is to provide a comprehensive framework for evaluating uncertainty in estimates of river migration and width change by: (1) summarizing relevant research and methods for evaluating uncertainty; (2) highlighting and testing approaches used to estimate channel migration and uncertainty; (3) systematically evaluating how spatial autocorrelations, riparian vegetation, and geomorphic conditions influence uncertainty; and (4) evaluating and improving techniques for dealing with measurements that fall below the minimum level of detection. Beyond planform adjustment of river channels, the guidance and results presented herein are applicable to measuring changes in other delineated boundaries, including glacier retreat or advance, erosion or deposition along coastlines and lakeshores, changes in wetland extent, expansion or contraction of vegetation (e.g., deforestation), cliff retreat, and political boundary disputes. Ensuring effective management of the river corridor requires that we appropriately quantify and report uncertainty in river migration measurements, lest we run the risk of inappropriately prescribing costly channel and riparian management strategies, including bank stabilization and invasive restoration or rehabilitation practices.

A second challenge that pervades hydrologic, geomorphic and other environmental science research is the issue of temporal and spatial measurement scales.

(Blöschl, 1996; Kirchner et al., 2001; Sadler and Jerolmack, 2015; Donovan and Belmont, 2019). The rates of many landscape processes are unsteady over time and non-uniform in space (Ganti et al., 2016). Thus, the time and space scales over which we measure change may have an important influence on the outcome and can bias our ability to understand and predict change (Schumm and Lichty, 1965; Harvey, 2002).

Timescale dependence occurs when measurements of process rates are directly influenced by the timescale over which they are measured, leading to biased comparisons of rates measured over different time intervals. This in turn, confounds our ability to untangle the complexity of environmental responses to external variables (Gurnell et al., 1994; Larsen et al., 2006; Micheli and Larsen, 2011; Gallen et al., 2015; Schook et al., 2017). Timescale dependence has been demonstrated for a multitude of unsteady processes, including sediment accumulation, aggradation, progradation, and degradation (Sadler, 1981; Gardner et al., 1987; Lindsay and Ashmore, 2002; Kessler et al., 2013; Sadler and Jerolmack, 2015), river incision (Finnegan et al., 2014; Gallen et al., 2015), mountain erosion (Kirchner et al., 2001), cliff erosion (Cambers, 1976), and slope adjustments (Penning-Rowsell and Townshend, 1978).

Process hiatuses (e.g., rapid change followed by periods of dormancy) and reversals (e.g., incision vs. aggradation) appear to be largely responsible for timescale dependence across a variety of unsteady processes (Sadler, 1981; Gardner et al., 1987; Finnegan et al., 2014; Sadler and Jerolmack, 2015). In the case of river migration, channel reversals may lead to underestimating measured migration rates by erasing part of the migration record between sequential aerial images. Despite this intuitive connection, the potential for timescale dependence in river migration measurements has

not been previously addressed. In Chapter 3, we analyze empirical and synthetic datasets to address the following questions: Does timescale dependence exist for river migration measurements? If so, how does it affect our ability to accurately measure and compare changes in migration rates over time? What mechanisms cause measurement timescale dependence, and to what degree? Can timescale dependence and actual changes in channel migration be disentangled in order to determine if/when/where real changes in migration rates have occurred?

The second component of measurement scale – space – reflects a third challenge that has resurfaced in new ways with the use aerial imagery and software to quantify changes in river morphology. While aerial imagery archives and new measurement platforms allow us to track detailed changes across Earth's surface at a variety of scales, the scale at which change is documented can will impact the results and may bias our interpretation of the driving mechanisms. When measurements of meander migration are averaged over the scale of a meander bend, rates of river migration are observed to be largest for bends with a moderate degree of curvature (Hickin, 1974; Nanson and Hickin, 1983; Hickin and Nanson, 1984). However, if change is measured at smaller, sub-bend scales, rates of erosion are observed to continuously increased with curvature (Sylvester et al., 2019). Additionally, the spatially continuous sub-bend measurements and geospatial analyses revealed a spatial lag of about 2 to 5 channel widths between patterns of curvature and migration rate. The role of curvature as a driver of bend migration informs our assessment of the driving mechanics and appears to depend upon measurement scale (Furbish, 1988; Hickin and Nanson, 1984; Howard and Knutson, 1984; Nanson and Hickin, 1983). The contrast between empirical measurements obtained

at bend-averaged and sub-meander scales highlight the need to better understand how spatial scale impacts curvature-migration relationships in natural river meanders.

Chapter 4 explores how spatial scale of measurement can impact curvature-migration relationships in natural river meanders. We examine the evolution of curvature and migration at sub-meander scales using repeated aerial images spanning large temporal (76 years) and spatial scales (25 river-km). Fine-scale measurements provide an opportunity to reevaluate the contrasting forms of curvature-migration relationships. Specifically, we ask: is there empirical evidence that migration rates peak at a critical radius of curvature that is 2 to 3 times the channel width (R/W ~2-3), or if they exhibit a direct relationship between curvature and migration? If the latter, what form does the relationship take? Is the peaked relationship between migration and curvature an artifact of using bend-averaged measurements, which fail to capture sub-meander scale variability? We also evaluate whether there is a spatial lag between curvature and migration. A clearer relation between bend curvature and migration rate can support a better understanding of the underlying mechanisms and an improved basis for predicting meander dynamics.

References

Allan, J.D., 2004. Landscapes and Riverscapes: The Influence of Land Use on Stream Ecosystems. Annual Review of Ecology, Evolution, and Systematics 35, 257–284. https://doi.org/10.1146/annurev.ecolsys.35.120202.110122

Anderson, S., 2018. Uncertainty in quantitative analyses of topographic change: Error propagation and the role of thresholding: Uncertainty in repeat topographic analyses. Earth Surface Processes and Landforms. https://doi.org/10.1002/esp.4551

Bangen, S., Hensleigh, J., McHugh, P., Wheaton, J., 2016. Error modeling of DEMs from topographic surveys of rivers using fuzzy inference systems. Water Resources Research 52, 1176–1193. https://doi.org/10.1002/2015WR018299

Belmont, P., 2011. Floodplain width adjustments in response to rapid base level fall and knickpoint migration. Geomorphology 128, 92–102. https://doi.org/10.1016/j.geomorph.2010.12.026

Belmont, P., Gran, K.B., Schottler, S.P., Wilcock, P.R., Day, S.S., Jennings, C., Lauer, J.W., Viparelli, E., Willenbring, J.K., Engstrom, D.R., Parker, G., 2011. Large shift in source of fine sediment in the Upper Mississippi River. Environmental Science & Technology 45, 8804–8810. https://doi.org/10.1021/es2019109

Blöschl, G., 1996. Scale and Scaling in Hydrology (Ph.D. Dissertation). Technische Universitat Wien lnstitut fur Hydraulik, Gewasserkunde und Wasserwirtschaft, Vienna, Austria.

Brasington, J., Langham, J., Rumsby, B., 2003. Methodological sensitivity of morphometric estimates of coarse fluvial sediment transport. Geomorphology 53, 299–316. https://doi.org/10.1016/S0169-555X(02)00320-3

Braudrick, C.A., Dietrich, W.E., Leverich, G.T., Sklar, L.S., 2009. Experimental evidence for the conditions necessary to sustain meandering in coarse-bedded rivers. Proceedings of the National Academy of Sciences 106, 16936–16941. https://doi.org/10.1073/pnas.0909417106

Call, B.C., Belmont, P., Schmidt, J.C., Wilcock, P.R., 2017. Changes in floodplain inundation under nonstationary hydrology for an adjustable, alluvial river channel. Water Resources Research 53, 3811–3834. https://doi.org/10.1002/2016WR020277

Cambers, G., 1976. Temporal Scales in Coastal Erosion Systems. Transactions of the Institute of British Geographers 1, 246. https://doi.org/10.2307/621987

Constantine, C.R., Dunne, T., Hanson, G.J., 2009. Examining the physical meaning of the bank erosion coefficient used in meander migration modeling. Geomorphology 106, 242–252. https://doi.org/10.1016/j.geomorph.2008.11.002

Constantine, J.A., Dunne, T., Ahmed, J., Legleiter, C., Lazarus, E.D., 2014. Sediment supply as a driver of river meandering and floodplain evolution in the Amazon Basin. Nature Geoscience 7, 899–903. https://doi.org/10.1038/ngeo2282

Crosato, A., 2009. Physical explanations of variations in river meander migration rates from model comparison. Earth Surface Processes and Landforms 34, 2078–2086. https://doi.org/10.1002/esp.1898

Dietrich, W.E., Smith, J.D., Dunne, T., 1979. Flow and Sediment Transport in a Sand Bedded Meander. The Journal of Geology 87, 305–315. https://doi.org/10.1086/628419

Donovan, M., Belmont, P., 2019. Timescale Dependence in River Channel Migration Measurements. Earth Surface Processes and Landforms. https://doi.org/10.1002/esp.4590

Donovan, M., Miller, A., Baker, M., 2016. Reassessing the role of milldams in Piedmont floodplain development and remobilization. Geomorphology 268, 133–145. https://doi.org/10.1016/j.geomorph.2016.06.007

Donovan, M., Miller, A., Baker, M., Gellis, A., 2015. Sediment contributions from floodplains and legacy sediments to Piedmont streams of Baltimore County, Maryland. Geomorphology 235, 88–105. https://doi.org/10.1016/j.geomorph.2015.01.025

Edwards, G., Lowell, K.E., 1996. Modeling uncertainty in photointerpreted boundaries. Photogrammetric Engineering and Remote Sensing 62, 377–390.

Finnegan, N.J., Schumer, R., Finnegan, S., 2014. A signature of transience in bedrock river incision rates over timescales of 104–107 years. Nature 505, 391–394. https://doi.org/10.1038/nature12913

Furbish, D.J., 1988. River-bend curvature and migration: How are they related? Geology 16, 752–755. https://doi.org/10.1130/0091-7613(1988)016<0752:RBCAMH>2.3.CO;2

Gaeuman, D., Symanzik, J., Schmidt, J.C., 2005. A Map Overlay Error Model Based on Boundary Geometry. Geographical Analysis 37, 350–369. https://doi.org/10.1111/j.1538-4632.2005.00585.x

Gallen, S.F., Pazzaglia, F.J., Wegmann, K.W., Pederson, J.L., Gardner, T.W., 2015. The dynamic reference frame of rivers and apparent transience in incision rates. Geology 43, 623–626. https://doi.org/10.1130/G36692.1

Ganti, V., von Hagke, C., Scherler, D., Lamb, M.P., Fischer, W.W., Avouac, J.-P., 2016. Time scale bias in erosion rates of glaciated landscapes. Science Advances 2, e1600204–e1600204. https://doi.org/10.1126/sciadv.1600204

Gardner, T.W., Jorgensen, D.W., Shuman, C., Lemieux, C.R., 1987. Geomorphic and tectonic process rates: Effects of measured time interval. Geology 15, 259–261. https://doi.org/10.1130/0091-7613(1987)15<259:GATPRE>2.0.CO;2

Ghoshal, S., James, L.A., Singer, M.B., Aalto, R., 2010. Channel and Floodplain Change Analysis over a 100-Year Period: Lower Yuba River, California. Remote Sensing 2, 1797–1825. https://doi.org/10.3390/rs2071797

Gran, K.B., Finnegan, N., Johnson, A.L., Belmont, P., Wittkop, C., Rittenour, T., 2013. Landscape evolution, valley excavation, and terrace development following abrupt postglacial base-level fall. Geological Society of America Bulletin 125, 1851–1864. https://doi.org/10.1130/B30772.1

Gurnell, A.M., Downward, S.R., Jones, R., 1994. Channel planform change on the river dee meanders, 1876–1992. Regulated Rivers: Research & Management 9, 187–204. https://doi.org/10.1002/rrr.3450090402

Harvey, A.M., 2002. Effective timescales of coupling within fluvial systems. Geomorphology 44, 175–201.

Hickin, E., Nanson, G., 1984. Lateral Migration Rates of River Bends. J. Hydraul. Eng. 110, 1557–1567. https://doi.org/10.1061/(ASCE)0733-9429(1984)110:11(1557)

Hickin, E.J., 1974. The development of meanders in natural river-channels. American Journal of Science 274, 414–442.

Howard, A.D., Knutson, T.R., 1984. Sufficient conditions for river meandering: A simulation approach. Water Resources Research 20, 1659–1667. https://doi.org/10.1029/WR020i011p01659

Hughes, M.L., McDowell, P.F., Marcus, W.A., 2006. Accuracy assessment of georectified aerial photographs: Implications for measuring lateral channel movement in a GIS. Geomorphology 74, 1–16. https://doi.org/10.1016/j.geomorph.2005.07.001

Kasvi, E., Laamanen, L., Lotsari, E., Alho, P., 2017. Flow Patterns and Morphological Changes in a Sandy Meander Bend during a Flood—Spatially and Temporally Intensive ADCP Measurement Approach. Water 9, 106. https://doi.org/10.3390/w9020106

Kessler, A.C., Gupta, S.C., Brown, M.K., 2013. Assessment of river bank erosion in Southern Minnesota rivers post European settlement. Geomorphology 201, 312–322. https://doi.org/10.1016/j.geomorph.2013.07.006

Kiiveri, H.T., 1997. Assessing, representing and transmitting positional uncertainty in maps. International Journal of Geographical Information Science 11, 33–52. https://doi.org/10.1080/136588197242482

Kirchner, J.W., Finkel, R.C., Riebe, C.S., Granger, D.E., Clayton, J.L., King, J.G., Megahan, W.F., 2001. Mountain erosion over 10 yr, 10 k.y., and 10 m.y. time

scales. Geology 29, 591. https://doi.org/10.1130/0091-7613(2001)029<0591:MEOYKY>2.0.CO;2

Larsen, E.W., Fremier, A.K., Girvetz, E.H., 2006. Modeling the effects of variable annual flow on river channel meander migration patterns, Sacramento River, California, USA. JAWRA 42, 1063–1075.

Lauer, J.W., Parker, G., 2008. Net local removal of floodplain sediment by river meander migration. Geomorphology 96, 123–149. https://doi.org/10.1016/j.geomorph.2007.08.003

Lawler, D.M., 1993. The measurement of river bank erosion and lateral channel change: a review. Earth Surface Processes and Landforms 18, 777–821.

Lea, D.M., Legleiter, C.J., 2016. Refining measurements of lateral channel movement from image time series by quantifying spatial variations in registration error. Geomorphology 258, 11–20. https://doi.org/10.1016/j.geomorph.2016.01.009

Lindsay, J.B., Ashmore, P.E., 2002. The effects of survey frequency on estimates of scour and fill in a braided river model. Earth Surface Processes and Landforms 27, 27–43. https://doi.org/10.1002/esp.282

Miall, A.D., 2006. Reconstructing the architecture and sequence stratigraphy of the preserved fluvial record as a tool for reservoir development: A reality check. AAPG Bulletin 90, 989–1002. https://doi.org/10.1306/02220605065

Micheli, E.R., Larsen, E.W., 2011. River channel cutoff dynamics, Sacramento River, California, USA. River Research and Applications 27, 328–344. https://doi.org/10.1002/rra.1360

Motta, D., Abad, J.D., Langendoen, E.J., Garcia, M.H., 2012. A simplified 2D model for meander migration with physically-based bank evolution. Geomorphology 163–164, 10–25. https://doi.org/10.1016/j.geomorph.2011.06.036

Mount, N., Louis, J., 2005. Estimation and propagation of error in measurements of river channel movement from aerial imagery. Earth Surface Processes and Landforms 30, 635–643. https://doi.org/10.1002/esp.1172

Mount, N.J., Louis, J., Teeuw, R.M., Zukowskyj, P.M., Stott, T., 2003. Estimation of error in bankfull width comparisons from temporally sequenced raw and corrected aerial photographs. Geomorphology 56, 65–77. https://doi.org/10.1016/S0169-555X(03)00046-1

Nanson, G.C., Hickin, E.J., 1983. Channel Migration and Incision on the Beatton River. Journal of Hydraulic Engineering 109, 327–337. https://doi.org/10.1061/(ASCE)0733-9429(1983)109:3(327)

Parker, G., Shimizu, Y., Wilkerson, G.V., Eke, E.C., Abad, J.D., Lauer, J.W., Paola, C., Dietrich, W.E., Voller, V.R., 2011. A new framework for modeling the migration of meandering rivers. Earth Surface Processes and Landforms 36, 70–86. https://doi.org/10.1002/esp.2113

Passalacqua, P., Belmont, P., Staley, D.M., Simley, J.D., Arrowsmith, J.R., Bode, C.A., Crosby, C., DeLong, S.B., Glenn, N.F., Kelly, S.A., Lague, D., Sangireddy, H., Schaffrath, K., Tarboton, D.G., Wasklewicz, T., Wheaton, J.M., 2015. Analyzing high resolution topography for advancing the understanding of mass and energy transfer through landscapes: A review. Earth-Science Reviews 148, 174–193. https://doi.org/10.1016/j.earscirev.2015.05.012

Penning-Rowsell, E.C., Townshend, J.R.G., 1978. The Influence of Scale on the Factors Affecting Stream Channel Slope. Transactions of the Institute of British Geographers 3, 395. https://doi.org/10.2307/622120

Reid, L.M., Dunne, T., 2005. Sediment Budgets as an Organizing Framework in Fluvial Geomorphology, in: Tools in Fluvial Geomorphology. John Wiley & Sons, Ltd, pp. 463–500.

Sadler, P.M., 1981. Sediment Accumulation Rates and the Completeness of Stratigraphic Sections. The Journal of Geology 89, 569–584.

Sadler, P.M., Jerolmack, D.J., 2015. Scaling laws for aggradation, denudation and progradation rates: the case for time-scale invariance at sediment sources and sinks. Geological Society, London, Special Publications 404, 69–88. https://doi.org/10.1144/SP404.7

Schaffrath, K.R., Belmont, P., Wheaton, J.M., 2015. Landscape-scale geomorphic change detection: Quantifying spatially variable uncertainty and circumventing legacy data issues. Geomorphology 250, 334–348. https://doi.org/10.1016/j.geomorph.2015.09.020

Schook, D.M., Rathburn, S.L., Friedman, J.M., Wolf, J.M., 2017. A 184-year record of river meander migration from tree rings, aerial imagery, and cross sections. Geomorphology 293, 227–239. https://doi.org/10.1016/j.geomorph.2017.06.001

Schumm, S.A., Lichty, R.W., 1965. Time, space, and causality in geomorphology. American Journal of Science 263, 110–119. https://doi.org/10.2475/ajs.263.2.110

Schwenk, J., Lanzoni, S., Foufoula-Georgiou, E., 2015. The life of a meander bend: Connecting shape and dynamics via analysis of a numerical model. Journal of Geophysical Research: Earth Surface 120, 690–710. https://doi.org/10.1002/2014JF003252

Slater, L.J., Singer, M.B., Kirchner, J.W., 2015. Hydrologic versus geomorphic drivers of trends in flood hazard. Geophysical Research Letters 42, 370–376. https://doi.org/10.1002/2014GL062482

Stout, J.C., Belmont, P., Schottler, S.P., Willenbring, J.K., 2014. Identifying Sediment Sources and Sinks in the Root River, Southeastern Minnesota. Annals of the Association of American Geographers 104, 20–39. https://doi.org/10.1080/00045608.2013.843434

Sylvester, Z., Durkin, P., Covault, J.A., 2019. High curvatures drive river meandering. Geology 47, 263–266. https://doi.org/10.1130/G45608.1

Trimble, S.W., 1983. A sediment budget for Coon Creek basin in the Driftless Area, Wisconsin, 1853-1977. American Journal of Science 283, 454–474. https://doi.org/10.2475/ajs.283.5.454

Unwin, D.J., 1995. Geographical information systems and the problem of "error and uncertainty." Progress in Human Geography 19, 549–558. https://doi.org/10.1177/030913259501900408

Vericat, D., Wheaton, J.M., Brasington, J., 2017. Revisiting the Morphological Approach: Opportunities and Challenges with Repeat High-Resolution Topography, in: Tsutsumi, D., Laronne, J. (Eds.), Gravel-Bed Rivers: Processes and Disasters, Gravel Bed Rivers. John Wiley and Sons Ltd., pp. 121–155.

Wente, S., 2000. Proximity-based measure of land use impacts to aquatic ecosystem integrity. Environmental Toxicology and Chemistry 19, 1148–1152. https://doi.org/10.1897/1551-5028(2000)019<1148:PBMOLU>2.3.CO;2

Werbylo, K.L., Farnsworth, J.M., Baasch, D.M., Farrell, P.D., 2017. Investigating the accuracy of photointerpreted unvegetated channel widths in a braided river system: a Platte River case study. Geomorphology 278, 163–170. https://doi.org/10.1016/j.geomorph.2016.11.003

Wheaton, J.M., Brasington, J., Darby, S.E., Sear, D.A., 2010. Accounting for uncertainty in DEMs from repeat topographic surveys: Improved sediment budgets. Earth Surface Processes and Landforms 35, 136–156. https://doi.org/10.1002/esp.1886

CHAPTER 2

ACCOUNTING FOR UNCERTAINTY IN REMOTELY-SENSED MEASUREMENTS OF RIVER PLATFORM CHANGE

1. Introduction

River channels are among the most dynamic landforms on Earth's surface, sweeping laterally across valley bottoms- often in subtle and sometimes catastrophic-ways over event-, decadal-, and millennial timescales. Remotely-sensed imagery is increasingly used to delineate channel boundaries to measure changes in river planform such as lateral migration (Hickin and Nanson, 1984; Gurnell et al., 1994; Gaeuman et al., 2005b; Lauer and Parker, 2008; Constantine et al., 2014; Donovan et al., 2015, 2016; Morais et al., 2016), as well as channel width (Winterbottom, 2000; Pavelsky and Smith, 2008; Swanson et al., 2011; Downs et al., 2013; Lauer et al., 2017). These measurements provide a basis for understanding effective management strategies for erosion along the riparian corridor (Micheli et al., 2004; Piégay et al., 2005), providing input to sediment budgets (Allmendinger et al., 2007; Belmont et al., 2011; Smith et al., 2011), and automated characterization of single- versus multi-threaded river planforms (Rowland et al., 2016). Such measurements also inform our understanding of important issues including erosional hazards caused by migrating streams (Lawler, 1993; Piégay et al., 1997, 2005; Hughes et al., 2006; Rhoades et al., 2009), understanding the impact of anthropogenic modifications to the fluvial system (Shields et al., 2000; Donovan and Belmont, 2019), and managing riparian habitat (Ward et al., 2002). Ensuring effective management of the river corridor requires that we appropriately quantify and report uncertainty in river migration measurements, lest we run the risk of inappropriately

prescribing costly channel and riparian management strategies, including bank stabilization and invasive restoration or rehabilitation practices.

Increased availability and resolution of aerial photography, satellite imagery, unmanned aerial vehicle (UAV) imagery, and LiDAR or digital elevation/terrain models (DEM/DTMs) of Earth's surface have greatly enhanced the precision, spatial extent and temporal frequency with which we can analyze river channel migration (Harpold et al., 2015). Despite an abundance of remotely sensed data and new capabilities enabled by continually evolving software packages, studies of fluvial change based upon remote sensing lack a robust and consistent methodology for quantifying and handling uncertainty (Kiiveri, 1997; Schook et al., 2017; Werbylo et al., 2017). Several studies have provided recent advances to our understanding of uncertainty in measurements of channel width and lateral migration from remotely sensed imagery (Mount et al., 2003; Mount and Louis, 2005; Hughes et al., 2006; Lea and Legleiter, 2016; Werbylo et al., 2017), but no comprehensive framework has been developed. In this way, the methods for measurement of river migration rates lags considerably behind other measurements of topographic change for which rigorous, repeatable and generalizable uncertainty methods have been developed (Brasington et al., 2003; Wheaton et al., 2010; Passalacqua et al., 2015; Schaffrath et al., 2015; Bangen et al., 2016; Vericat et al., 2017; Anderson, 2018).

The goal of this paper is to provide a comprehensive framework for evaluating uncertainty in estimates of river migration and width change by: (1) summarizing relevant research and methods for evaluating uncertainty; (2) highlighting and testing approaches used to estimate channel migration and uncertainty; and (3) filling in gaps regarding how spatial autocorrelations, riparian vegetation, and geomorphic conditions

influence uncertainty. This paper does not attempt to address all possible approaches or available tools for analyzing channel migration, but rather discusses the primary considerations and key components of the uncertainty inherent in such measurements. Beyond planform adjustment of river channels, the guidance and results presented herein are applicable to measuring changes in delineated boundaries, including glacier retreat or advance, erosion or deposition along coastlines and lakeshores, changes in wetland extent, expansion or contraction of vegetation (e.g., deforestation), cliff retreat, and political boundary disputes. Furthermore, it will help generate and constrain uncertainty and error estimates for models utilizing such data.

2. Error and uncertainty in Geographic Information Systems

2.1. Background

Measurements of planform change over broad spatial and temporal scales are often derived from series of remotely-sensed images. Such measurements are often made within geographic information systems (GIS) due to their ability to compile and measure spatial (e.g., x, y, z), temporal, and thematic components. Respectively, these three components describe a measurement's location and size within space, the time, speed and/or duration of the measurement, and any associated descriptions or classifying attributes. Measurements of planform change derived from remotely-sensed images contain spatial and temporal components that manifest in magnitudes and rates of change. Such measurements also contain some amount of error, which can be defined as the difference between a measurement of reality, and reality itself (Unwin, 1995; Crosetto & Tarantola, 2001). For planform changes, temporal error is generally absent because the date of image acquisition is usually known. Thematic/classification errors are also

irrelevant, leaving only spatial/locational uncertainty in the horizontal and (sometimes) vertical dimensions, to consider. Spatial uncertainty is estimated as the total *possible* error in a given measurement, the components of which are summarized in Table 2-1. Estimating the total possible error provides a value with which to quantify a level of detection (LoD) threshold. The LoD is a threshold for determining which measurements are statistically significant. Measurements that fall below the LoD, called 'nondetects', occur due to measurement error exceeding the magnitude of measured change. By quantifying uncertainty alongside measurements of river planform change, we provide transparent and informative data for best management practices along the riparian corridor.

When documenting channel planform and migration change using aerial images, total uncertainty should include uncertainty in image georeferencing and orthorectification, as well as uncertainty in manual- or algorithm-derived channel delineations (Libby et al., 2016). The choice of transformation (e.g., linear, polynomial, kriging, spline, etc.) can have the largest impact on orthorectification uncertainty. A second-order polynomial transformation is recommended for most applications, because it minimizes both image distortion and georeferencing error (Hughes et al., 2006). The quantity, quality, and spatial distribution of georeferenced control points (GCPs) are key factors influencing georeferencing uncertainty, summarized in Table 2-1 (Lea and Legleiter, 2016). Delineation error has received considerably less attention in the literature. Gurnell et al. (1994) quantified digitization error for a single-threaded highly sinuous channel using average offset of repeated streambank digitizations on 1:10,000 scale maps. They found an average of ±2 meters offset over 18 river km, but were unable

to evaluate how error varied spatially or may be affected by overhanging vegetation or shadows, similar to semi- and fully-automated channel delineations (Güneralp, Filippi, & Hales, 2013, 2014). Working in a mix of braided and anastomosing morphologies, Werbylo et al., 2017 found that while digitizations of multiple users resulted in no significant differences on average channel width, at-a-section differences in width varied by as much as 37 meters. The authors conclude that digitizations are more consistent for imagery obtained at high resolution and that flow conditions are the most significant factor impacting error and inconsistency in delineations, with higher flows providing more consistent delineations.

Accurately estimating uncertainty is not only essential for filtering out unreliable measurements, but also for retaining reliable measurements. The latter is particularly relevant for short-term measurements of smaller changes that are rendered obsolete if uncertainty is overestimated (Liro, 2015; Lea & Legleiter, 2016; Donovan & Belmont, 2019). However, when uncertainty cannot be properly quantified, results should be constrained using upper and lower bounds of uncertainty (Kiiveri, 1997; Crosetto & Tarantola, 2001; Donovan et al., 2015; Passalacqua et al., 2015; Lauer et al., 2017) or simply highlighting locations where the measurement is more or less a reflection of noise (i.e., random variability) to provide an estimate of reliability for end users. Using probability and fuzzy positional boundaries has been proposed as a generic approach to estimate probabilistic positional uncertainty in GIS (Kiiveri, 1997; Wheaton et al., 2010). For any application, appropriately evaluating and disclosing uncertainty will improve the quality of results and subsequent applications.

Table 2-1.
Factors affecting uncertainty in remotely-sensed images and measurements of planform change

Factors affecting uncertainty in remotely sensed images and measurements of planform changes			
Type	**Expected influencial factors**	**Considerations**	**Reference**
Georeferencing uncertainty	Image warping (camera optics)	Periphery of images affected relatively more than centers	Fryer & Brown (1986)
	Georeferenced control points	Hard points reduce error compared to soft points	Mount et al. (2003); Hughes et al. (2006)
	Image resolution/quality	Coarser resolution decreases ability to find GCPs	-
	Anthropogenic changes	Urban development changes availability of GCPs	-
	Georectification transformation	2nd-order polynomial is consistently the best choice	Hughes et al. (2006); Donovan et al. (2015)
Digitization (i.e.,delineation) uncertainty	Vegetation density	Vegetation cover reduces visibility of channel edge	Güneralp et al. (2013, 2014); Winterbottom (2000)
	Shadows along river boundary	Shadows reduce visibility of channel edge	Güneralp et al. (2013, 2014)
	Scale of image during delineation	Increased scale (zooming in) reduces delineation error	Liro et al. (2015)
	Water level	Will impact which vegetated-edge boundaries are visible	Lauer et al. (2017), Werbylo et al. (2017)
	Arbitrary user inconsistency	Users are prone to inconsistency in boundary interpretations	Gurnell et al. (1994); This study
	Topographic data availability	High-resolution DEMs increase delineation accuracy	Mount et al. (2013); Donovan et al. (2015)
Automated delineation/ classification uncertainty	Manual vs. [semi]automated	Automated approaches are generally less accurate and vary by which algorithm or software tool is used	Pavlesky & Smith (2008); Rowland et al. (2016); Schwenk et al. (2017)
	Channel width & complexity	Narrow channels and highly complex bar arrangements can reduce automated [and manual] classification accuracy	Rowland et al., (2016); [Werbylo et al., (2017)]
Detecting changes in delineated boundaries	Magnitude of changes	Larger changes more likely to exceed level of detection	This study
	Duration between images	Broader timescales span periods of greater change	Donovan & Belmont (2019)
	Reference datum changes	After adjusting images to a common datum, differences may arise due to distinct datum offsets	Anders & Byrnes (1991)
	LoD threshold calculation	Uniform LoD thresholds erroneously reduce number (and quality)* of significant measurements	Lea & Legleiter (2016); *This study

2.2. Techniques and developments in quantifying uncertainty

2.2.1. Georeferencing uncertainty

Georeferencing is the process of placing scanned aerial photographs onto a coordinate plane using known feature locations, referred to as georeferenced control points (GCPs). Optimally, and most often, GCPs are derived from orthorectified images to support maximal accuracy. However, large errors still exist in georeferenced images as a result of errors in the GCPs, associated images, and geometric distortion from cameras/sensors (Fryer & Brown, 1986), scanners, or varying relief. These errors directly affect insights derived from research using image-based delineations for change detection. An estimate of georeferencing uncertainty (i.e., possible X-Y positional error) reflects offset between points on the image and their actual locations. GCPs should preferably be ‘hard’ points: easily distinguished immobile feature edges such as buildings, houses, earth-bound anthropogenic structures, rather than ‘soft’ points such as

vegetation, waterbodies, roads, or signs. A minimum of 5 to 8 hard GCPs is recommended (respectively, Mount et al., 2003 and Hughes et al., 2006) in order to minimize georeferencing uncertainty, with diminishing returns on uncertainty reduction beyond 8-10 GCPs (Hughes et al., 2006; Donovan et al., 2015; Lea & Legleiter, 2016). Homogeneous placement of GCPs reduces warping in georectified images, with moderate improvements when placing GCPs along the floodplain versus uplands (Lea and Legleiter, 2016). Multiple studies confirm that when georectifying images, a second-order polynomial interpolation minimizes error and reduces warping relative to higher-order transformations (N.J Mount et al., 2003; Hughes et al., 2006; Lea & Legleiter, 2016). A summary of factors affecting georeferencing uncertainty is found in Table 2-1.

2.2.2. Approaches to river channel digitization and classification

Subsequent to quantifying uncertainty associated with georeferencing aerial imagery, the images are used to digitize the boundary of the stream via automated or manual methods. Regardless of the method used, channel-margin delineations are most often defined by the edge of riparian vegetation in order to eliminate variability arising from fluctuating water levels (Winterbottom, 2000; D. A. Gaeuman, Schmidt, & Wilcock, 2003; Nelson, Erwin, & Schmidt, 2013; Rowland et al., 2016; Werbylo et al., 2017). The exception to this is when using delineations to estimate discharge or to determine if/how channel width has changed for a given flow value, in which case, variability as a function of water stage is desired (Bjerklie et al., 2005; Smith and Pavelsky, 2008; Lauer et al., 2017). Vegetated channel-margin delineations are more prone to error and inconsistency for braided and anastomosing systems, where width-related metrics are more sensitive to stage (Werbylo et al., 2017). An alternative approach

to delineations uses the break in slope at the top of near vertical channel banks, but this approach depends on availability of high resolution topographic data and is unsuccessful where banks are not well defined (Osterkamp & Hedman, 1982; Nick J. Mount, Tate, Sarker, & Thorne, 2013; Donovan et al., 2015). While the edge of riparian vegetation provides a rational and typically discernable boundary, individuals must consider their data quality and research goals when defining an appropriate channel margin.

The scope of each project's questions and goals help inform whether to use manual or automated delineations, which can both help answer a wide variety of questions, but are each better suited for specific goals. Herein, we describe appropriate contexts and questions for each approach. Rowland et al. (2016) provided a detailed summary of methods and software using remotely sensed imagery to analyze river planform properties and dynamics (Micheli & Kirchner, 2002; Micheli et al., 2004; Güneralp & Rhoads, 2008; Legleiter & Kyriakidis, 2007; Aalto, Lauer, & Dietrich, 2008; Pavelsky & Smith, 2008; Lauer & Parker, 2008; Peixoto, Nelson, & Wittmann, 2009; Baki & Gan, 2012; Fisher, Bookhagen, & Amos, 2013; Hossain, Gan, & Baki, 2013; Nick J. Mount et al., 2013).

While manual delineations are most common (Blundell & Opitz, 2006) and accurate, semi- or fully-automated methods save time by eliminating the tedious nature of manual delineation (Güneralp et al., 2013; Rowland et al., 2016; Schwenk, Khandelwal, Fratkin, Kumar, & Foufoula-Georgiou, 2017). Studies attempting to span broad spatial and/or temporal scales may therefore opt for automated delineations/classifications, thereby sacrificing accuracy to increase the extent of their analyses and save time. One caveat is that such studies must occur along sufficiently wide and active rivers (Peixoto et

al., 2009; J. A. Constantine et al., 2014; Schwenk et al., 2017), because manual delineations are able to extend the spatial extent of delineations/classifications to lower-order streams relative to automated approaches. When conducted by an informed user, manual methods improve overall delineation/classification accuracy because they accommodate interpretation of occasionally complex or anomalous features and thus are flexible across varying hydrologic and geomorphic conditions. Because algorithms and automated classifications adhere to a set of input criteria, they are more likely to misclassify channels or images outside the range of conditions for which they were developed.

Despite the limitations mentioned above, automated approaches such as SCREAM (Spatially Continuous Riverbank Erosion and Accretion Measurements; Rowland et al., 2016), are increasingly applied to multiple rivers with diverse morphologies and a broad range of image resolutions. SCREAM identifies and rasterizes channel locations from images to provide a suite of outputs including channel width and migration, sinuosity, bank aspect and channel islands (Rowland et al., 2016). In practice, automated channel classification algorithms such as RivWidth (Pavelsky & Smith, 2008) and SCREAM (Rowland et al., 2016), yield similar estimates of bankfull width for a variety of river planform morphologies. However, only SCREAM accounted for exposed channel bars and islands, and thus, width estimates had slightly higher discrepancies for multi-threaded channels.

Vectorized streambank delineations are often used to derive a single channel centerline. Changes in the location of the centerline over time can be used to estimate linear migration rates (Lauer & Parker, 2008; Donovan & Belmont, 2019; Sylvester et al.,

2019). In other cases, polygons of the channel extent are delineated to measure areal change (D. A. Gaeuman et al., 2003; Rhoades et al., 2009; Donovan et al., 2015, 2016). Measuring migration as the difference in channel centerline position is a simple and efficient method to provide linear migration measurements over user-specified channel lengths. Linear migration rates and areal changes from polygons can both be normalized as a proportion of the channel width for comparisons across rivers of different size (J. M. Hooke, 1980; Donovan et al., 2015; Spiekermann, Betts, Dymond, & Basher, 2017; Sylvester et al., 2019). Estimating migration from centerlines conflates migration of each bank, and thereby reduces the ability to detect which mechanisms are influencing observed meander-bend migration (Miller & Friedman, 2009), as well as expected relations with flow (Schook et al., 2017). Thus, measuring migration separately for cutbanks on the outside of meander bends and point bars on the inside of bends is better suited for questions regarding local-scale mechanisms driving meander migration, at the expense of computation time.

An alternative to measuring linear channel adjustment is to compare polygons or rasters of channel position to estimate the area and/or volume of deposition and erosion (D. Gaeuman, Schmidt, & Wilcock, 2005; D. Gaeuman, Symanzik, et al., 2005). This method is especially useful for braided or anastomosing systems, which may exhibit multiple linear adjustments within a single cross-section that should not be conflated. Channel polygons (vector or raster) are most often derived using image classification and assisted or unassisted machine learning algorithms. Such approaches benefit from the relative speed and ease of automation, but are limited by image resolution, shallow or transparent river reaches, inconsistent lighting and cloud cover, variable hydrologic or

fluvial conditions, and vegetation and shadows overlapping the river boundary. Although raster and polygon outputs are generally similar, discrepancies increase between raster and vector-based delineations for lower order streams (Melville & Martz, 2004).

Differencing channel polygons is well-suited for measuring the area of erosion or accretion, but estimating volumetric sediment fluxes by combining linear migration rates with LiDAR or cross-section information consistently yields results similar to polygon-based calculations (Donovan et al., 2015; Rowland et al., 2016). Areas and volumes of erosion and/or deposition are most accurately and optimally estimated by differencing raster DEMs (DEMs of Difference; i.e., DoDs) derived from automated or semi-automated algorithms (Wheaton et al., 2010; Bangen et al., 2016; Vericat et al., 2017; S. Kelly & Belmont, 2018). However, such methods are limited to areas with repeat surveys of high-resolution topography (HRT), which are expensive to obtain and process due to equipment and software unavailable throughout the majority of history. Best practices and considerations for handling uncertainty in HRT DoDs are outside the scope of this paper, but can be found in Wheaton et al., (2010), Passalacqua et al., (2015) and Anderson, (2018).

2.2.3. Uncertainty in river channel digitization and identification

A modest body of research has evaluated components of uncertainty for manual and automated channel boundary delineations and classifications (Downward, Gurnell, & Brookes, 1994; Gurnell et al., 1994; Melville & Martz, 2004; Rhoades et al., 2009; Liro, 2015). While automated channel delineations and classifications are increasingly common, manual delineations remain the most prevalent and accurate, and thus, serve as validation for estimating uncertainty of automated results (Rowland et al., 2016). Manual

delineation error is greatly reduced by increasing digitization scale (i.e., zooming in), and to a minor degree, aerial photo scale (Liro, 2015). Mid-channel and side bars, as well as proximity to overhanging trees and shadows, are known to reduce the accuracy of semi-automated algorithms delineating wetted channel edges (Güneralp et al., 2013; 2014). However, the impact of such features and conditions on human delineation error is unknown; we attempt to fill this gap herein.

The magnitude, location, and type of offset due to inconsistent digitization and georeferencing distortions have unique implications for estimates of migration and width change (Rowland et al., 2016). For example, when bank delineations are biased in such a way that they result in a channel that is systematically narrower or wider than reality (Fig. 2-1a), centerline migration measurements will not be affected because the centerline(s) is/are not altered significantly. However, this scenario affects measurements of both channel width and width change. If the channel delineation is systematically offset in a single direction (Fig. 2-1a), channel width will remain unaffected, while migration will be exaggerated or damped. When only one bank is offset from its true location, measurements of width change will have an error equal to the magnitude of offset. However, the impact is halved for migration because the effect is damped when banklines are collapsed to a single centerline.

In the case of raster-based binary river classification, such as SCREAM, RivWidth or RivMap (Pavelsky & Smith, 2008; Rowland et al., 2016; Schwenk et al., 2017), ‘delineation error’ is equivalent to errors in feature identification and extraction. Each automation tool will have unique magnitudes and distributions of error due to

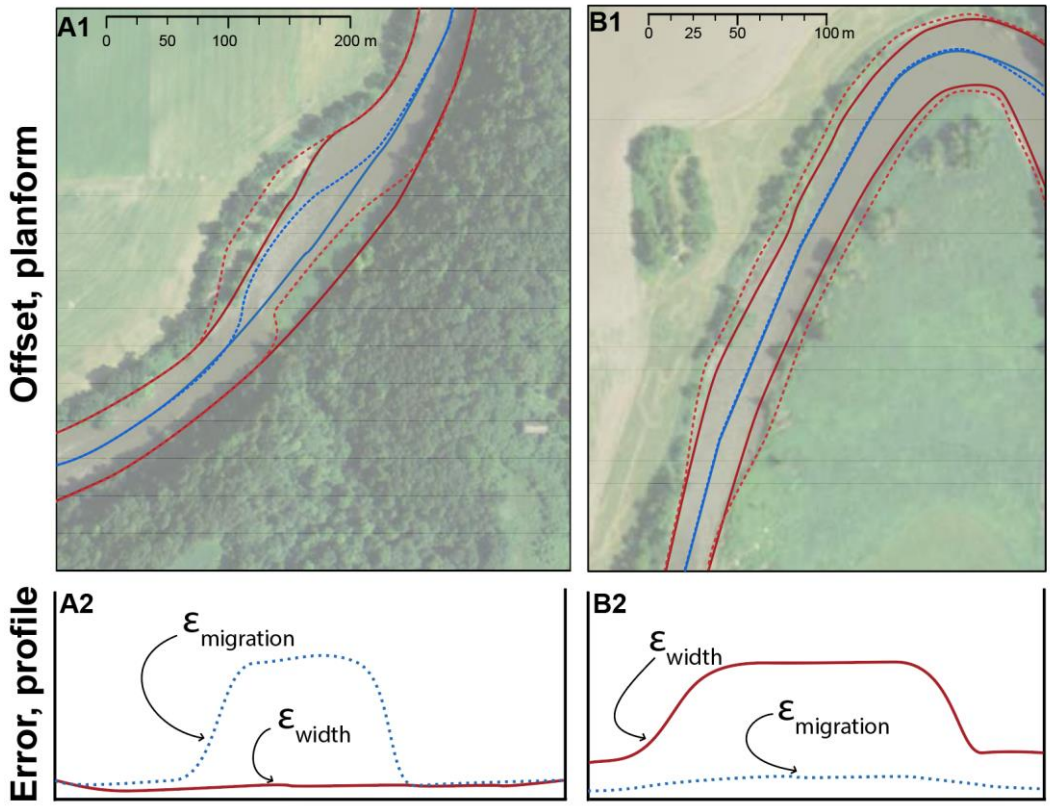

Fig. 2-1. Aerial imagery and hypothetical bank delineations illustrating the types of offsets (A1, B1), along with how such offsets have unique impacts on channel width and migration measurements (A2, B2). In Fig. A1 and B1, the dashed lines indicate an alternative choice of delineation (red) and the centerlines associated with those banklines. The lines in Fig. A2 and B2, illustrate- as a longitudinal profile- error in width (solid red line) and migration (dashed blue line).

unique classification algorithms and river width. For both automated classifications and manual delineations, the ability to detect migration will vary with image resolution, river size, rate of change, and time interval between photos. We hypothesize that georeferencing error will cause local systematic (i.e., directional) errors that impact migration measurements, but not necessarily width change measurements. However, over sufficiently broad reaches, georeferencing offsets should exhibit non-uniform/directional offsets. Due to the nature of changes in river width (i.e., narrowing and widening), width

measurements are impacted by digitization inconsistency more than georeferencing offsets. We explain our approach to testing these hypotheses in the methods, and illustrate the results in subsequent sections.

2.3.4. Level of detection (LoD) threshold

The LoD is a threshold for determining whether measurements of migration or width change are statistically significant. This threshold should account for the total uncertainty arising from georeferencing (not orthorectification) and digitization uncertainty (or feature identification, in the case of automated classifications) (N. Mount & Louis, 2005; N.J Mount et al., 2003). Research estimating migration and width change from repeat aerial images maintains a common practice of applying a uniform LoD threshold, typically ranging from 2 to 5 meters based off the Root Mean Square Error (RMSE) or standard error (SE) of GCPs or delineations (Gurnell et al., 1994; Micheli & Kirchner, 2002; N. Mount & Louis, 2005; Rowland et al., 2016). Uniform error has also been estimated using photo scale (D. A. Gaeuman et al., 2003; Nelson et al., 2013), digitization scale (Downs et al., 2013; Liro, 2015), stated error from the source of the imagery (Draut, Logan, McCoy, McHenry, & Warrick, 2008), and qualitative descriptions of uncertainty in National Ocean Service T-sheets and U.S. Coastal Geodetic Surveys (Anders & Byrnes, 1991). However, uncertainty related to GCPs is inherently non-uniform and directional due to unique offsets of the GCPs in both x- and y-planes.

Three primary problems arise from assuming uniform LoDs, regardless of the how the LoD is estimated or what assumptions are made. First, actual at-a-point error is directionally skewed in the x- or y-plane (i.e., an ellipse), while uniform error thresholds can only be projected with equal error in all directions (i.e., a circle). Thus, uniform

thresholds cannot accurately discern whether the error lies in the same or opposite direction of the channel migration or width change measurement. Second, RMSE-based LoDs increase loss of data/measurements relative to spatially variable LoDs (Liro, 2015; Lea & Legleiter, 2016), for reasons demonstrated in subsequent sections. Third, we hypothesize that uniform LoDs reduce the quality of retained measurements due to excessive loss of measurements of small changes and erroneous retention of large changes that may simply reflect georeferencing offset or image warping (Fig. 2-1b). These two issues are especially problematic for fluvial processes, which follow heavy-tailed distributions that are largely composed of small values and may be strongly skewed by a few large outliers. Discarding small but valid changes in combination with retaining large but erroneous changes causes a systematic overestimation of average migration rates.

Lea and Legleiter (2016) overcome the aforementioned issues by estimating spatially-variable (SV) uncertainty from both georeferencing uncertainty and digitization error. A raster of SV-uncertainty is used as an LoD to compare with migration trajectories from the Planform Statistics Toolbox (Lauer & Parker, 2008) in order to distinguish statistically significant measurements. Their approach calculates non-uniform LoD ellipses at all points around the river as the sum-of-squares including all sources of uncertainty (Eqs. 1 and 2).

$$\sqrt{\varepsilon_{xt1}^2 + \varepsilon_{xt2}^2 + \varepsilon_{dig}^2} = \varepsilon_x \; ; \qquad \text{Eq. 1}$$

$$\sqrt{\varepsilon_{yt1}^2 + \varepsilon_{yt2}^2 + \varepsilon_{dig}^2} = \varepsilon_y \; ; \qquad \text{Eq. 2}$$

$$\sqrt{\varepsilon_x^2 + \varepsilon_y^2} = \varepsilon_{xy} \; ; \qquad \text{Eq. 3}$$

where ε_x and ε_y are georeferencing uncertainty in the x- and y-planes for time 1 (*t*1) and *t*2, respectively, ε_{dig} is digitization uncertainty, and ε_{xy} is total uncertainty at a location (e.g., the LoD error ellipse, Eq. 3). This approach increased the number of statistically significant measurements retained relative to RMSE or 90th percentile uniform error thresholds (Lea & Legleiter, 2016).

Measurements below the LoD can be entirely removed, treated as values of zero (i.e., no migration occurred), or modelled based on the expected distribution of measured values (Donovan & Belmont, 2019). Replacing measurements below LoD with zero is generally preferable to removing them entirely. However, a disproportionate number (> 50%) of zero-values can compromise comparative statistics (e.g., Paired *t* Test, Kolmogorov-Smirnov, Mann-Whitney Wilcoxon) that count each pair of zeros as a 'tie' (Martín-Fernández, Barceló-Vidal, & Pawlowsky-Glahn, 2003). In these cases, it may seem prudent to discard uncertain measurements, but this not only reduces sample size, but also introduces error into estimates of net change and uncertainty (Anderson, 2018). Details on imputation and replacement strategies for values falling below the LoD can be found in section 2.3.5.

Areal or volumetric estimates of channel change using polygons contain the same sources of error, but must account for error differently because outputs/results are 2-D geometric features (i.e., polygons, rather than 1-D lines). Polygonal results are commonly beset with small polygon slivers that arise from slight misalignment due to georeferencing and digitization error (Chrisman, 1987; Bailey, 1988). Slivers are often assumed erroneous, rather than real change. Thus, a common and simple approach to address error is to remove polygons smaller than a threshold size (Edwards & Lowell,

1996; Donovan et al., 2015). More advanced approaches clip polygons using buffers of uncertainty scaled to georeferencing RMSE (Rhoades et al., 2009). Unfortunately, because both approaches lack a spatially variable threshold, both also unnecessarily remove significant measurements of erosion or deposition simply because they are of low magnitude. However, error models have been developed to incorporate heterogeneity of error for polygon/areal-based estimates of channel change (D. Gaeuman, Symanzik, et al., 2005). Rather than assuming errors are spatially independent of one another, they assume error is spatially correlated at the scale of local digitization inconsistencies and broadly over the scale of GCP placement, similar to Lea and Legleiter (2016).

2.3.5. Handling values below the LoD ('nondetects')

Earth-science literature increasingly reports uncertainty associated with planform change measurements, but there appears to be few discussions and no consensus regarding how to handle nondetect measurements that fall below the LoD/uncertainty threshold. Common methods include discarding nondetect measurements (Rhoades et al., 2009), imputing nondetects with values of '0' (Donovan & Belmont, 2019) or substituting nondetects with 0, 0.5, 0.7, or $1/\sqrt{2}$ of the LoD threshold (Martín-Fernández et al., 2003; Lee & Helsel, 2005; Helsel, 2006), and retaining nondetect measurements in order to bracket results with a range of upper and lower bounds based on the degree of uncertainty (Fraley, Miller, & Welty, 2009; Dean & Schmidt, 2011; Donovan et al., 2016). Despite their use in contemporary research, these methods should be avoided because they introduce systematic errors and bias the mean and variance increasingly as the proportion of nondetects increases relative to the entire sample size (Tauber, 1999;

Singh & Nocerino, 2002; Martín-Fernández et al., 2003). When observations or process understanding suggest no channel migration has occurred, it may be appropriate to record nondetect migration measurements as zeros, which are termed ‘rounded zeros’. Researchers must consider, however, that the individual data points can no longer be log-transformed or used as a denominator in subsequent normalizations.

When nondetects account for only a small proportion (10-15%) of the data, EPA’s Unified Guidance suggests that a simple substitution method is acceptable, based on insignificant changes to the mean and variance. However, when dealing with data fraught with nondetects, Maximum Likelihood Estimators (MLE), imputation via Regression on Order Statistics (ROS), and the Kaplan-Meier (KM) method are three approaches that provide more robust representations of summary statistics (i.e., mean, median, variance; Helsel, 2005). Each approach is unique, using some combination of detectable (i.e., known) data, nondetects (some methods, but not all), and an assumed or known data distribution based upon detectable observations. We describe the mechanics of each approach in the methods.

3. Methods & Study area

3.1. Measuring migration and spatial autocorrelation

We develop guidelines to evaluate uncertainty for channel migration derived from manual channel delineations using a set of 13 aerial photographs spanning 76 years and 120 river-km of the Root River, MN, USA (Fig. 2-2A). With 441 images spanning nearly eight decades and an entire river network, we were able to evaluate the relationship between uncertainty (Eqs. 1, 2, and 3) and a variety of variables, including image resolution, acquisition date, local lighting, vegetation type/cover, and channel planform.

Streambank delineations and interpolated centerlines from each georeferenced image (Souffront, 2014, M.S. Thesis) were used to calculate migration magnitude and rate at 10-meter increments using the Planform Statistics Toolbox (Lauer, 2007; Lauer & Parker, 2008). The Planform Statistics Toolbox measures total migration as the distance between nodes on the initial and terminal channel centerlines, but does not identify meander bend cutoffs, which we manually identified and filtered out.

We initially measured migration along the entire reach at 10-meter increments. However, measurements at such close intervals are likely autocorrelated due to the natural tendency for rivers to move in coherent spatial units that scale with the size of the river (Donovan & Belmont, 2019). Additionally, autocorrelation may arise from systematic offsets in digitization at local (100 – 500 m) scales, and at broader scales (10^2 – 10^3 m) due to offsets in image georeferencing and expected similarities in migration rates for adjacent stream reaches and meander bends. Autocorrelated measurements are not independent and are thus not statistically independent observations; they also underestimate standard errors and bias statistical comparisons that assume independent measurements. We computed Geary's C to estimate the length scale over which migration rates were influenced by the combined effects of spatial autocorrelation and local-scale systematic delineation biases (Geary, 1954). While Moran's I is more commonly used for characterizing global spatial autocorrelations, it fails to capture local autocorrelation due to the simple regression structure used. In contrast, Geary's C is able to detect local spatial autocorrelation, which is more relevant for analyzing channel planform adjustments, which are autocorrelated over meander-bend scale (local), rather than an entire longitudinal profile (global). Geary's C values typically range from 0 to 2

and estimate the level of correlation between all possible data points at specified lag distance bins. Values near to 1 indicate weak or absence of positive spatial autocorrelation. Values approaching 0 indicate positive autocorrelation, and are common at smaller lags. Values close to 2 indicate an increasing negative autocorrelation. To improve interpretability of results, we transform Geary's C values to standard correlation coefficients for plotting in correlograms, ranging from -1 to 1 to indicate negative to positive autocorrelation. Scripts for calculating Geary's C are provided in a supplementary file, 'GearyC.R'.

3.2. Georeferencing uncertainty

We analyze georeferencing uncertainty analyses using 13 sets of GCPs (n = 185 – 302) spanning 120 km of the Root River (Table 2-2). Rather than using the original GCPs, we quantified georeferencing error using an independent set of GCPs found on a high-resolution composite image from 2015 (USDA FSA APFO, 2015). Georectification transformations use least-squares fitting algorithms to optimize (i.e., minimize) georeferencing offset using the original input GCPs, but not necessarily areas in between (Ladd, Nagchaudhuri, Earl, Mitra, & Bland, 2006). Thus, using an independent set of GCPs ensured that error was not underestimated because it included areas aside from the original input GCPs. We primarily selected 'hard' GCPs (i.e., immobile or unlikely to have moved) that could be found on both historical and 2015 images. We evaluated spatial correlation of GCP error over a range of distances in order to determine whether or not georeferencing error is spatially correlated, and if so, over what distance (D. Gaeuman, Symanzik, et al., 2005).

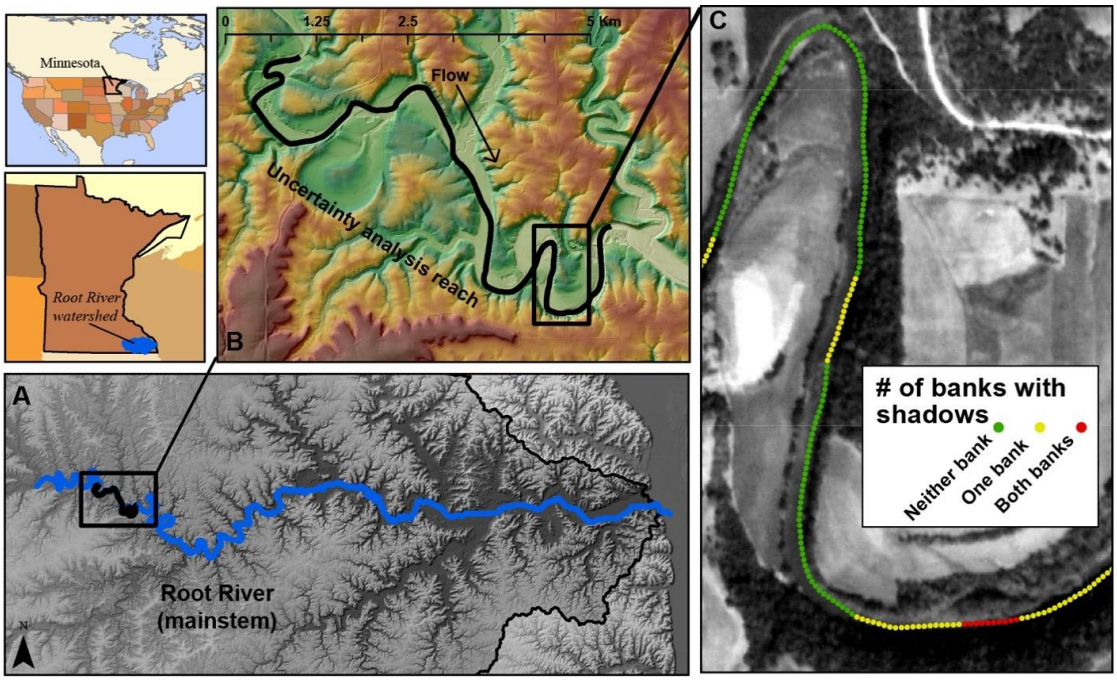

Fig. 2-2. (Topleft) Locations of Minnesota within North America, and the Root River within southeastern Minnesota. (A) 120 km of the mainstem Root River (blue) with 13 overlapping years of aerial photography. Inset black box is (B) the 11 km study reach analyzed in detail for this study. Second inset black box is (C) a single channel centerline divided into points each 10-m, with colors indicating whether shadows covered both, one, or neither streambanks. We categorized the banks in the same way for locations where vegetation covered the bank.

3.3. Digitization uncertainty

We chose an 11-km reach of the Root River with multiple morphologic features and variable degrees of overhanging vegetation and shadows in order to quantify digitization uncertainty and determine whether it varies with fluvial and riparian conditions (Fig. 2-2B). The reach also allowed us to evaluate whether point bars reduced consistency in manual riverbank delineation, similar to semi-automated algorithms (Güneralp et al., 2013, 2014). Similar to (Gurnell et al., 1994), a single user repeatedly delineated 11-km of vegetation-streambank boundary four times without the aid of previous iterations, yielding 52 streambank delineations across 13 years with imagery (13

years × 4 delineations). We did not limit the user to a specific map scale/zoom in order to reflect 'normal' working conditions, which do not impose such constraints. When vegetation covered the bank, we delineated bank location through the crown of the tree, unless we observed the bank-vegetation interface elsewhere. Channel centerlines were interpolated from each bank delineation, consistent with the prevalent method for measuring migration rates. Because centerlines should be identical for users with 100% delineation consistency, we calculated centerline offset at 10-meter increments as a measure of uncertainty arising from digitization inconsistency. This resulted in 78 centerline comparisons (13 years × 6 centerline comparisons) spanning 11-km and 13 years of imagery, for approximately 86,000 measurements to estimate digitization uncertainty. We calculated Geary's C values from these centerline comparisons to quantify the length scales over which digitization introduces autocorrelation into migration measurements.

To determine whether image resolution influenced digitization uncertainty, first we visually compared the means and distributions of false migration of all 11-km of the 13 images using Kruskal-Wallis nonparametric analysis of variance (ANOVA) and a comparison of image resolution versus false migration. Subsequently, we evaluate whether a single user's digitization inconsistency increases for channel reaches with overhanging vegetation or shadows, as has been observed when using semi-automated delineation algorithms (Güneralp et al., 2013, 2014). At each 10-m increment, we classified the channel centerline as 0, 1, or 2; respectively classifying whether neither bank, one bank, or both banks were obscured by shadow (Fig. 2-2C). We repeated this approach for vegetation, attributing 0, 1 or 2 to indicate absence or presence of vegetation

obscuring one or both banks for each year with photo record. A Kruskal-Wallis test revealed whether any group/class exhibited significant differences. In cases where differences existed, we followed up with a Kolmogorov-Smirnov test to test for a stochastic increase in uncertainty for each class (Massey, 1951; Fay & Proschan, 2010).

3.4. Spatially-variable level of detection

We generated a spatially-variable level of detection (SV-LoD) raster for each year with images that included total uncertainty from georeferencing and digitization (Eqs. 1, 2 and 3). The sum of squares of positional offset in the x- and y-planes at each GCP and mean digitization inconsistency were interpolated using second-order polynomials, which yield low mean RMSE and minimize image warping relative to all eight possible transformations (Hughes et al., 2006; Lea & Legleiter, 2016).

We compared the percent and magnitudes of migration measurements retained (n = 66 comparisons) to respectively evaluate the relative quantity and quality of retained measurements. Comparing the percent of retention between SV- and uniform-LoD thresholds confirmed whether SV thresholds improved (i.e., increased) the quantity of retained measurements. We evaluated the quality of retained measurements by testing whether distributions under SV thresholds shifted left (i.e., reduction) relative to uniform LoD thresholds. This assumes that a reduction in the distribution indicates that the quality of retained measurements has increased because SV-LoDs are more likely to retain measurements of small magnitude that are erroneously discarded by uniform LoDs. We visually inspected shifts in addition to performing one-way Kolmogorov-Smirnov tests to evaluate whether SV distributions increased the retention of low-magnitude measurements relative to uniform LoD thresholds, as indicated by a reduction/leftward-

shift in the distribution. Lastly, we used linear regressions to estimate percent retention as a function of pixel resolution, initial image year, temporal measurement interval, along with river-averaged migration and its natural logarithm.

3.5. Handling nondetects

Common approaches for handling nondetects in geomorphology include: removing nondetects or substituting nondetects with 0, 0.5, 0.7, or $1/\sqrt{2}$ of the LoD threshold (Martín-Fernández et al., 2003; Lee & Helsel, 2005; Helsel, 2006) and retaining nondetect measurements in order to bracket results with a range of upper and lower bounds based on the degree of uncertainty (Fraley et al., 2009; Dean & Schmidt, 2011; Donovan et al., 2016). However, these methods introduce error into estimates of net change and uncertainty (Anderson, 2018) and skew statistical parameters by introducing a disproportionate number of arbitrary values (Helsel, 2006), respectively. Thus, we propose and test three alternative methods developed by statisticians and discipines outside of Earth science: Maximum Likelihood Estimation (MLE), imputation via Regression on Order Statistics (ROS), and Kaplan-Meier (KM). Each method is unique in its approach to estimating summary statistics for nondetect data and are known to outperform one another depending on the underlying data distribution, proportion of nondetects, sample size, and the number of detection limits (Helsel, 2005). Among research on geomorphic change detection, bracketing results with the sum of uncertainties is common; the benefits and drawbacks of this approach are detailed in (Anderson, 2018). Our scripts for running MLE, ROS and KM are available in the supplementary .R file.

Following its name, the MLE estimates the 'most likely' mean and standard deviation by fitting both detected observations and nondetects to a distribution chosen by a knowledgeable expert. Although MLE assumes a normal distribution, it is commonly used with transformed lognormal data. MLE generally underperforms for small datasets ($n < 50$ detectable observations) with large skewness, or when outliers are present, relative to ROS or K-M. ROS depends less on assumptions of distribution shape because it estimates nondetect data using probability plots of detectable data. Kaplan-Meier is a standard in medical, industrial, and water chemistry statistics for estimating the mean and standard deviation of data containing censored (i.e., partially known) measurements. K-M does not assume a parametric distribution, but requires at least 8-10 measurements, less than 50-70% nondetects, and is biased when the highest and/or lowest values are nondetects. K-M also requires multiple levels of detection, and thus, is appropriate with an SV-LoD, but not a uniform LoD. For a robust description of K-M, see Hosmer et al., (2008). Additional guidance and details on MLE, ROS, and K-M are provided online (Huston & Juarez-Colunga, 2009; ITRC, 2013).

We evaluated each approach by quantitatively comparing their predicted mean (μ), median, distribution fit, and standard deviation (σ) with known values from modelled distributions ($n = 400$) containing varying proportions of nondetects (8-30%). The 'best estimate' of mean, median and variance from the MLE, KM, and ROS were those with the minimum difference relative to the modelled/raw values. We ranked the distribution fits relative to the original modelled distribution using a Pairwise Wilcoxon Rank Sum test statistic with an adjusted p-value (based on Benjamini and Hochberg, (1995)) to reduce the rate of false-positive results and allow for distribution comparison. With this

adjustment, the test is sensitive to differences in distributions, not only central tendencies. We plot the empirical cumulative density functions (ECDFs) from each approach to visually confirm the quantitative results and further inform a discussion of when each approach is most appropriate. We also varied the measurement sample size (n= 100, 1000, or 10,000) in modelled simulations to evaluate whether sample size influenced which approach (i.e., MLE, KM, ROS) best predicted the statistical parameters. This also allowed us to explore the implications of different combinations of spatial and temporal data extent (spatial coverage x measurement interval), which directly affect sample size.

Modelled migration rates followed a lognormal distribution with means drawn from the range of 13 empirical distributions, each with ~13,000 measurements spanning 120 km of the Root River. Deviance scaled directly and significantly with the mean migration rates, and thus was predicted using Eq. 4, similar to Donovan & Belmont (2019).

$$\sigma = 0.25\mu + 1.09 \quad \text{Eq. 4}$$

We calculated the probability of significance for each modelled migration rate using the relationship ($r^2 = 0.89$) between empirical migration rate and chance of statistical significance based on 864,204 empirical migration rates (Fig. 2-3). We did not include migration rates beyond 9 m/yr when regressing the data because 100% of those rates were significant, and including those reduced the logarithmic regression fit for values that may be nondetects. This approach resulted in 10 to 53% of nondetects for each model iteration, which had 100, 1,000 or 10,000 sample measurements.

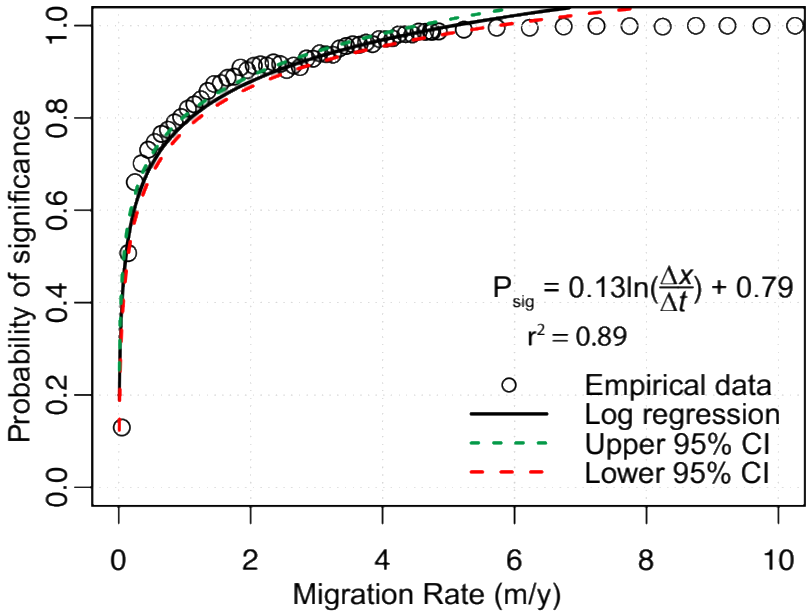

Fig. 2-3. Empirical data (black dots) used to generate the probability that a modelled migration rate will be significant or nondetect. The probability of significance (P_{sig}) for a given migration rate increases logarithmically with the magnitude of the rate, and beyond ~9 m/yr, 100% of measurements were significant. In order to improve the model fit for values with a chance of being nondetects, values with 100% chance of significance were not included in the regression.

4. Results & Discussion

4.1 Spatial autocorrelation for measurements of migration and uncertainty

Correlograms of autocorrelation values illustrate a waning spatial autocorrelation of channel migration rates over length-scales that are approximately 1-4 channel widths (50-200 meters), at which point autocorrelation was weak or nonexistent (Fig. 2-4). The trends in autocorrelation values of migration rates were similar to those for user digitization inconsistency. Thus, we were unable to ascertain the length scales over which autocorrelation reflects digitization inconsistency as opposed to coherent units of channel migration. This suggests similar scales of autocorrelation for both manual channel digitization and river migration across a wide range of geomorphic conditions and river

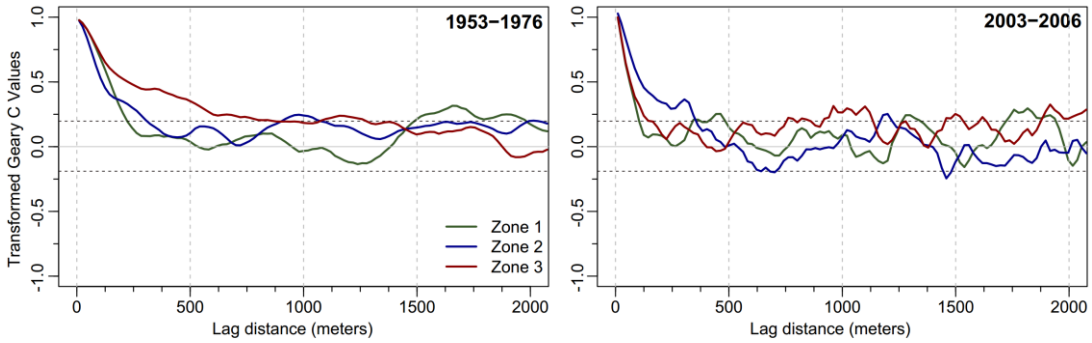

Fig. 2-4. Correlograms of spatial autocorrelation for measurements of channel migration. Lag distance indicates the length over which autocorrelation was measured. Geary's C values, which typically range from 0-2, were transformed to the typical range of correlation values, spanning -1 to 1.

widths. Thus, measuring migration over lengths ≥ 6 channel widths (400 meters) for the Root River ensured autocorrelation did not confound statistical results and inferences.

When testing the assumption that GCPs exhibit local spatial correlation (D. Gaeuman, Symanzik, et al., 2005), we found strong autocorrelations were rare (values > 0.7 or < -0.7) (6-28%), whereas weak autocorrelations dominated the data ($-0.3 > r < 0.3$) (62-81%), with the remaining 14-38% of data exhibiting moderate autocorrelations (values between 0.3-0.7 or -0.3- -0.7). The few GCPs with strong autocorrelation did not dominate any particular spatial scale, suggesting it is invalid to assume that nearby GCPs are more or less similar than distant GCPs. The lack of local or global autocorrelation reinforces the need for spatially variable LoDs because neither neighboring GCPs nor distant GCPs were similar in magnitude or autocorrelated.

4.2. Factors influencing digitization uncertainty

We analyze an 11-km reach of the Root River to build upon the literature quantifying the factors that influence the magnitude, location, and types of offset from

digitization. Mean and median digitization uncertainty across all years was 1.4 meters. Despite unique approaches to calculating uncertainty, this result is consistent, albeit slightly less than Gurnell et al. (1994) (2 meters). Within the 11-km segment, pixel resolution ranged from 0.5-5.8 m^2, thereby including nearly the full pixel range (0.3-5.8 m^2) for all 441 images spanning the 120-km mainstem Root River. Despite a variety of pixel resolutions, the distributions of digitization offset were not significantly different ($p = 0.95$, Fig. 2-5) based on a Kruskal-Wallis Rank Sum Test and the lack of a systematic trend between digitization offset and pixel resolution. Neither image date nor pixel resolution appear to have a systematic influence on the degree of digitization inconsistency for a single user. The consistency in these results across a variety of image resolutions (0.5-5.8 m^2) and conditions suggests that average and median digitization uncertainty for a single experienced user will lie between 1.5 and 2 meters, and need not be calculated for all future studies. It remains plausible that follow-up evaluations may be pertinent for studies with resolutions outside this range, or for substantially different geomorphic conditions. The framework provided herein for evaluating digitization uncertain remains transferrable to other environments to explore potential differences. Similar methods were applied to braided and anastomosing planforms by Werbylo et al., (2017), who found that measurements of at-a-section channel width derived from multiple digitizers differ up to 20% of channel width, while river-averaged widths exhibited no significant differences.

Digitization uncertainty was generally consistent across all years (i.e., high precision) in cases where the bank is masked by shadow and/or vegetation cover (Fig. 2-6). Higher degrees of inconsistency (> 5 meters) occurred along meander bends with

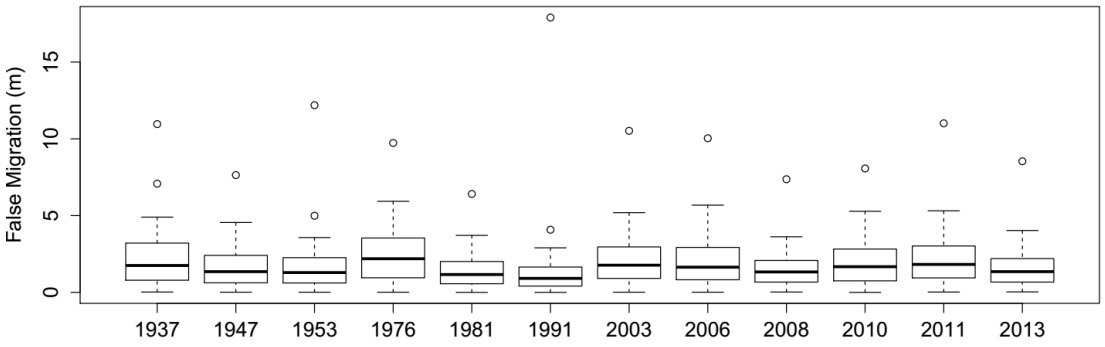

Fig. 2-5. Digitization inconsistency for 11.2 km of the Root River for each of the 13 years with aerial images (~1120 migration transects measured for each photo year). The overall magnitudes and distributions were relatively consistent across all photos, regardless of pixel resolution.

various types of vegetation cover (e.g. thick vegetation, scattered brush, grass) because users are inconsistent in their choice of vegetation boundary. Similar inconsistencies have been observed for semi-automated algorithms (Güneralp et al., 2013, 2014). Most of the remaining offsets in digitization (≤ 1 meter) were minor and were scattered uniformly across the 11-km reach. Thus, we demonstrate that users remain consistent in delineating the channel-vegetation boundary regardless of shadows and vegetation, but not in cases where multiple vegetation boundaries exist. Thus, for such reaches, users should determine which vegetation-boundary best reflects the dominant- or channel-forming discharge. Optimally, verification would utilize ground-truthing along ambiguous reaches. Alternatively, where high-resolution topography is available, local peaks in curvature may be used as a characteristic signal of the streambank-floodplain transition (Donovan et al., 2015). In areas where riparian vegetation and geomorphic conditions differ substantially to obscure delineations, the framework laid out herein should be applied to evaluate for consistency of results.

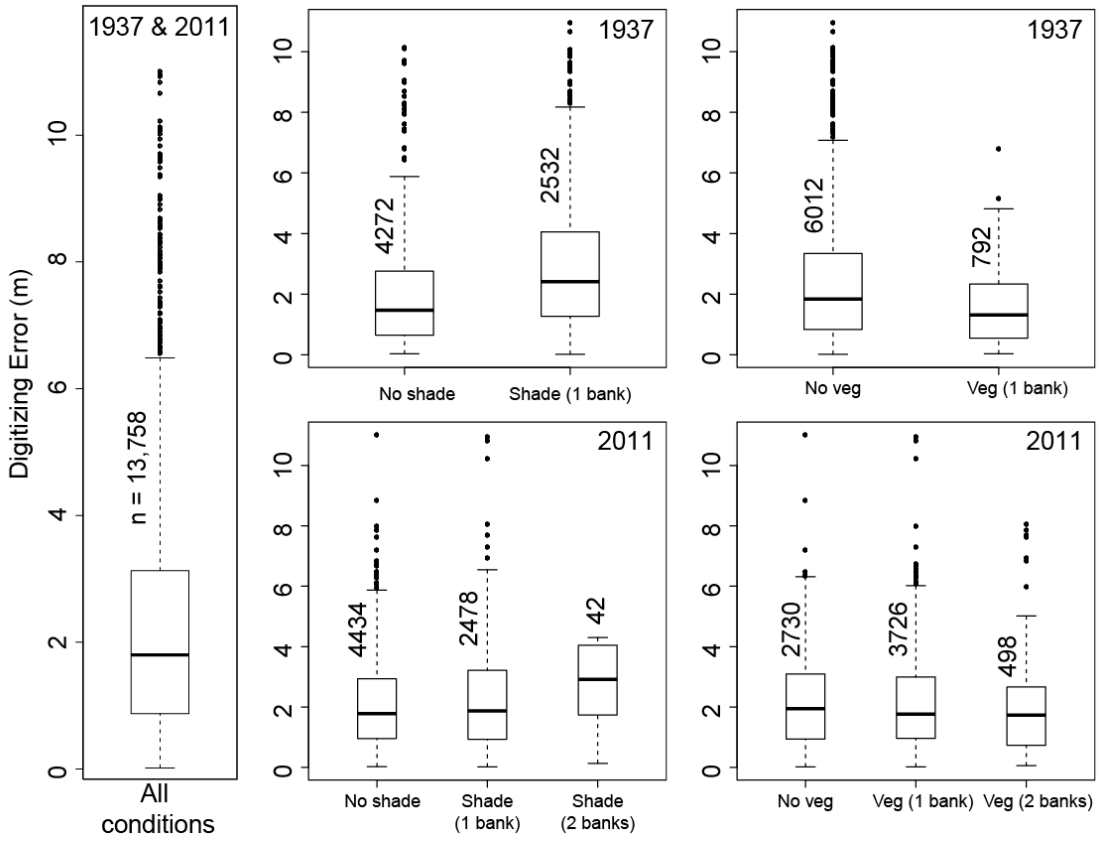

Fig. 2-6. Digitization inconsistency binned by the presence of shadows and vegetation on either one, both, or neither adjacent streambanks. Numbers adjacent to individual boxplots indicate the sample size of each category.

4.3 Georeferencing uncertainty

Georeferencing uncertainty varied widely across the study reach within each year's images (Fig. 2-7) and across all years (Fig. 2-8), and generally decreased towards the present, likely a reflection of reduced distortion and warping with improved camera lenses and developments in self-calibrating sensors (Clarke & Fryer, 1998). Because georeferencing error generally distorts images over scales equal to and greater than GCP spacing, river width measurements are unaffected unless warping occurs over scales less than a channel width. Thus, we do not explore the impact of georeferencing uncertainty

on width calculations. Neither the RMSE of georeferencing error, nor the distributions of error, appear to have any significant relationship to the mean pixel resolution of each year (Table 2-2) based on graphical assessment, and thus, were not explored statistically. The RMSE was approximately the 75th percentile for most years (Fig. 2-8, red points), which illustrates how a small number of extreme outliers in georeferencing uncertainty inflate the RMSE relative to the median (i.e., the actual central tendency in a long-tailed, non-normal distribution). We describe implications of using this inflated RMSE value in the next section.

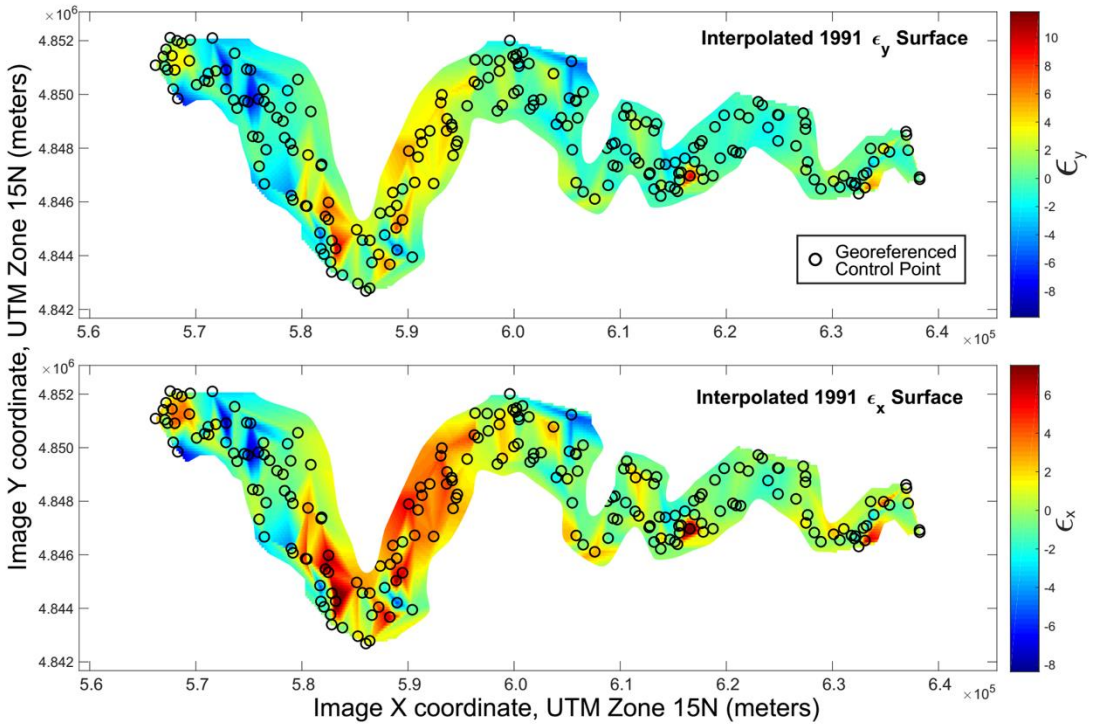

Fig. 2-7. Spatially variable georeferencing uncertainty, in meters, across the x- and y-coordinate planes (bottom and top, respectively). For total uncertainty, we used Eq. 1 and 2 as components for calculating a final error ellipse for each pixel. Note that the color gradient scales change for each panel, due to different ranges of error in the x- and y-planes.

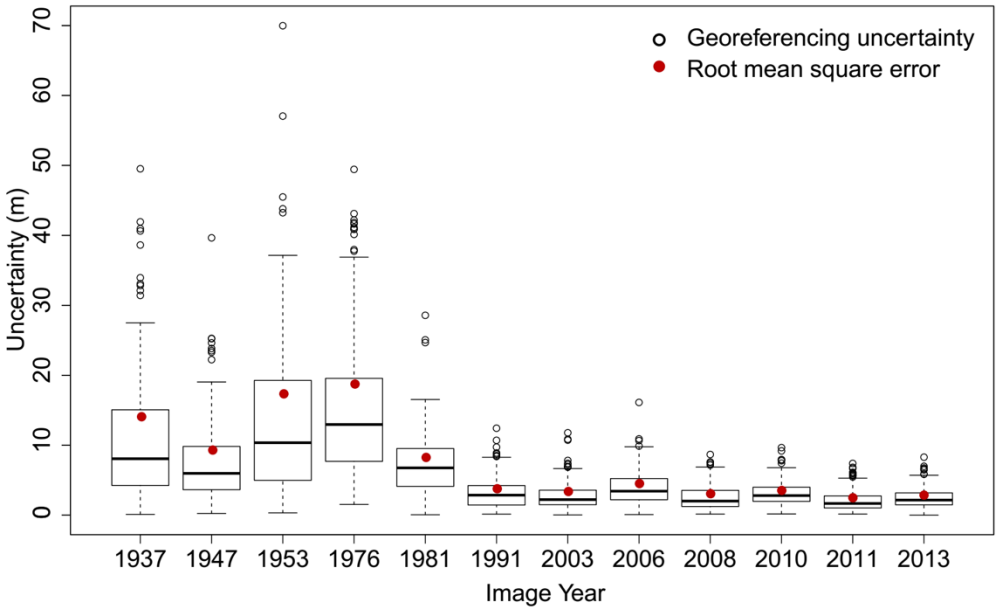

Fig. 2-8. The distribution of georeferencing uncertainty for each image year (black), based on the set of georeferenced control points (GCPs, n = 185-302). The red dots indicate the root mean square error (i.e., mean) of each distribution, a common uniform uncertainty threshold. However, using the RMSE threshold leads to excessive data loss of any measurement below the red dots.

4.4 Calculating and evaluating LoD thresholds

Final LoD thresholds reflect the sum of squares of georeferencing and digitization uncertainties. While SV LoDs reflect a different sum of squares for each pixel, RMSE LoDs calculate a single, average sum of squares. As explained earlier, however, extreme outliers in georeferencing error disproportionately inflate the mean error (i.e., RMSE) relative to the majority of values within a lognormal distribution (Fig. 2-8, red dots). Thus, using an inflated RMSE value as the LoD inherently removes the majority of migration measurements, which are predominately low-magnitude values (Fig. 2-9, black distribution). After using a singular RMSE LoD, the majority of low-magnitude migration values are thus ‘nondetects’, while the few upper percentiles remain to dominate the migration distribution. As a result, the mean migration rate- a widely used

Table 2-2.
Overview of image characteristics, georeferencing control points, and error for each year with imagery. We used imagery from 2015 as a reference layer for calculating offset/error, and thus does not have error values. This assumes the 2015 imagery is the most spatially accurate representation of the study area.

Year	# of GCPs	Color profile	Mean image resolution* (m)	Georeferencing error (m)				Digitization error* (m)		
				RMSE	10%	50%	90%	10%	50%	90%
1937	198	B&W	0.9	14.1	2.7	8.1	22.0	0.3	1.8	4.9
1947	214	B&W	1.0	9.3	1.9	6.0	14.5	0.2	1.4	3.7
1953	199	B&W	2.1	17.4	2.4	10.4	27.9	0.3	1.3	3.6
1976	185	B&W	2.2	18.8	4.5	13.0	31.4	0.4	2.2	4.9
1981	223	RGB	3.2	8.3	2.7	6.8	12.1	0.2	1.2	3.0
1991	220	B&W	1.0	3.8	0.8	2.9	5.9	0.2	0.9	2.9
2003	226	RGB	1.0	3.4	0.7	2.2	5.5	0.4	1.8	4.3
2006	227	RGB	2.0	4.5	1.2	3.4	7.0	0.4	1.6	4.7
2008	228	RGB	1.0	3.1	0.8	2.0	5.2	0.3	1.3	2.9
2010	232	RGB	1.0	3.5	1.2	2.8	5.2	0.3	1.7	4.4
2011	233	RGB	0.5	2.5	0.6	1.7	4.0	0.4	1.8	4.5
2013	233	RGB	1.0	2.9	0.9	2.2	4.6	0.3	1.4	3.2
2015	302	RGB	1.0	-	-	-	-	-	-	-

*Average resolution and digitization error come from the 11-km subreach.

Summary statistics for each year's imagery and the associated digitization uncertainty are available in Table 2-2. Second-order polynomial interpolation of SV error improved the number of retained migration measurements for all years, corroborating results from the original implementation of this method (Lea & Legleiter, 2016). Furthermore, in all comparisons (n = 67), SV-LoD thresholds retained more migration measurements (μ=62%, range=25-81%) than uniform LoD thresholds (μ=35%, range=12-52%). Distributions of retained measurements consistently demonstrate that SV-LoDs retain additional measurements of smaller magnitude and fewer measurements of large magnitude (Fig. 2-9).

For three different years, we evaluated migration measurements that were retained with the SV-LoD, but not the uniform LoD. Visual observations of values retained by

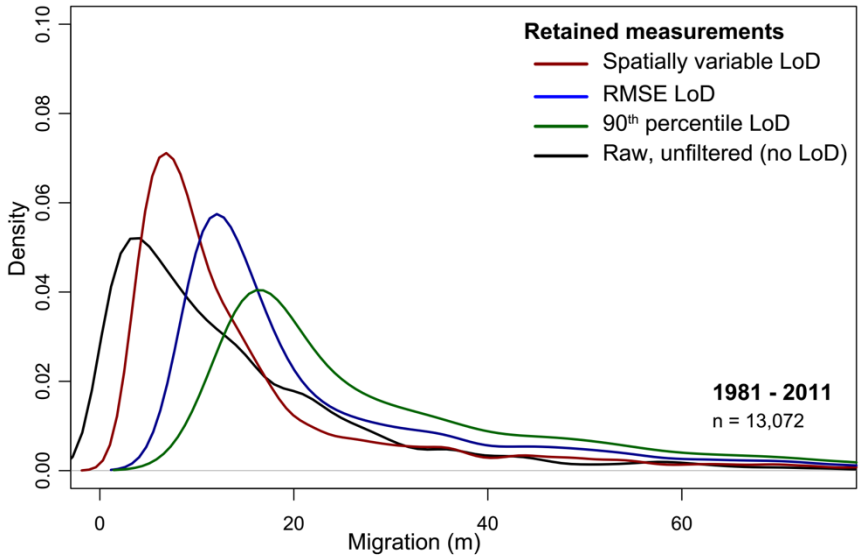

Fig. 2-9. A comparison of probability density functions among of all measurements (black) and retained (i.e., 'significant') measurements for each type of LoD (SVE-red, RMSE-blue, and 90th percentile threshold-green). Illustrated distributions are for measurements of migration (m) between 1981 and 2011, with similar trends in the remaining 65 comparisons. The SV-LoD (red) retained a higher proportion of low-magnitude measurements, and relatively fewer large-magnitude measurements. This suggests that a SV-LoD not only improved the quantity, but also the quality of retained measurements.

only the SV-LoD suggest that a little over half of these values were real, verifiable changes, generally characterized by gradual systematic shifts in the river apparent in multiple images and/or visual evidence from the LiDAR hillshade and/or images. 'Questionable' retained measurements were often non-systematic migration along reaches that were fully or partially masked by shadows or vegetation, which possibly led to inaccurate delineations. Thus, despite consistent delineations (i.e., delineation precision) under the same conditions, the interpreted location of the riverbanks (i.e., delineation accuracy) still appears to vary significantly when visual conditions change along a stable reach (Figs. 2-3 and 2-6).

Anomalously high-magnitude measurements that result from extreme image

warping or georeferencing error that shifted the river boundary (Fig. 2-10) are more likely to be retained by the SV-LoD than the uniform LoD. The uniform LoD may retain these large measurements simply because they exceeded the RMSE, whereas the SV-LoD is likely to discard them by properly accounting for local maxima in uncertainty. The use of a spatially-variable LoD will thus improve results by reducing the likelihood of including inaccurate measurements, and is generalizable/applicable to any context.

We tested for systematic trends in the percent of retained measurements to evaluate whether factors such as image year, image resolution, or migration distance, exhibited strong relationships with the proportion of retained measurements. Of these

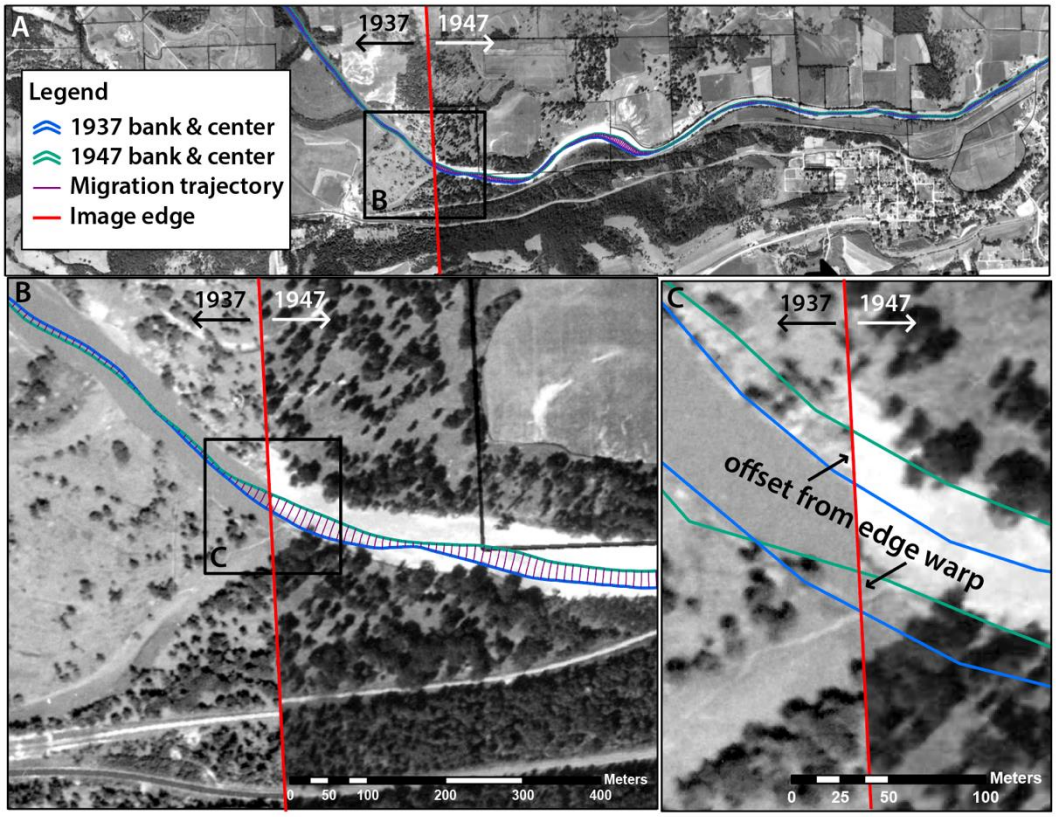

Fig. 2-10. An example of image warping near the edge of two images, which intersect at the red line. The warping resulted in offset channel centerlines (B) and delineated banklines (C). Evidence of warping along the channel in B and C is confirmed by the offset roads in the bottom of B.

factors, the most significant was the natural logarithm of mean migration distance (Fig. 2-11, $p < 0.001$, $r^2 = 0.92$). When mean migration falls below the minimum LoD- equivalent to mean and median digitization uncertainty (1.4 meters, dashed-blue line, Fig. 2-11)- there is a drastic reduction in the proportion of 'significant' migration measurements. For migration above this threshold, the number of significant measurements increases relatively slowly, as some diminishing proportion of measurements still have a total uncertainty that exceeds the LoD threshold.

4.5. Treatment of nondetect measurements

We summarize the model results for each approach- Maximum Likelihood Estimator (MLE), Kaplan-Meier (KM), Regression on Order Statistics (ROS), zero

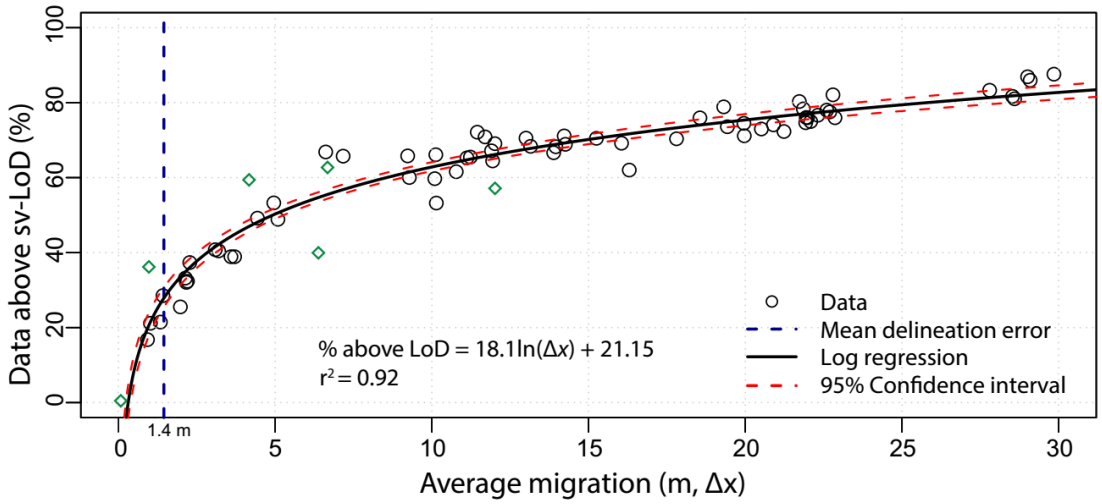

Fig. 2-11. Relation between mean migration and the percent of retained measurements. Each black point reflects the percent of significant measurements for a given river-averaged migration (over the 120-km of the Root River) between two sets/dates of imagery (n= 864,204). The proportion of significant measurements increases rapidly as mean migration passes the average (mean and median) digitization error (blue vertical line, 1.4 meters). Beyond this threshold, the number of retained measurements increases asymptotically. Green diamonds represent averaged migration measured over portions (1-37 km) of the Root River, rather than the entire 120-km (black points).

thresholding, and removing nondetects- to best approximate the mean, median, standard deviation, and overall distribution of modelled data in Table 2-3. We quantified 'best fits'for the mean, median and standard deviation as the method which best approximated (i.e, minimum difference) a known, modelled distribution. We ran 400 simulations, each with a unique lognormal distribution containing a range of nondetects (47-90%) and sample sizes (n = 100, 1,000 or 10,000). Detailed methods for generating and comparing the statistical parameters are described in Section 3.5, and can be found in the supplementary .R file "Nondetect Method Comparison'.

Across all sample sizes, the MLE and KM methods provide the best estimate of the mean in a similar number of simulations. MLE performed better for model iterations handles nondetects in estimating the new mean. KM also performed well in estimating

Table 2-3.
Results from 400 simulations comparing known/modelled values with estimated statistical parameters (i.e., mean, median, standard deviation, distribution) from each method. MLE- Maximum likelihood estimator; KM- Kaplan Meier; ROS- Regression on Order Statistics; ZRO- nondetects treated as '0'; RMV- nondetects removed entirely. Bolded values indicate which method performed the best.

Sample size	Statistical criteria	Best fits (%)					Total
		MLE	**KM**	**ROS**	**ZRO**	**RMV**	
n = 100	Mean	50%	33%	0%	0%	17%	100%
	Median	19%	41%	3%	0%	37%	100%
	Variance (σ)	2%	7%	80%	0%	11%	100%
	Distribution	91%	1%	0%	8%	0%	100%
n = 1,000	Mean	50%	34%	1%	0%	15%	100%
	Median	1%	77%	0%	0%	22%	100%
	Variance (σ)	1%	1%	98%	0%	0%	100%
	Distribution	99%	0%	0%	1%	0%	100%
n = 10,000	Mean	47%	30%	1%	0%	22%	100%
	Median	0%	79%	0%	0%	21%	100%
	Variance (σ)	0%	16%	84%	0%	0%	100%
	Distribution	98%	0%	0%	2%	0%	100%

the median across all sample sizes with the exception of small sample sizes containing a high proportion of nondetects, where removing nondetects (RMV) resulted in better estimates of the median. In the majority of simulations (86 – 97%), ROS provided the best approximation of variance. Finally, the best estimates of the entire distribution largely came from the MLE (85 – 92%). Two characteristic sets of ECDFs are plotted alongside the raw/modelled data as the gold standard (Fig. 2-12). Below, we illustrate and describe the conditions in which each method is most appropriate in a flow chart (Fig. 2-13).

5. Conclusions, recommendations, and future challenges

Earth-science literature has become increasingly aware of the importance of calculating and disclosing uncertainty inherent in GIS-based measurements. In the early 1990s, (Anders & Byrnes, 1991) acknowledged the need to address the key sources of

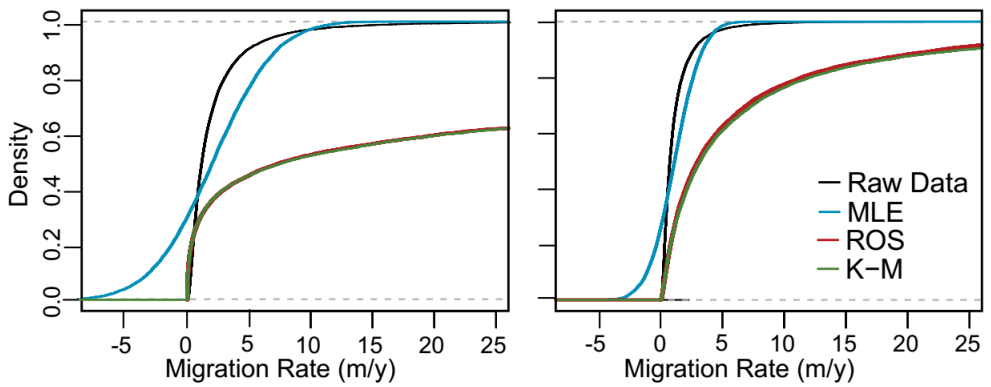

Fig. 2-12. Empirical cumulative density functions (ECDFs) for the modelled (i.e., 'raw') migration data, alongside three approaches used to model nondetect measurements. The two sets of ECDFs reflect the majority of model iterations (n = 400). While the three methods are only meant to estimate summary statistics (mean, median, variance), visualizing the distributions help interpret the results in Table 2-2.

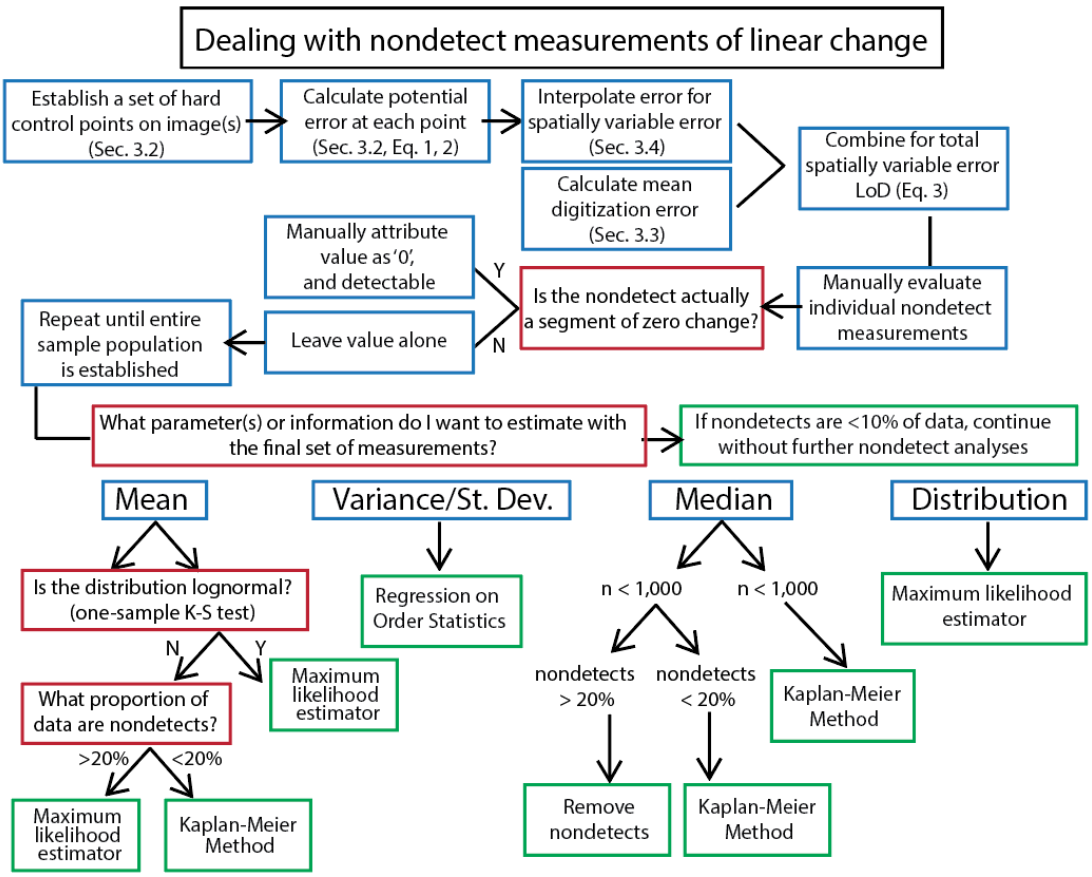

Fig. 2-13. A flow chart illustrating how to handle nondetect measurements, from start to finish.

uncertainty in boundary delineations derived from aerial images. This body of research grew throughout the following decade to describe how to estimate uncertainty and levels of detection (LoDs) using traditional methods of error propagation (Edwards & Lowell, 1996; Kiiveri, 1997; Crosetto & Tarantola, 2001). Subsequent research quantified how specific variables influence uncertainty (D. A. Gaeuman et al., 2003; Nelson et al., 2013;Güneralp et al., 2013, 2014; Liro, 2015). Meanwhile, other fields and researchers were identifying appropriate methods for handling nondetect measurements below LoD thresholds (Shumway, Azari, & Kayhanian, 2002; Martín-Fernández et al., 2003; Helsel, 2006; Lee & Helsel, 2005). Unfortunately, a disconnect remains between these

developments and the application within earth-science research (Lea and Legleiter, 2016; Donovan & Belmont, 2019). Herein, we have collected, summarized, and tested methodological and applied research relevant to calculations of planform changes derived from remotely-sensed imagery. The subsequent paragraphs provide a comprehensive framework including both general guidance and specific factors to consider when evaluating uncertainty in planform change measurements.

Our use of 441 images spanning 8 decades and encompassing multiple riparian conditions, geomorphic environments, and a wide array of resolutions and image quality (e.g., grayscale and color) allow us to provide a general framework for handling uncertainty that is broadly applicable to rivers of varying scale, geomorphology, and river pattern. Nonetheless, we recognize the need to include considerations and caveats for our specific analyses, which stem from a single threaded meandering river (Root River, MN) spanning widths of 30-80 meters. Many of these considerations are detailed in the background material, but are restated in the context of our results, below. While specific unforeseen considerations will vary with each application, the practices, conclusions, and recommendations for calculating and evaluating uncertainty are generally applicable to many remote sensing applications, including glacier retreat or advance, erosion or deposition along coastlines and lakeshores, changes in wetland extent, expansion or contraction of vegetation (e.g., deforestation), cliff retreat, and political boundary disputes. We encourage readers to consider their specific context, questions, and needs when applying our findings. To reconstruct the analyses conducted herein to explore their own datasets, we have made scripts are available as supplementary .R files. For example, our approach focuses on measuring change as a linear adjustment, but as

explained in the background, anabranching and braided channels exhibit complex planforms and adjustments may be better approximated by a volume, mass, or percent of erosion/deposition.

Surprisingly, inconsistencies in streambank delineations were generally not significantly greater for images of lower quality (resolution) or channel reaches with shadows and/or vegetation cover. Thus, a single, experienced user can be expected to have a similar degree of precision (i.e., consistency) regardless of image quality, shadows, and/or vegetation, at least for settings with a range of environments similar to those encountered along our 120 km stretch of the Root River. Arbitrary inconsistency in user-defined delineations dominate delineation uncertainty, but we expect that image quality will dominate delineation uncertainty when pixel size exceeds the resolution necessary for detecting the riparian-fluvial boundary (0.5 – 3.5 m^2 were used herein), such as in (Werbylo et al., 2017). Vegetation type, or an absence thereof, will also impact whether pixel resolution leads to more or less accurate delineations. Furthermore, pixel size may exceed or span the width of small tributaries and/or sufficiently narrow channels, which exacerbate the impact of small delineation offsets per channel width.

In cases where image quality weakens or invalidates delineations, field measurements or high-resolution topography should be used to verify or replace image-based river delineations. Locations along meander bends with various types of vegetation cover (e.g. thick vegetation, scattered brush, grass) exhibit the highest uncertainty due to ambiguity in which vegetated boundary to use. Future studies should explore how to incorporate spatially variable delineation uncertainty. Performing digitizations with a single user is optimal because it reduces digitization uncertainty by approximately 0.5

meters relative to multiple users, which has been shown to have a central tendency of ±2 meters (Micheli & Kirchner, 2002) and range up to ±37 meters (Werbylo et al., 2017). Specifying a standard for delineation will help reduce errors and biases in long-term monitoring of river channels and riparian conditions that rely on multiple users for manual delineations. We recommend delineating the vegetated boundary that best approximates bankfull width to avoid inconsistency along such reaches, whenever possible. Additional considerations may be necessary for delineations of braided or gravel-bed rivers that have less clear channel boundaries than typical meandering rivers (Winterbottom, 2000).

Our analyses of georeferencing uncertainty support previous research recommending the use of second-order polynomials to optimize the combination of retained measurements and reduced image warping. We found significant differences in georeferencing uncertainty for images predating the 1990s (Fig. 2-8), likely due to reduced image quality and fewer reliable control points to georeference. An absence of local and global autocorrelation for GCPs reinforced our other results, identifying the need for spatially variable LoDs (SV-LoD) because errors associated with GCPs were uncorrelated irrespective of the distance between them. Spatial autocorrelation for both delineation bias and measured migration rates were autocorrelated from 1-6 channel widths (50- to 400-meters). The scale of autocorrelation arising from coherent reaches of similar migration will likely vary with river size and are not directly transferrable to other systems. Thus, autocorrelation should be explored in future studies, and additional exploration may improve models of river meander migration.

Our analyses demonstrate how spatially-variable LoDs improve the quality of

retained measurements relative to a singular RMSE-based LoD for two reasons. First, SV-LoDs are able to detect and eliminate erroneous large-magnitude migration values (false-positives) that arise from georeferencing offset or image warping in cases where the local spatially variable uncertainty is equally large (Fig. 2-7). In contrast, RMSE-based LoDs retain such measurements simply due to their large magnitude. Second, SV-LoDs retain the abundance of small, but legitimate, channel adjustments that often fall below the RMSE LoD (Fig. 2-8). Thus, we recommend the use of a SV-LoD in order to more accurately quantify uncertainty, as well as improve the quantity and quality of retained measurements. Currently, using the Planform Statistics Toolbox (Lauer and Parker, 2008) in combination with Lea and Legleiter's (2016) Matlab script quantifying spatially variable error provides an accurate, efficient, and nearly seamless means to quantify linear river migration and spatially variable uncertainty. For braided and/or anabranching channels, or rivers with many permanent vegetated islands, polygonal (area-based) methods of quantifying changes and associated spatially variable estimates (D. Gaeuman, Symanzik, et al., 2005) may be more suitable.

After applying a LoD threshold for parsing significant and nondetect measurements, a few approaches may be appropriate for handling nondetects, contingent upon expert knowledge and scope/goals of the research (Fig. 2-12). In both linear and areal measurements of channel change, observations of 'zero' or nearly-zero change are generally flagged as 'nondetects', despite the possibility that no change actually occurred. In such cases, we recommend using expert discretion to discern if these measurements qualify as 'significant' measurements of zero, or nearly zero, change. Because the majority of river channels exhibit negligible adjustments between two photos, this

exercise is likely to improve the accuracy of the final data distribution, as it reduces the odds of erroneously filtering measurements of real geomorphic change (Anderson, 2018). This recommendation is not justification for determining the significance of any/all measurements, but merely for evaluating nondetect measurements along known stagnant reaches. We evaluated the ability of three new approaches (i.e., Kaplan-Meier, Regression on Order Statistics, and Maximum Likelihood Estimation) to estimate statistical parameters (mean, median, standard deviation, and distribution fit) for modelled distributions with known proportions of nondetects (Table 2-3). MLE and K-M consistently perform well for approximating the mean of raw data at small measurement sample sizes (n = 100). However, at sample sizes > 1000, MLE will best approximate the mean. ROS will perform best for estimating the variance at all sample sizes and exhibits improvements in median estimates as sample size increases. KM is consistently the most robust in its overall distribution fit. The specific approach chosen for handling nondetects remains contingent upon each case, but should be guided and informed by the descriptions of each method and their requirements (Section 2.3.5), references to external resources, and results of our analyses.

Herein, we provided a comprehensive summary and evaluation of research on uncertainty as applied to studies of river planform change. Decades of research have built our understanding of uncertainty in remotely-sensed data, and will undoubtedly continue to be refined with improved technologies, software, statistical approaches, and most importantly, critical thinking. Future work should aim to improve upon the guidance provided herein to improve accuracy and uncertainty in measurements of fluvial change. There has been little consensus on applying knowledge gleaned from over two decades of

research on identifying and quantifying uncertainty. This likely reflects the complicated nature of calculating uncertainty, the variety of tools (and thus, output formats) used to evaluate planform change, and in some cases, the absence of uncertainty estimates. Thus, we encourage improving the simplicity, generalizability, and open-source opportunities of tools and packages used for calculating planform change and associated uncertainty, thereby enabling a common platform to measure and compare results.

References

Aalto, R., Lauer, J.W., Dietrich, W.E., 2008. Spatial and temporal dynamics of sediment accumulation and exchange along Strickland River floodplains (Papua New Guinea) over decadal-to-centennial timescales. Journal of Geophysical Research 113. https://doi.org/10.1029/2006JF000627

Allmendinger, N.E., Pizzuto, J.E., Moglen, G.E., Lewicki, M., 2007. A sediment budget for an urbanizing watershed, 1951-1996, Montgomery County, Maryland, U.S.A. Journal of the American Water Resources Association 43, 1483–1498.

Anders, F.J., Byrnes, M., 1991. Accuracy of shoreline change rates as determined from maps and aerial photographs. Shore and Beach 59, 17–26.

Anderson, S., 2018. Uncertainty in quantitative analyses of topographic change: Error propagation and the role of thresholding: Uncertainty in repeat topographic analyses. Earth Surface Processes and Landforms. https://doi.org/10.1002/esp.4551

Bailey, R.G., 1988. Problems with using overlay mapping for planning and their implications for geographic information systems. Environmental Management 12, 11–17. https://doi.org/10.1007/BF01867373

Baki, A.B.M., Gan, T.Y., 2012. Riverbank migration and island dynamics of the braided Jamuna River of the Ganges–Brahmaputra basin using multi-temporal Landsat images. Quaternary International 263, 148–161. https://doi.org/10.1016/j.quaint.2012.03.016

Bangen, S., Hensleigh, J., McHugh, P., Wheaton, J., 2016. Error modeling of DEMs from topographic surveys of rivers using fuzzy inference systems. Water Resources Research 52, 1176–1193. https://doi.org/10.1002/2015WR018299

Belmont, P., Gran, K.B., Schottler, S.P., Wilcock, P.R., Day, S.S., Jennings, C., Lauer, J.W., Viparelli, E., Willenbring, J.K., Engstrom, D.R., Parker, G., 2011. Large shift in source of fine sediment in the Upper Mississippi River. Environmental Science & Technology 45, 8804–8810. https://doi.org/10.1021/es2019109

Benjamini, Y., Hochberg, Y., 1995. Controlling the False Discovery Rate: A Practical and Powerful Approach to Multiple Testing. Journal of the Royal Statistical Society. Series B (Methodological) 57, 289–300.

Bjerklie, D.M., Moller, D., Smith, L.C., Dingman, S.L., 2005. Estimating discharge in rivers using remotely sensed hydraulic information. Journal of Hydrology 309, 191–209. https://doi.org/10.1016/j.jhydrol.2004.11.022

Blundell, B., J.S., Opitz, D.W., 2006. Object recognition and feature extraction from imagery: The Feature Analyst® approach (2006), in: ISPRS Proceedings. Presented at the International Conference on Object-based Image Analysis (OBIA 2006), Salzburg Unversity, Austria.

Brasington, J., Langham, J., Rumsby, B., 2003. Methodological sensitivity of morphometric estimates of coarse fluvial sediment transport. Geomorphology 53, 299–316. https://doi.org/10.1016/S0169-555X(02)00320-3

Chrisman, N.R., 1987. The accuracy of map overlays: A reassessment. Landscape and Urban Planning 14, 427–439. https://doi.org/10.1016/0169-2046(87)90054-5

Clarke, T.A., Fryer, J.G., 1998. The Development of Camera Calibration Methods and Models. The Photogrammetric Record 16, 51–66. https://doi.org/10.1111/0031-868X.00113

Constantine, J.A., Dunne, T., Ahmed, J., Legleiter, C., Lazarus, E.D., 2014. Sediment supply as a driver of river meandering and floodplain evolution in the Amazon Basin. Nature Geoscience 7, 899–903. https://doi.org/10.1038/ngeo2282

Crosetto, M., Tarantola, S., 2001. Uncertainty and sensitivity analysis: tools for GIS-based model implementation. International Journal of Geographical Information Science 15, 415–437. https://doi.org/10.1080/13658810110053125

Dean, D.J., Schmidt, J.C., 2011. The role of feedback mechanisms in historic channel changes of the lower Rio Grande in the Big Bend region. Geomorphology 126, 333–349. https://doi.org/10.1016/j.geomorph.2010.03.009

Donovan, M., Belmont, P., 2019. Timescale Dependence in River Channel Migration Measurements. Earth Surface Processes and Landforms. https://doi.org/10.1002/esp.4590

Donovan, M., Miller, A., Baker, M., 2016. Reassessing the role of milldams in Piedmont floodplain development and remobilization. Geomorphology 268, 133–145. https://doi.org/10.1016/j.geomorph.2016.06.007

Donovan, M., Miller, A., Baker, M., Gellis, A., 2015. Sediment contributions from floodplains and legacy sediments to Piedmont streams of Baltimore County, Maryland. Geomorphology 235, 88–105. https://doi.org/10.1016/j.geomorph.2015.01.025

Downs, P.W., Dusterhoff, S.R., Sears, W.A., 2013. Reach-scale channel sensitivity to multiple human activities and natural events: Lower Santa Clara River, California, USA. Geomorphology 189, 121–134. https://doi.org/10.1016/j.geomorph.2013.01.023

Downward, S.R., Gurnell, A.M., Brookes, A., 1994. A methodology for quantifying river channel planform change using GIS. IAHS Publication, Proceedings of the Canberra Symposium 224, 449–456.

Draut, A.E., Logan, J.B., McCoy, R.E., McHenry, M., Warrick, J.A., 2008. Channel Evolution on the Lower Elwha River, Washington, 1939-2006 (Report No. 2008–5127), Scientific Investigations Report. U.S. Geological Survey, Washington.

Edwards, G., Lowell, K.E., 1996. Modeling uncertainty in photointerpreted boundaries. Photogrammetric Engineering and Remote Sensing 62, 377–390.

Fay, M.P., Proschan, M.A., 2010. Wilcoxon-Mann-Whitney or t-test? On assumptions for hypothesis tests and multiple interpretations of decision rules. Statistics Surveys 4, 1–39. https://doi.org/10.1214/09-SS051

Fisher, G.B., Bookhagen, B., Amos, C.B., 2013. Channel planform geometry and slopes from freely available high-spatial resolution imagery and DEM fusion: Implications for channel width scalings, erosion proxies, and fluvial signatures in tectonically active landscapes. Geomorphology 194, 46–56. https://doi.org/10.1016/j.geomorph.2013.04.011

Fraley, L.M., Miller, A.J., Welty, C., 2009. Contribution of in-channel processes to sediment yield of an urbanizing watershed. JAWRA Journal of the American Water Resources Association 45, 748–766. https://doi.org/10.1111/j.1752-1688.2009.00320.x

Fryer, J.G., Brown, D.C., 1986. Lens distortion for close-range photogrammetry. Photogrammetric Engineering and Remote Sensing 52, 51–58.

Gaeuman, D., Schmidt, J.C., Wilcock, P.R., 2005a. Complex channel responses to changes in stream flow and sediment supply on the lower Duchesne River, Utah. Geomorphology 64, 185–206. https://doi.org/10.1016/j.geomorph.2004.06.007

Gaeuman, D., Symanzik, J., Schmidt, J.C., 2005b. A Map Overlay Error Model Based on Boundary Geometry. Geographical Analysis 37, 350–369. https://doi.org/10.1111/j.1538-4632.2005.00585.x

Gaeuman, D.A., Schmidt, J.C., Wilcock, P.R., 2003. Evaluation of in-channel gravel storage with morphology-based gravel budgets developed from planimetric data. Journal of Geophysical Research: Earth Surface 108, n/a-n/a. https://doi.org/10.1029/2002JF000002

Geary, R.C., 1954. The Contiguity Ratio and Statistical Mapping. The Incorporated Statistician 5, 115. https://doi.org/10.2307/2986645

Güneralp, İ., Filippi, A.M., Hales, B., 2014. Influence of river channel morphology and bank characteristics on water surface boundary delineation using high-resolution passive remote sensing and template matching. Earth Surface Processes and Landforms 39, 977–986. https://doi.org/10.1002/esp.3560

Güneralp, İ., Filippi, A.M., Hales, B.U., 2013. River-flow boundary delineation from digital aerial photography and ancillary images using support vector machines. GIScience & remote sensing 50, 1–25.

Güneralp, İ., Rhoads, B.L., 2008. Continuous Characterization of the Planform Geometry and Curvature of Meandering Rivers: Planform Geometry and Curvature of Meandering Rivers. Geographical Analysis 40, 1–25. https://doi.org/10.1111/j.0016-7363.2007.00711.x

Gurnell, A.M., Downward, S.R., Jones, R., 1994. Channel planform change on the river dee meanders, 1876–1992. Regulated Rivers: Research & Management 9, 187–204. https://doi.org/10.1002/rrr.3450090402

Harpold, A.A., Marshall, J.A., Lyon, S.W., Barnhart, T.B., Fisher, B., Donovan, M., Brubaker, K.M., Crosby, C.J., Glenn, N.F., Glennie, C.L., Kirchner, P.B., Lam, N., Mankoff, K.D., McCreight, J.L., Molotch, N.P., Musselman, K.N., Pelletier, J., Russo, T., Sangireddy, H., Sjöberg, Y., Swetnam, T., West, N., 2015. Laser vision: lidar as a transformative tool to advance critical zone science. Hydrology and Earth System Sciences Discussions 12, 1017–1058. https://doi.org/10.5194/hessd-12-1017-2015

Helsel, D.R., 2006. Fabricating data: How substituting values for nondetects can ruin results, and what can be done about it. Chemosphere 65, 2434–2439. https://doi.org/10.1016/j.chemosphere.2006.04.051

Helsel, D.R., 2005. More Than Obvious: Better Methods for Interpreting Nondetect Data. Environmental Science & Technology 39, 419A-423A. https://doi.org/10.1021/es053368a

Hickin, E., Nanson, G., 1984. Lateral Migration Rates of River Bends. J. Hydraul. Eng. 110, 1557–1567. https://doi.org/10.1061/(ASCE)0733-9429(1984)110:11(1557)

Hooke, J.M., 1980. Magnitude and distribution of rates of river bank erosion. Earth Surface Processes 5, 143–157. https://doi.org/10.1002/esp.3760050205

Hosmer, D.W., Lemeshow, S., May, S., 2008. Applied Survival Analysis: Regression Modeling of Time-to-Event Data, Wiley Series in Probability and Statistics. John Wiley & Sons, Inc., Hoboken, NJ, USA. https://doi.org/10.1002/9780470258019

Hossain, M.A., Gan, T.Y., Baki, A.B.M., 2013. Assessing morphological changes of the Ganges River using satellite images. Quaternary International 304, 142–155. https://doi.org/10.1016/j.quaint.2013.03.028

Hughes, M.L., McDowell, P.F., Marcus, W.A., 2006. Accuracy assessment of georectified aerial photographs: Implications for measuring lateral channel movement in a GIS. Geomorphology 74, 1–16. https://doi.org/10.1016/j.geomorph.2005.07.001

Huston, C., Juarez-Colunga, E., 2009. Guidelines for computing summary statistics for data-sets containing non-detects, Statistical Guidance. Department of Statistics and Actuarial Science, Simon Fraser University, British Columbia, CA.

ITRC, 2013. Groundwater Statistics and Monitoring Compliance, Statistical Tools for the Project Life Cycle. ITRC, Nondetects 5.7.

Kelly, S., Belmont, P., 2018. High Resolution Monitoring of River Bluff Erosion Reveals Failure Mechanisms and Geomorphically Effective Flows. Water 10, 394. https://doi.org/10.3390/w10040394

Kiiveri, H.T., 1997. Assessing, representing and transmitting positional uncertainty in maps. International Journal of Geographical Information Science 11, 33–52. https://doi.org/10.1080/136588197242482

Ladd, G.B., Nagchaudhuri, A., Earl, T.J., Mitra, M., Bland, G.L., 2006. Rectification, Georeferencing, and Mosaicking of Images Acquired with Remotely Operated Aerial Platforms. Presented at the ASPRS 2006 Annual Conference, ASPRS, Reno, NV, p. 10.

Lauer, J.W., 2007. Channel Planform Statistics Toolbox. National Center for Earth-Surface Dynamics, University of Minnesota.

Lauer, J.W., Echterling, C., Lenhart, C., Belmont, P., Rausch, R., 2017. Air-photo based change in channel width in the Minnesota River basin: Modes of adjustment and implications for sediment budget. Geomorphology 297, 170–184. https://doi.org/10.1016/j.geomorph.2017.09.005

Lauer, J.W., Parker, G., 2008. Net local removal of floodplain sediment by river meander migration. Geomorphology 96, 123–149. https://doi.org/10.1016/j.geomorph.2007.08.003

Lawler, D.M., 1993. The measurement of river bank erosion and lateral channel change: a review. Earth Surface Processes and Landforms 18, 777–821.

Lea, D.M., Legleiter, C.J., 2016. Refining measurements of lateral channel movement from image time series by quantifying spatial variations in registration error. Geomorphology 258, 11–20. https://doi.org/10.1016/j.geomorph.2016.01.009

Lee, L., Helsel, D., 2005. Statistical analysis of water-quality data containing multiple detection limits: S-language software for regression on order statistics. Computers & Geosciences 31, 1241–1248. https://doi.org/10.1016/j.cageo.2005.03.012

Legleiter, C.J., Kyriakidis, P.C., 2007. Forward and Inverse Transformations between Cartesian and Channel-fitted Coordinate Systems for Meandering Rivers. Mathematical Geology 38, 927–958. https://doi.org/10.1007/s11004-006-9056-6

Libby, D., J., Larson, P.H., Howell, D.W., Aeikens, A.L., Scheeler, D.J., Millett, J.J., Williams, V.A., Hilgendorf, Z., Chadwick-Camp, M., 2016. Assessing Error and Uncertainty in Remote Analysis of Channel Change Dynamics and Morphology. Case Study: Minnesota River, Minnesota, USA.

Liro, M., 2015. Estimation of the impact of the aerialphoto scale and the measurement scale on the error in digitization of a river bank. Zeitschrift für Geomorphologie 59, 443–453. https://doi.org/10.1127/zfg/2014/0164

Martín-Fernández, J.A., Barceló-Vidal, C., Pawlowsky-Glahn, V., 2003. Dealing with Zeros and Missing Values in Compositional Data Sets Using Nonparametric Imputation. Mathematical Geology 35, 253–278. https://doi.org/10.1023/A:1023866030544

Massey, F.J., Jr., 1951. The Kolmogorov-Smirnov Test for Goodness of Fit. Journal of the American Statistical Association 46, 68–78. https://doi.org/10.2307/2280095

McMillan, M., Hu, Z., 2017. A watershed scale spatially-distributed model for streambank erosion rate driven by channel curvature. Geomorphology. https://doi.org/10.1016/j.geomorph.2017.03.017

Melville, J.K., Martz, L.W., 2004. A Comparison of Data Sources for Manual and Automated Hydrographical Network Delineation. Canadian Water Resources Journal 29, 267–282. https://doi.org/10.4296/cwrj267

Micheli, E.R., Kirchner, J.W., 2002. Effects of wet meadow riparian vegetation on streambank erosion. 1. Remote sensing measurements of streambank migration

and erodibility. Earth Surface Processes and Landforms 27, 627–639. https://doi.org/10.1002/esp.338

Micheli, E.R., Kirchner, J.W., Larsen, E.W., 2004. Quantifying the effect of riparian forest versus agricultural vegetation on river meander migration rates, central Sacramento River, California, USA. River Research and Applications 20, 537–548. https://doi.org/10.1002/rra.756

Miller, J.R., Friedman, J.M., 2009. Influence of flow variability on floodplain formation and destruction, Little Missouri River, North Dakota. Geological Society of America Bulletin 121, 752–759. https://doi.org/10.1130/B26355.1

Morais, E.S., Rocha, P.C., Hooke, J., 2016. Spatiotemporal variations in channel changes caused by cumulative factors in a meandering river: The lower Peixe River, Brazil. Geomorphology 273, 348–360. https://doi.org/10.1016/j.geomorph.2016.07.026

Mount, N., Louis, J., 2005. Estimation and propagation of error in measurements of river channel movement from aerial imagery. Earth Surface Processes and Landforms 30, 635–643. https://doi.org/10.1002/esp.1172

Mount, N.., Louis, J., Teeuw, R.., Zukowskyj, P.., Stott, T., 2003. Estimation of error in bankfull width comparisons from temporally sequenced raw and corrected aerial photographs. Geomorphology 56, 65–77. https://doi.org/10.1016/S0169-555X(03)00046-1

Mount, N.J., Tate, N.J., Sarker, M.H., Thorne, C.R., 2013. Evolutionary, multi-scale analysis of river bank line retreat using continuous wavelet transforms: Jamuna River, Bangladesh. Geomorphology 183, 82–95. https://doi.org/10.1016/j.geomorph.2012.07.017

Nelson, N.C., Erwin, S.O., Schmidt, J.C., 2013. Spatial and temporal patterns in channel change on the Snake River downstream from Jackson Lake dam, Wyoming. Geomorphology 200, 132–142. https://doi.org/10.1016/j.geomorph.2013.03.019

Osterkamp, W.R., Hedman, E.R., 1982. Perennial-streamflow characteristics related to channel geometry and sediment in Missouri River basin (Report No. 1242), Professional Paper.

Passalacqua, P., Belmont, P., Staley, D.M., Simley, J.D., Arrowsmith, J.R., Bode, C.A., Crosby, C., DeLong, S.B., Glenn, N.F., Kelly, S.A., Lague, D., Sangireddy, H., Schaffrath, K., Tarboton, D.G., Wasklewicz, T., Wheaton, J.M., 2015. Analyzing high resolution topography for advancing the understanding of mass and energy transfer through landscapes: A review. Earth-Science Reviews 148, 174–193. https://doi.org/10.1016/j.earscirev.2015.05.012

Pavelsky, T.M., Smith, L.C., 2008. RivWidth: A Software Tool for the Calculation of River Widths From Remotely Sensed Imagery. IEEE Geoscience and Remote Sensing Letters 5, 70–73. https://doi.org/10.1109/LGRS.2007.908305

Peixoto, J.M.A., Nelson, B.W., Wittmann, F., 2009. Spatial and temporal dynamics of river channel migration and vegetation in central Amazonian white-water floodplains by remote-sensing techniques. Remote Sensing of Environment 113, 2258–2266. https://doi.org/10.1016/j.rse.2009.06.015

Piégay, H., Cuaz, M., Javelle, E., Mandier, P., 1997. Bank erosion management based on geomorphological, ecological and economic criteria on the Galaure River, France. Regulated Rivers: Research & Management 13, 433–448. https://doi.org/10.1002/(SICI)1099-1646(199709/10)13:5<433::AID-RRR467>3.0.CO;2-L

Piégay, H., Darby, S.E., Mosselman, E., Surian, N., 2005. A review of techniques available for delimiting the erodible river corridor: a sustainable approach to managing bank erosion. River Research and Applications 21, 773–789. https://doi.org/10.1002/rra.881

Rhoades, E.L., O'Neal, M.A., Pizzuto, J.E., 2009. Quantifying bank erosion on the South River from 1937 to 2005, and its importance in assessing Hg contamination. Applied Geography 29, 125–134. https://doi.org/10.1016/j.apgeog.2008.08.005

Rowland, J.C., Shelef, E., Pope, P.A., Muss, J., Gangodagamage, C., Brumby, S.P., Wilson, C.J., 2016. A morphology independent methodology for quantifying planview river change and characteristics from remotely sensed imagery. Remote Sensing of Environment 184, 212–228. https://doi.org/10.1016/j.rse.2016.07.005

Schaffrath, K.R., Belmont, P., Wheaton, J.M., 2015. Landscape-scale geomorphic change detection: Quantifying spatially variable uncertainty and circumventing legacy data issues. Geomorphology 250, 334–348. https://doi.org/10.1016/j.geomorph.2015.09.020

Schook, D.M., Rathburn, S.L., Friedman, J.M., Wolf, J.M., 2017. A 184-year record of river meander migration from tree rings, aerial imagery, and cross sections. Geomorphology 293, 227–239. https://doi.org/10.1016/j.geomorph.2017.06.001

Schwenk, J., Khandelwal, A., Fratkin, M., Kumar, V., Foufoula-Georgiou, E., 2017. High spatiotemporal resolution of river planform dynamics from Landsat: The RivMAP toolbox and results from the Ucayali River: Annual Planform Morphodynamics, Ucayali. Earth and Space Science 4, 46–75. https://doi.org/10.1002/2016EA000196

Shields, F.D., Simon, A., Steffen, L.J., 2000. Reservoir effects on downstream river channel migration. Environmental Conservation 27, 54–66.

Shumway, R.H., Azari, R.S., Kayhanian, M., 2002. Statistical Approaches to Estimating Mean Water Quality Concentrations with Detection Limits. Environmental Science & Technology 36, 3345–3353. https://doi.org/10.1021/es0111129

Singh, A., Nocerino, J., 2002. Robust estimation of mean and variance using environmental data sets with below detection limit observations. Chemometrics and Intelligent Laboratory Systems 60, 69–86. https://doi.org/10.1016/S0169-7439(01)00186-1

Smith, L.C., Pavelsky, T.M., 2008. Estimation of river discharge, propagation speed, and hydraulic geometry from space: Lena River, Siberia: RIVER DISCHARGE AND HYDRAULIC GEOMETRY. Water Resources Research 44. https://doi.org/10.1029/2007WR006133

Smith, S., Belmont, P., Wilcock, P.R., 2011. Closing the gap between watershed modeling, sediment budgeting, and stream restoration, in: Simon, A., Bennett, S.J., Castro, J.M. (Eds.), Geophysical Monograph Series, Stream Restoration in Dynamic Fluvial Systems: Scientific Approaches, Analyses, and Tools. American Geophysical Union, Washington, D. C., pp. 293–317.

Souffront, M., 2014. Channel Adjustment and Channel-Floodplain Sediment Exchange in the Root River, Southeastern Minnesota (M.S. Thesis). Utah State University, Logan, Utah.

Spiekermann, R., Betts, H., Dymond, J., Basher, L., 2017. Volumetric measurement of river bank erosion from sequential historical aerial photography. Geomorphology 296, 193–208. https://doi.org/10.1016/j.geomorph.2017.08.047

Swanson, B.J., Meyer, G.A., Coonrod, J.E., 2011. Historical channel narrowing along the Rio Grande near Albuquerque, New Mexico in response to peak discharge reductions and engineering: magnitude and uncertainty of change from air photo measurements. Earth Surface Processes and Landforms 36, 885–900. https://doi.org/10.1002/esp.2119

Sylvester, Z., Durkin, P., Covault, J.A., 2019. High curvatures drive river meandering. Geology 47, 263–266. https://doi.org/10.1130/G45608.1

Tauber, F., 1999. Spurious Clusters in Granulometric Data Caused by Logratio Transformation. Mathematical Geology 31, 491–504. https://doi.org/10.1023/A:1007532222145

Unwin, D.J., 1995. Geographical information systems and the problem of “error and uncertainty.” Progress in Human Geography 19, 549–558. https://doi.org/10.1177/030913259501900408

USDA FSA APFO, 2015. National Agricultural Imagery Program (NAIP), Minnesota, 2015, Digital Orthorectified Images (DOQ).

Vericat, D., Wheaton, J.M., Brasington, J., 2017. Revisiting the Morphological Approach: Opportunities and Challenges with Repeat High-Resolution Topography, in: Tsutsumi, D., Laronne, J. (Eds.), Gravel-Bed Rivers: Processes and Disasters, Gravel Bed Rivers. John Wiley and Sons Ltd., pp. 121–155.

Ward, J.V., Tockner, K., Arscott, D.B., Claret, C., 2002. Riverine landscape diversity. Freshwater Biology 47, 517–539. https://doi.org/10.1046/j.1365-2427.2002.00893.x

Werbylo, K.L., Farnsworth, J.M., Baasch, D.M., Farrell, P.D., 2017. Investigating the accuracy of photointerpreted unvegetated channel widths in a braided river system: a Platte River case study. Geomorphology 278, 163–170. https://doi.org/10.1016/j.geomorph.2016.11.003

Wheaton, J.M., Brasington, J., Darby, S.E., Sear, D.A., 2010. Accounting for uncertainty in DEMs from repeat topographic surveys: Improved sediment budgets. Earth Surface Processes and Landforms 35, 136–156. https://doi.org/10.1002/esp.1886

Winterbottom, S.J., 2000. Medium and short-term channel planform changes on the Rivers Tay and Tummel, Scotland. Geomorphology 34, 195–208. https://doi.org/10.1016/S0169-555X(00)00007-6

CHAPTER 3

TIMESCALE DEPENDENCE IN RIVER CHANNEL MIGRATION MEASUREMENTS

1. Introduction

1.1. Fundamental concepts and motivations

Measuring river meander migration rates from historical aerial images is useful for developing a predictive understanding of channel and floodplain evolution (Lauer and Parker, 2008; Crosato, 2009; Braudrick et al., 2009; Parker et al., 2011), bedrock incision and strath terrace formation (Constantine et al., 2009; Finnegan and Dietrich, 2011; Motta et al., 2012; Gran et al., 2013), as well as providing constraints for sediment budgets (Trimble, 1983; Reid and Dunne, 2005; Belmont et al., 2011) and bank erosion models (Larsen et al., 2006; Motta et al., 2012). Historical meander migration rates are also used to study if, and to what extent, channel migration rates have changed over time. Rivers respond to climate and land use changes via nonlinear adjustments to channel, width, depth, planform pattern, vertical incision or aggradation, and lateral migration (Nanson and Hickin, 1983; Simon, 1989; Gaeuman et al., 2005; Swanson et al., 2011; Toone et al., 2014; Larsen et al., 2006; Call et al., 2017). Ultimately, channel adjustments shape fluvial and riparian habitats and may pose risks for nearby human infrastructure (Wente, 2000; Allan, 2004). Accurate measurements of migration rates are essential for advancing our understanding of river adjustment across a range of spatial and temporal scales.

Increased availability of historical and contemporary landscape-scale data (e.g., aerial photographs and high-resolution topography, HRT) have improved the accuracy

and precision of channel migration measurements over short (<1 year) and long (> 50 years) timescales, and thus interpretations of fluvial patterns, processes and trends (Lindsay and Ashmore, 2002; Ghoshal et al., 2010; Donovan et al., 2015; Passalacqua et al., 2015). However, timescale dependence of process rate measurements, often referred to as 'Sadler effects' (Sadler, 1981), may bias interpretations and hinder attempts to untangle the complexity of river responses to changing climate and land use conditions (Gurnell et al., 1994; Larsen et al., 2006; Micheli and Larsen, 2011; Schook et al., 2017). We use 'timescale dependence', rather than 'Sadler effects', because channel migration and accompanying measurements occur over much shorter timescales than geologic phenomena, and are affected by factors other than those discussed by Sadler (1981).

Timescale dependence has been demonstrated for a multitude of unsteady processes, including sediment accumulation, aggradation, progradation, and degradation (Sadler, 1981; Gardner et al., 1987; Lindsay and Ashmore, 2002; Kessler et al., 2013; Sadler and Jerolmack, 2015), river incision (Finnegan et al., 2014; Gallen et al., 2015), mountain erosion (Kirchner et al., 2001), cliff erosion (Cambers, 1976), and slope adjustments (Penning-Rowsell and Townshend, 1978). Spatially averaged (mean) erosion rates such as sediment yield appear to be independent of measurement timescale because they integrate across local extents of erosion and deposition (Sadler and Jerolmack, 2015; Ganti et al., 2016). While research has compared short-term erosion pin measurements with long-term measurements derived from tree rings or aerial image comparisons (Hooke, 1980; Nanson and Hickin, 1983; Thorne, 1981), the potential for timescale to disproportionately affect short- and long-term measurements of river migration has not been addressed.

Process hiatuses (e.g., rapid change followed by periods of dormancy) and reversals (e.g., incision vs. aggradation) appear to be largely responsible for timescale dependence across a variety of unsteady processes (Sadler, 1981; Gardner et al., 1987; Finnegan et al., 2014; Sadler and Jerolmack, 2015). In the case of channel migration, both factors likely influence measurement-scale dependence, with reversals defined as episodes of left vs. right migration, rather than incision vs. aggradation. Intuitively, channel reversals necessarily lead to underestimating the total/gross migration because observed/net migration approaches; with apparent rates approaching zero as the channel migrates back to the position in the initial photo. Highly confined channels with high sediment load may experience higher degrees of channel reversals as they 'bounce' off nearby valley walls more often than an unconfined channel with a wide meander belt.

In order to understand timescale dependency in channel migration measurements, we analyze empirical and synthetic datasets to address the following questions: Does timescale dependence exist for river migration measurements? If so, how does it affect our ability to accurately measure and compare changes in migration rates over time? What mechanisms cause measurement timescale dependence, and to what degree? Can timescale dependence and actual changes in channel migration be disentangled in order to determine if/when/where real changes in migration rates have occurred? We explore these questions using a statistical model as well as empirical data from the Root River, in southeastern Minnesota, USA. While we focus on channel migration measured from aerial images, our insights are applicable to process rates measured using other platforms, such as repeat topographic surveys, or HRT.

2. Study area and Data

We evaluate timescale dependence empirically using 12 sets of aerial photographs spanning 120 km of the Root River, Minnesota, a single-threaded, meandering sand- and gravel-bedded river that drains into the Mississippi River (Fig. 3-1). Images span 76 years (1937, 1947, 1953, 1976, 1981, 1991, 2003, 2006, 2008, 2010, 2011, and 2013). We selected the Root River because it exhibits three distinct geomorphic settings (Table 2-1) that provide an opportunity to explore differences in measurement-scale dependencies and channel migration patterns for each setting. These distinct geomorphic environments are relics of the Late Pleistocene and Holocene history of glaciation and base level changes and are characterized by different degrees of valley confinement, slope, and sinuosity (Souffront, 2014; Belmont et al., 2016a). While it is not the goal of this study to examine how changes in land use and flow affect migration rates, the

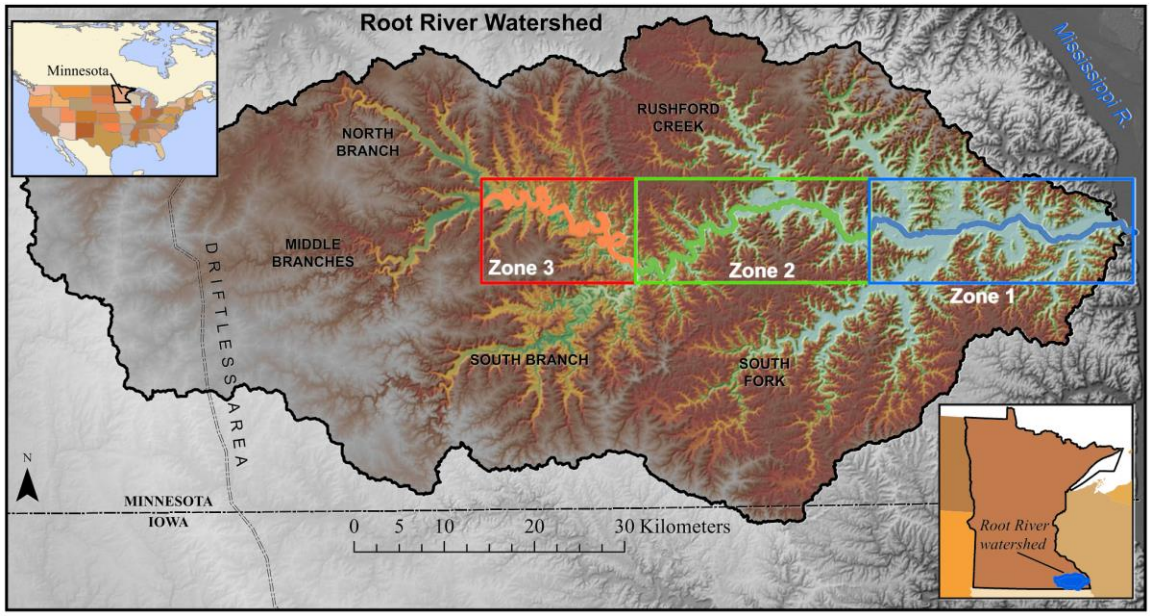

Fig. 3-1. The Root River watershed and three distinct geomorphic zones as defined by Souffront (2014). Each zone has a unique slope and degree of valley confinement. The extent of delineated river spans 120-km of river length, with Zones 3, 2, and 1 having lengths of 42, 38, and 32 km, respectively.

Table 3-1. Root River zones and morphological characteristics

Characteristic	Zone 3	Zone 2	Zone 1
Length (km)	46	47	34
Drainage area[a] (km^2)	160	301	431
Median channel width (m)	42	50	65
Median valley width (m)	261	683	1314
Sinuosity	1.10	1.23	1.04
Slope (m/m)	0.0010	0.0006	0.0005

[a]Farthest downstream point.

geomorphic setting provides useful context to interpret our results.

The 120 km study reach is partially within the so-called 'Driftless Area' of the upper Midwestern United States, which has been unglaciated for the past 500 kyr (Syverson and Colgan, 2004), but received glacial melt water and outwash from the glaciated western portion of the watershed following the Last Glacial Maximum (LGM). Deep valleys within the Driftless Area resulted from incision of the Mississippi River prior to the LGM (Baker et al., 1998; Knox, 2006). These alluvial valleys are surrounded by rolling uplands that are largely forested in steeper areas (> 10°) of the watershed, with corn and soybean farming on gently sloping areas. Row crops occupy approximately 75% of the watershed and are dominant throughout the previously glaciated western portion. Shallow karst underlies the majority of the Root River watershed, with typically less than 15 m of alluvial deposits overtop carbonate bedrock. Mainstem valleys and larger tributaries run across mantled karst with alluvial deposits exceeding 30 m.

While improved agricultural management in the 1940s reduced upland erosion from agricultural fields, the legacy of historical agricultural erosion still represents a significant sediment source in the form of large alluvial terrace and floodplain deposits along the modern Root River (Stout and Belmont, 2013; Stout et al., 2014; Belmont et al., 2016a). Historical milldams and small hydroelectric power dams exist along some

tributaries, as well as levees along the mainstem outlet along downstream reaches of Zone 3.

The Root River hydrologic regime has experienced significant increases in both low and high flows (80 and 60% increases, respectively) over the past 40 years resulting from enhanced artificial drainage of agricultural lands and increasing precipitation (Lenhart et al., 2011; Stout et al., 2014; Kelly et al., 2017). Changes in sediment loading over time have not been examined, although the land use history bears many similarities to the well-studied Coon Creek, directly across the Mississippi River (Trimble, 1999, 2009). The Root River watershed exhibits some of the steepest relationships between discharge (Q) and total suspended solids (TSS) throughout Minnesota (Vaughan et al., 2017), indicating the presence of considerable near-channel sediment sources that are highly vulnerable to erosion, especially under high flow conditions (Stout et al., 2014; Belmont et al., 2016a). Combining three distinct geomorphic settings with the spatially (120 km) and temporally (76 years) robust set of historical air photos provides an exemplary opportunity to explore timescale dependence of migration measurements along an alluvial river experiencing increased flow.

3. Methods

3.1. Measuring and evaluating temporal change

Approximately 2,880 km of streambanks were digitized from 12 sets of scanned georeferenced images (Souffront, 2014; M.S. Thesis) and used to interpolate channel centerlines for each year (1937, 1947, 1953, 1976, 1981, 1991, 2003, 2006, 2008, 2010, 2011, 2013). For every combination of two images (n = 66), curvature-driven cut-bank migration magnitude was measured at 10-meter increments along the channel centerlines

using the Planform Statistics Toolbox (Lauer, 2007; Lauer and Parker, 2008). We do not distinguish between cut-bank migration, down-valley translation, and/or bend expansion/contraction in our measurements, because results exhibit < 1% difference based on preliminary comparisons. Total migration was measured as distance between a node on the initial and terminal channel centerlines (Fig. 3-2). We manually identified and filtered out meander bend cutoffs for relevant measurements (i.e., affected image pairs) before performing subsequent analyses. Although the length of river filtered out as cutoffs increased with the measurement interval, the proportion of length filtered out was trivial compared to the entire 120 km study reach.

Because different geomorphic conditions can lead to unique channel responses (Montgomery, 1999), we binned migration rates into three distinct geomorphic zones previously classified by (Souffront, 2014) based primarily on slope and valley confinement (Fig. 3-1, Table 3-1). Lognormal distributions dominated our migration measurements, so we tested for significant increases in the medians, extremes, and distributions of each image pair using nonparametric statistics (Mann-Whitney Wilcoxon and Kolmogorov-Smirnov tests). We tested the alternative hypothesis that migration rates have increased with flow using one-tailed tests with alpha-values of 0.05 to ensure 95% confidence of avoiding a Type I error. Because 95% confidence levels can be excessive in water resource and environmental risk applications and are not always germane (Johnson, 1999; Belmont et al., 2016b), we also evaluated significance at alpha values of 0.1 and 0.2 (Appendix C, Table A1a & A1b).

Measurement intervals differed for image pairs between 2003-2013 ($\Delta t \sim$ 1-3 years) and those prior to 1991 ($\Delta t \sim$ 6-23 years), possibly confounding results. Thus, we

also compared pre-1991 rates with ensemble rates measured from 2003-2013 ($\Delta t = 10$, $n = 18$), providing the second line of evidence for whether migration rates have changed. In the case that fewer years exhibited differences after comparing migration measured over 2003-2013, timescale bias may have confounded or influenced inferences of channel response to hydrologic changes.

3.2. Measurement length-scale dependence

We computed and plotted correlograms of Geary's C (Geary, 1954) to quantify the lengths over which spatial measurement autocorrelation exists in our river migration data, which results from autocorrelation inherent in river migration as well as local-scale systematic delineation biases. Spatial autocorrelation generally persisted until 50-200 m length-scales, beyond which it was extremely weak to none (C-values > 0.8). Thus, we averaged migration rates over 400-meter increments to ensure autocorrelation did not compromise the validity of the statistical tests implemented. Nevertheless, we used a range of length scales above and below 400-meters to confirm that length scale had negligible effects on timescale dependency results. The Geary's C results informed our decision to model migration over 400-m increments. Specifically, knowing that migration rates are not autocorrelated at length scales longer than 400 m allows us to randomly sample the distributions of migration rates, which were derived from empirical data, without concern for spatial autocorrelation.

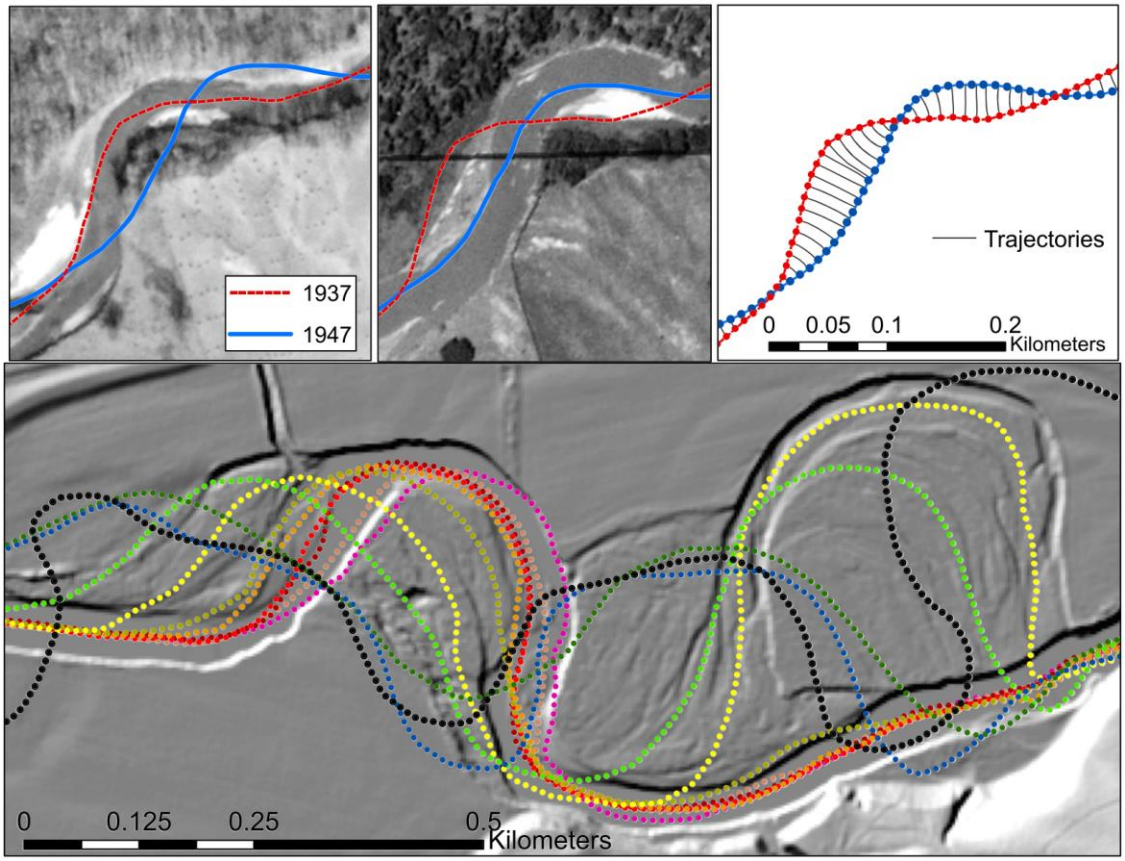

Fig. 3-2. Images depicting migration measurements as described in the text. Top left and center images show the 1937 and 1947 imagery, respectively, overlain by the channel centerlines. The top right image depicts 10-m increments at which the migration distance is calculated using the Planform Statistics Toolbox (Lauer, 2007). Bottom image illustrates 12 channel centerlines derived from the images spanning 1937–2013, with points at 10-m increments.

3.3. Quantifying uncertainty from georeferencing and digitization error

We quantified uncertainty as the sum of squares from spatially variable georeferencing uncertainty and uniform user delineation/digitization to estimate the minimum level of detection (LoD). Georeferencing uncertainty was calculated for at least 185 georeferenced control points (GCPs) for each year and interpolated to obtain uncertainty for each raster cell (Lea and Legleiter, 2016). Digitization uncertainty was estimated by comparing centerlines derived from 4-repeat streambank digitizations of the

same 11-km reach. We assigned values of zero to migration measurements below the minimum LoD (see flat portions, Fig. 3-4a – k).

3.4. Distinguishing timescale dependence

Following established methods for assessing timescale dependence (Gardner et al., 1987; Sadler and Jerolmack, 2015; Ganti et al., 2016), the mean channel migration (Δx, mean of all 400-m reaches) was plotted against the respective time interval (Δt, 1-76 years, $n = 66$) in log-log space (Fig. 3-5). Trends of $\log(\Delta x)$ over $\log(\Delta t)$ for each zone were compared to a 1:1 line visually and using an their 98% (3σ) confidence intervals to evaluate whether channel migration exhibited systematic bias with longer averaging time scales. Research assessing timescale dependence for timescales spanning multiple orders of magnitude (Gardner et al., 1987a; Sadler and Jerolmack, 2015; Ganti et al., 2016) compare mean adjustment (Δx) against the respective time interval (Δt) in log-log space with a 1:1 line. Significant deviations from the 1:1 line indicate a measurement-scale dependence, but can also reflect systematic shifts in rates over time. Because our aerial images span less than a century (76 years), and to avoid the possibility of confounding timescale dependence with systematic changes, we evaluate the process rate ($\Delta x/\Delta t$) over the time interval (Δt) on linear axes. We test whether systematic rate changes or sample bias are the source of observed timescale dependence by comparing historical and contemporary migration rates for a subset seven specific reaches (3-29 km, Appendix C, Fig. A3) having similar short measurement intervals ($\Delta t \leq 6$ years). This comparison used commensurate timescales and filled in our sample gap (i.e., historical data with short Δt), thereby providing an independent and unbiased third line of evidence indicating whether: 1) migration rates changed systematically over the period of study, and 2) observed

timescale dependence actually reflected a dearth of short-Δt measurements for historical data, rather than an actual change in migration rates. We further examined how sampling bias may affect timescale dependence using a statistical model (described later).

The overwhelming majority of past literature demonstrate that process reversals and hiatuses are mechanisms for causing timescale dependence and/or bias. We expected the Root River to have relatively low reversal rates due to its wide valley and meander belt. Nonetheless, we manually measured the length of channel that had reversed within the period of study to inform and support our statistical model that explores mechanisms of measurement bias. The criteria required that reversals be maintained for multiple years/images, ensuring exclusion of 'fake' reversals in the form of offset for single year due to georeferencing of digitization error. For this reason and due to the data structure, measuring reversal length by hand was necessary and allowed us to use our expert judgement that an automated classification would lack. In our evaluations, we omitted data after 1991 because the time intervals were too short to discern reversals from noise.

3.5. Discerning processes responsible for timescale dependence in channel migration

To explore the effects of hiatuses (e.g., rapid change followed by periods of dormancy) and reversals (migration opposite in direction to previous records) we developed a statistical model that simulates river migration and reversals, without involving unnecessary details regarding their underlying mechanisms. We developed the model to explore whether, and to what degree, migration hiatuses, channel reversals, and temporal shifts in migration rates affect migration measurement bias. To do so, we synthesized a 'complete' dataset representing annual migration measurements. Specifically, we generated 100-year synthetic annual migration rates for 100 reaches,

each 400-m in length. Rates were randomly selected from the range of lognormal distributions found in empirical data from the Root River with $\Delta t \leq 3$ years ($n_{years} = 7$, $n_{obs} = 2247$), including 0-values, which comprise 50 to 75% of the values. The model script randomly chose mean values from the entire range (0.31-1.42 m/yr) of empirical mean migration rates for years with $\Delta t \leq 3$ years and generated variance (σ) using an empirical linear relationship (Eq. 2; Appendix B, Fig. A2). For the initial year of the model, all migration rate values are positive, representing the rates of migration in either direction (i.e., right or left, the initial direction of movement of any given reach is irrelevant for our purposes). The model computed standard deviation based on the randomly selected average migration rate value using Eq. 2, because empirical data indicate that standard deviation varies directly, and significantly, as a function of the mean migration rate (Fig. 3-2).

$$\sigma = 0.36(\mu\left(\frac{\Delta x}{\Delta t}\right)) + 1.25 \quad (2)$$

Due to the high likelihood that the occurrence of channel reversals leads to underestimating measured migration rates, we evaluated the effect of reversal frequency using four model scenarios. In the absence of literature quantifying the temporal frequency or probability of channel reversals, we evaluated a range of plausible reversal frequencies (0%, 1%, 2%, 5%, and 10%), supported by observations for the Root River. The frequency of reversals explored in our model reflects a reasonable range of what we expect to occur in natural systems; reversal frequency varied from 1-6% across the definitive geomorphic zones of the Root River. Highest reversal frequency lie in the confined upper reaches and decreased downstream, which supports intuition that reversal

frequency is inversely related to valley width and our decision to model reversal frequencies from 1 to 10%. Reversal frequency was implemented by probabilistically reversing simulated migration (i.e., multiplying migration rates for individual reaches by -1) until the end of the 100-year model run, or until chance (1%, 2%, 5%, or 10%) reversed the 400-m segment back to its original direction (i.e., a positive value). The model tracked cumulative migration distance for each 400-m reach, and thus, negative values (i.e., reversals) reduced the modeled cumulative migration distance and rate. Similar to our analysis of empirical data, we calculated the mean for all 400-m segments to represent the ensemble mean annual river migration. We plotted all possible Δt combinations of average (mean) migration rate to evaluate how increasing reversal frequency affected timescale dependence.

In addition to hiatuses and reversals, systematic changes in migration rates may also cause trends in timescale dependence to diverge from a 1:1 relation, especially if recent photos dominate shorter timescales (Δt) and longer timescales are dominated by older photos acquired at lower frequencies. We conducted an additional set of model runs to explore the effect of older photo sets typically dominating longer timescales, coupled with the impacts of systematic changes in migration rates. We generated scenarios wherein contemporary migration rates (i.e., years 51-100) were increased and decreased by factors of 1.25, 2, 5, and 10 relative to historical rates (i.e., years 1-50, Fig. 3-3). These scenarios also had a 10% chance for channel reversals. Outputs from these eight scenarios of change allowed us to evaluate whether temporal changes in migration rates cause a false-positive timescale dependence, indicated by a shift/translation to the trends in Fig. 3-7a. We implemented a second test to verify or refute these results in which we

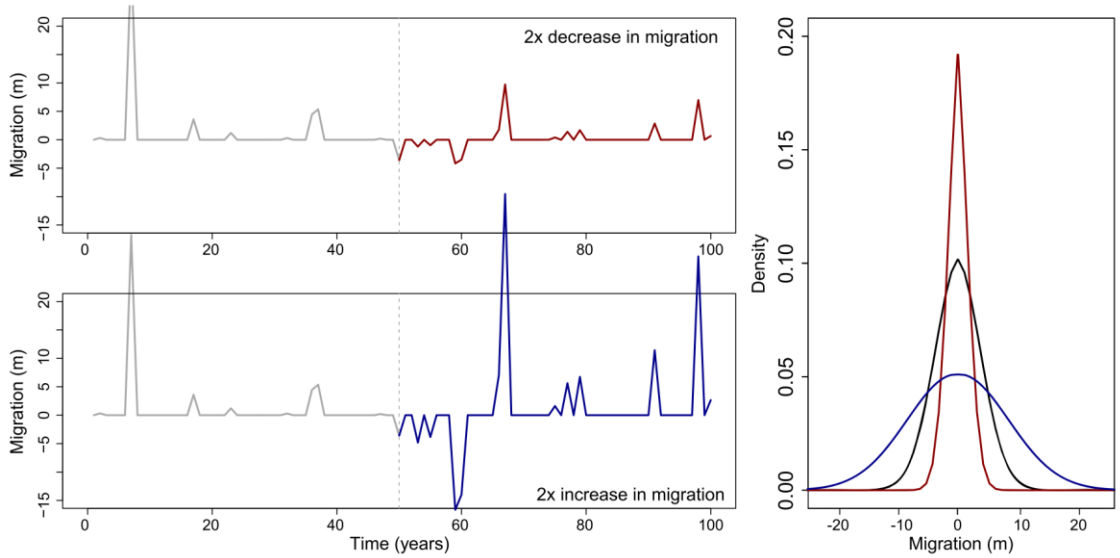

Fig. 3-3. Numerical simulations of annual migration for 100-years of a single 400-m reach. (Top) Red-colored 'modern' values are 50% less than the historical values from years 1–50. (Bottom) Blue-colored values (years 51-100) are double the historical rates rates from years 1-50.

compared the entire population of simulated migration measurements (n= 4950) to a sample of simulated measurements (n= 120) that reflected typical datasets having dominantly short Δt measurements from contemporary photos and long Δt measurements from historical photos (SI, Appendix D, Fig. A4).

4. Results and Discussion

4.1. Does timescale dependence exist for river migration measurements?

The entire 120 km dataset of migration rates for adjacent time intervals are illustrated in Fig. 3-4a-k, where channel cutoffs and measurements below the LoD are plotted as zeros. Measurements of mean channel migration exhibit a visual timescale dependence for each zone of the Root River (Fig. 3-5a). Loss of a record due to channel reversals would be similar to vertical reversals (e.g., sediment aggradation vs. erosion)

that cause bias in other measurements by erasing historical records (Sadler, 1981; Gardner et al., 1987b; Sadler and Jerolmack, 2015; Ganti et al., 2016). Reversals in migration direction (Fig. 3-6) occurred over 23 km (17%) of the Root River, and thus, were a possible mechanism underlying the timescale dependence. The percent and length of reversals declined from upstream to downstream reaches (66%, 32%, and 0.5% for Zones 3, 2, and 1, respectively), which is consistent with expectations because upstream reaches are exhibit higher migration rates and are confined within narrower valleys (Table 3-1). Post-hoc correlations and regressions showed a significant ($p < 0.001$, $r2 = 0.98$) indirect relationship between the frequency (length and percent) of reversals and valley width (Appendix A, Fig. A1). On the other hand, long-term rates may simply appear to have systematically low rates because our longer Δt values are dominated by historical air photos during periods when migration rates may simply have been slower. However, no systematic shifts were evident when comparing a subset of historical reaches ($n = 7$, 3-29 km, Appendix C, Fig. A3) with short measurement intervals ($\Delta t \leq 6$ years) to contemporary measurements with similar Δt. We further explore this possibility using a statistical model of migration.

4.2. How does timescale dependence vary with degrees of channel dormancy and reversals?

Numerical simulations using a statistical model allowed us to explore the role of channel dormancy and reversal frequency in migration measurements. When reversals were absent in modeled migration measurements, channel dormancy accounted for a very slight timescale dependence (~1% underestimate, Fig. 3-7). The degree of timescale dependence/bias increased with reversal probability/frequency- illustrated by decaying

cumulative migration rate (Δx/Δt) with increasing time interval (Δt). As reversals increase from 1% to 10%, migration distance and rate measured over 100 years are underestimated from 4% to nearly 30% relative to a channel with no reversals (Fig. 3-7). The bias decreases with measurement interval until gross migration is completely unbiased by reversals at Δt = 1. This finding suggests that decay in empirical migration rates with increasing measurement timescale (Fig. 3-5) may reflect measurements

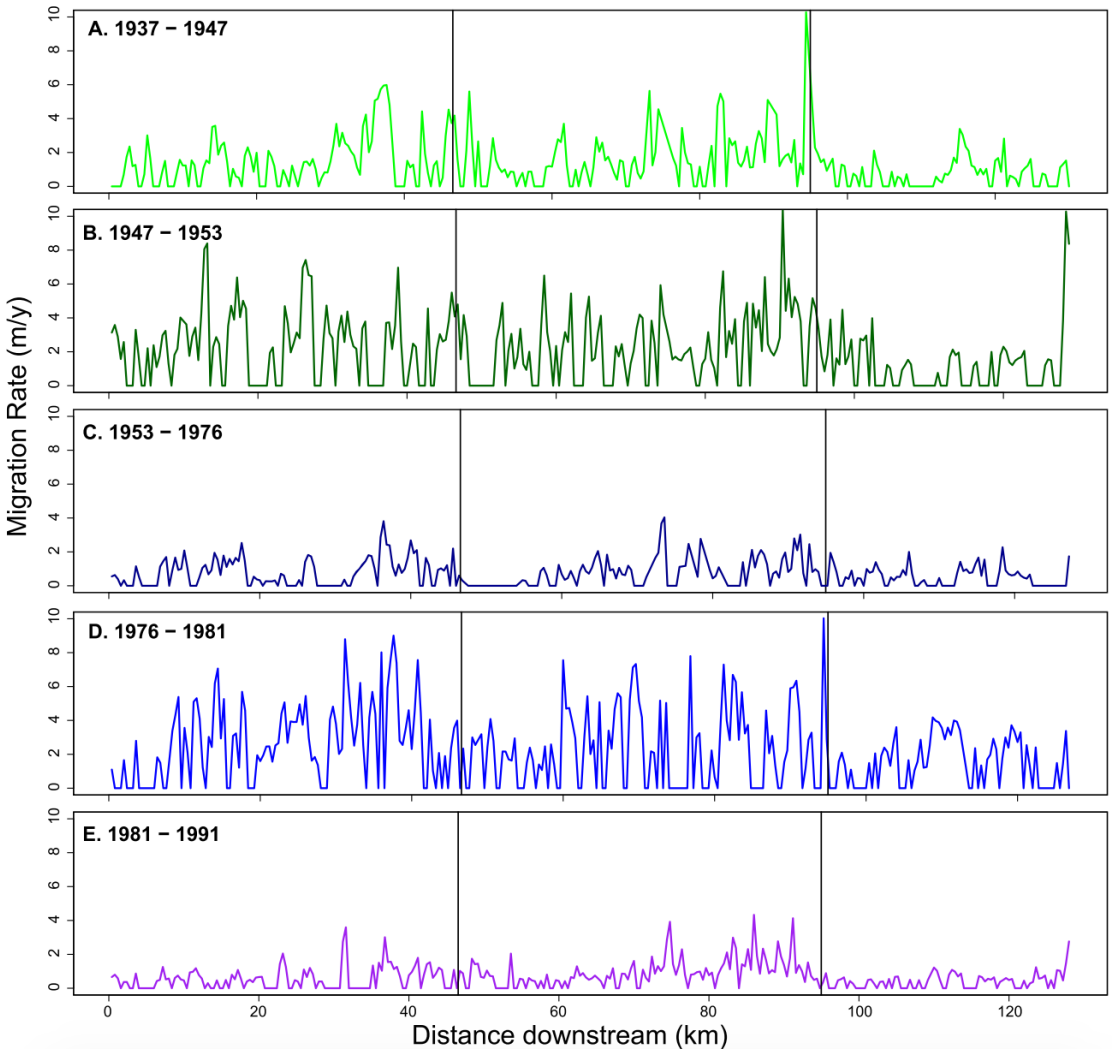

Fig. 3-4a. (A–E) Longitudinal profiles of migration rates for five measurements made between 1937 and 1991.

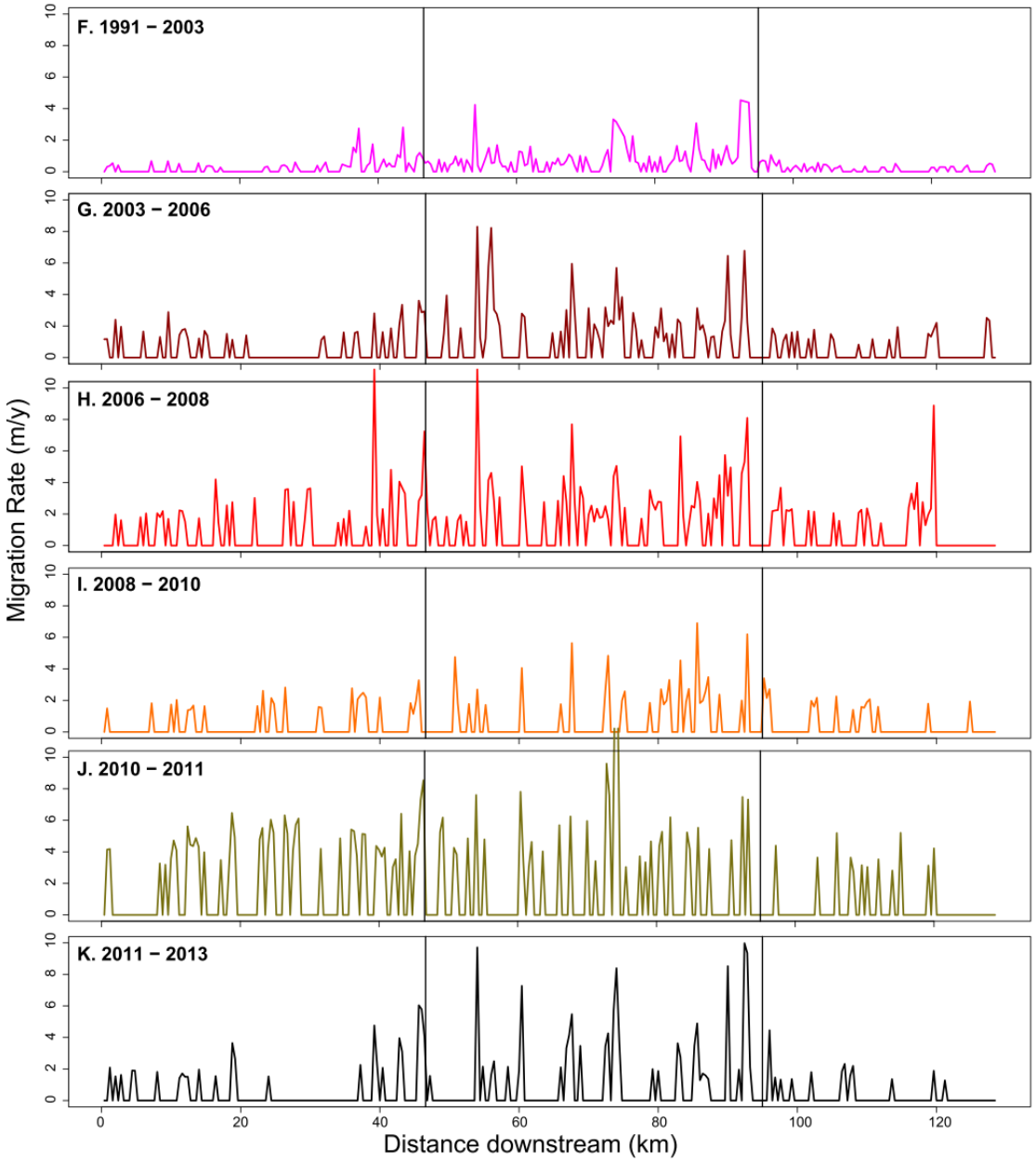

Fig. 3-4b. (F–K) Longitudinal profiles of migration rates for six measurements made between 1991 and 2013. Vertical black bars indicate demarcations of Zones 3, 2, and 1, from left to right.

incorporating more reversals and periods of dormancy. Rate convergence and asymptotic trends are also evident in the synthetic/modeled migration data (Appendix C, Figs. A4a & A4b).

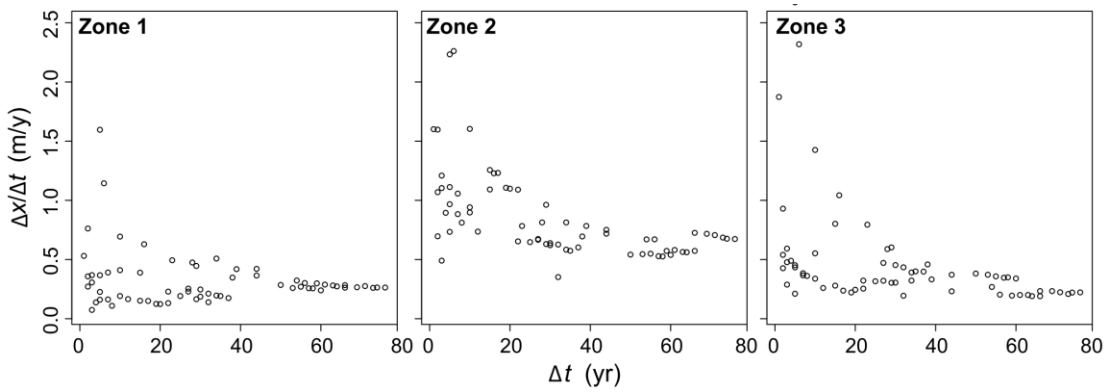

Fig. 3-5. Each black circle represent mean migration rates for a zone (34–48 km) of each aerial photo pair (e.g., 1937 – 1947, Fig. 3-4). Variability in migration dominates the signal in short-term rates, whereas rates converge over broader time intervals as broad measurement intervals dampen short-term variability. Measured migration rates systematically decrease and converge as Δt increases, indicating that migration measurements are dominated by channel dormancy and reversals at longer temporal scales.

4.3. How do actual changes in channel migration influence observed timescale dependence?

Additional simulations addressed whether actual temporal changes are distinguishable from timescale dependence, and whether the magnitude and direction of such changes make a difference. We sought to emulate a range of possible changes in migration rates, where each scenario involved a 1.25, 2, 5, or 10-fold change (increase and decrease) in migration rates half-way (50 years) through the 100-year simulations. All simulations included a 10% probability of reversals to maintain consistency. Increasing or decreasing modelled migration merely translated trends relative to the base case scenario of 10% reversals (Fig. 3-8). This finding matched the empirical trends of Zone 2, which are shifted/translated upward (Fig. 3-5, Zone 2, relative values of trend asymptotes) due to faster migration rates relative to Zones 1 and 3 (Fig. 3-9).

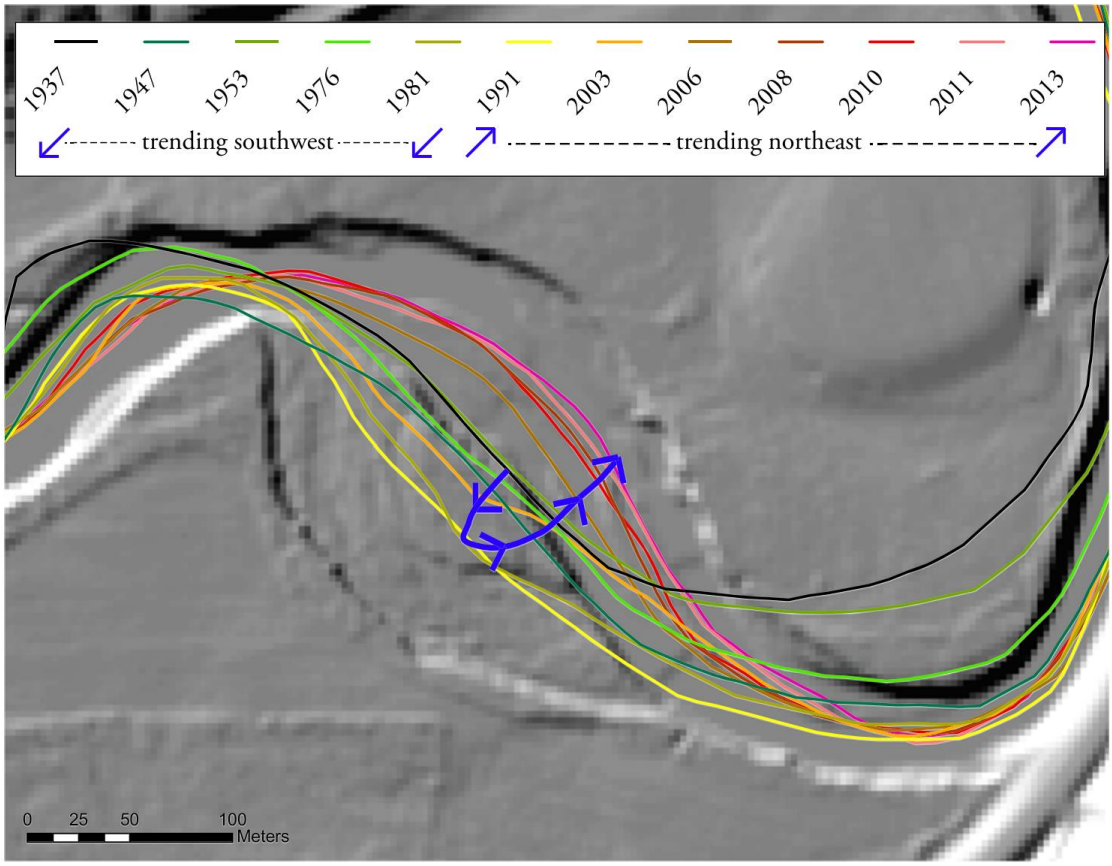

Fig. 3-6. One example of a reversal for a reach of the Root River. The reach migrated approximately 40 m southwest from 1937 to 1991, followed by 85 m of northeasterly migration between 1991 and 2013. For this reach, the observed net migration is 45 m (0.6 m/yr) if no photographs existed between 1937 and 2013, whereas the actual migration is 125 m (1.6 m/yr). The LiDAR hillshade confirms southwestward migration followed by a reversal to its location in 2013 (dark-pink line).

Because the slope of modelled trends remained consistent regardless of rate changes, we can infer that, systematic changes in river channel migration are not sufficient to emulate, nor exaggerate, patterns associated with timescale dependence without the inclusion of channel reversals. Subsequent model simulations showed that combining a change in rates with biased sampling (i.e., predominance of contemporary short-term measurements relative to historical long-term measurements) can exacerbate or confound timescale bias. This is the result of artificially increased (or decreased)

measurements for low- to mid-range time intervals (1-30 years), which effectively alters the slope of migration when plotted over Δt (Appendix C, Figs. A4a & A4b). Thus, if contemporary and historical data respectively dominate short- and long- term measurements/records, inferences on temporal change in channel behavior are not conclusive without additional, independent evidence.

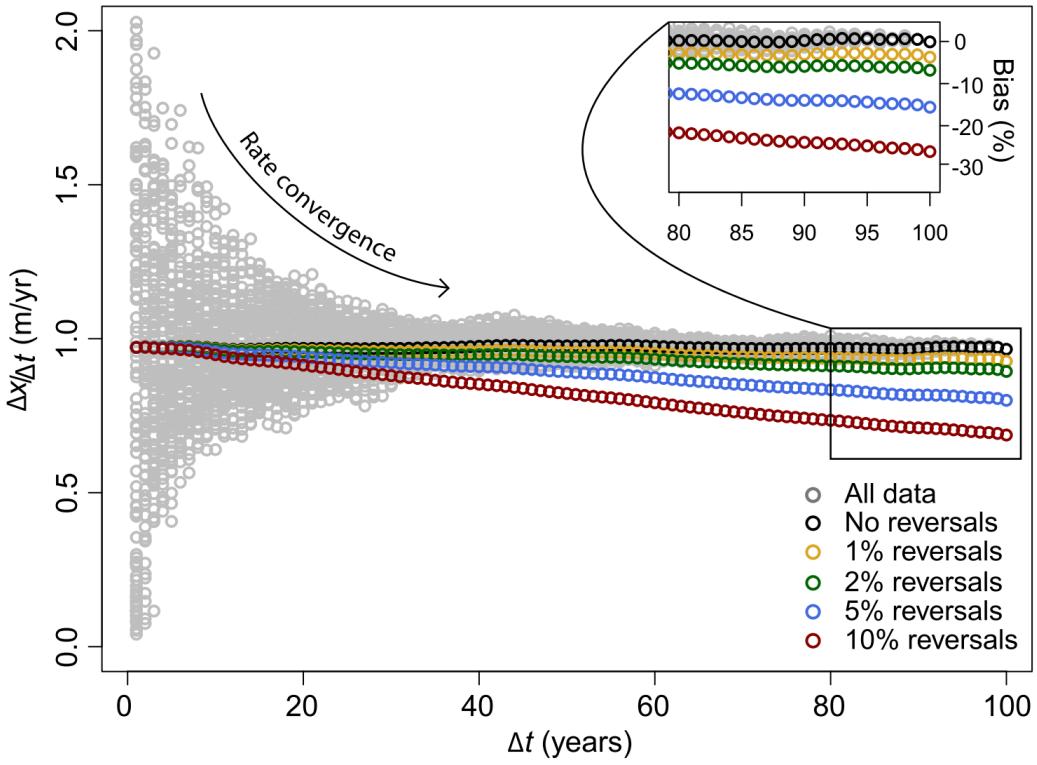

Fig. 3-7. The model results demonstrate how high variability of short-term modeled migration rates (Δx/Δt, grey circles) converges towards a long-term average, a trend similar to that in empirical migration measurements (Fig. 3-5). Black circles are mean rates over each measurement timescale (e.g., Δt = 1, 2, 3, …, 100). Colored circles reflect the same, with the addition of reversals to the model simulations. Measurement bias increases rapidly as reversal frequency and measurement timescale increase, illustrated by incrementally lower values of modelled migration rates (Δx/Δt) relative to the scenario with no reversals.

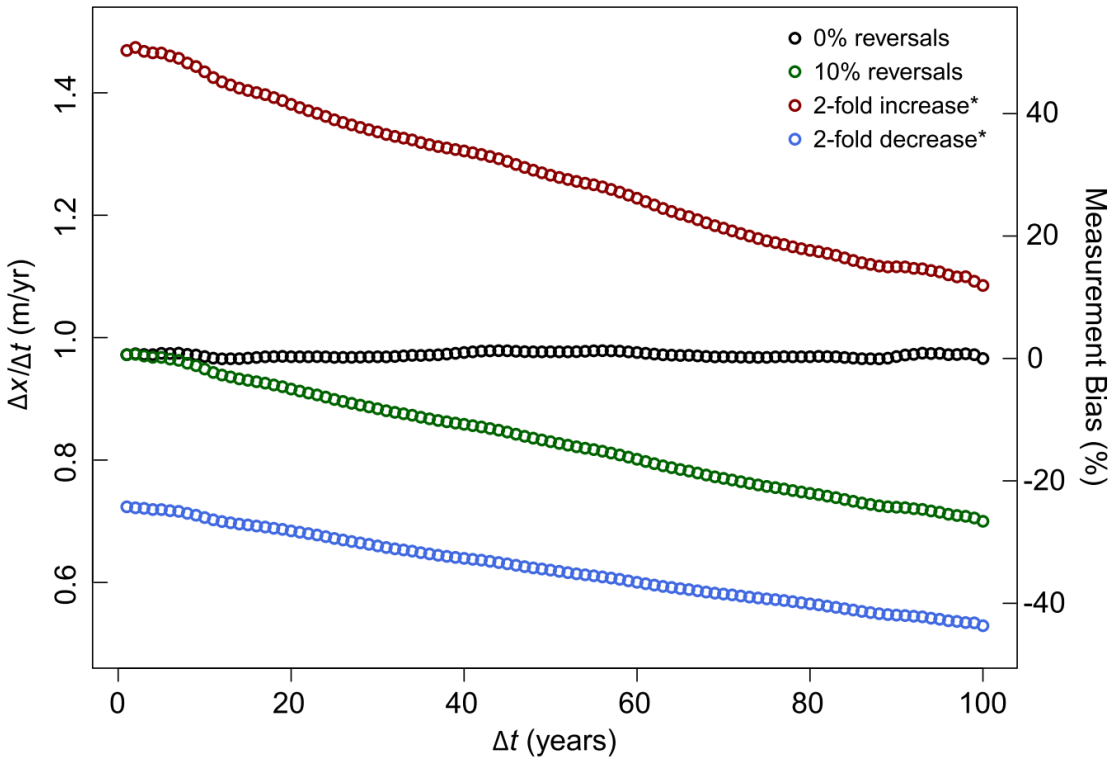

Fig. 3-8. Comparing observed migration rates (Δx/Δt) over increasing measurement timescale (Δt) for different scenarios of temporal change. Black and green points reflect scenarios without and with reversals, but no temporal changes. Red and blue points both incorporated reversals, but also had a 2-fold decrease and increase in migration after year 50, respectively. These scenarios are translated (up or down) versions of the simple reversal scenario (green) with no changes. Thus, temporal changes in migration alone are not sufficient to emulate, nor exaggerate, timescale dependence without the effect of reversals, which would be indicated by a change in the trend slope.

4.4. Predicting and adjusting measurements for timescale bias

Combined, the empirical and model results show us that timescale bias of migration measurements occurs, and this bias varies as a function of reversal frequency, measurement timescale, and changes in migration rate. While a lack of consistent short-timescale empirical measurements preclude the ability to eliminate timescale dependence, our model demonstrates that we can use estimates of reversal frequency to discern the percent of bias/underestimation in a given migration rate measurement for a given

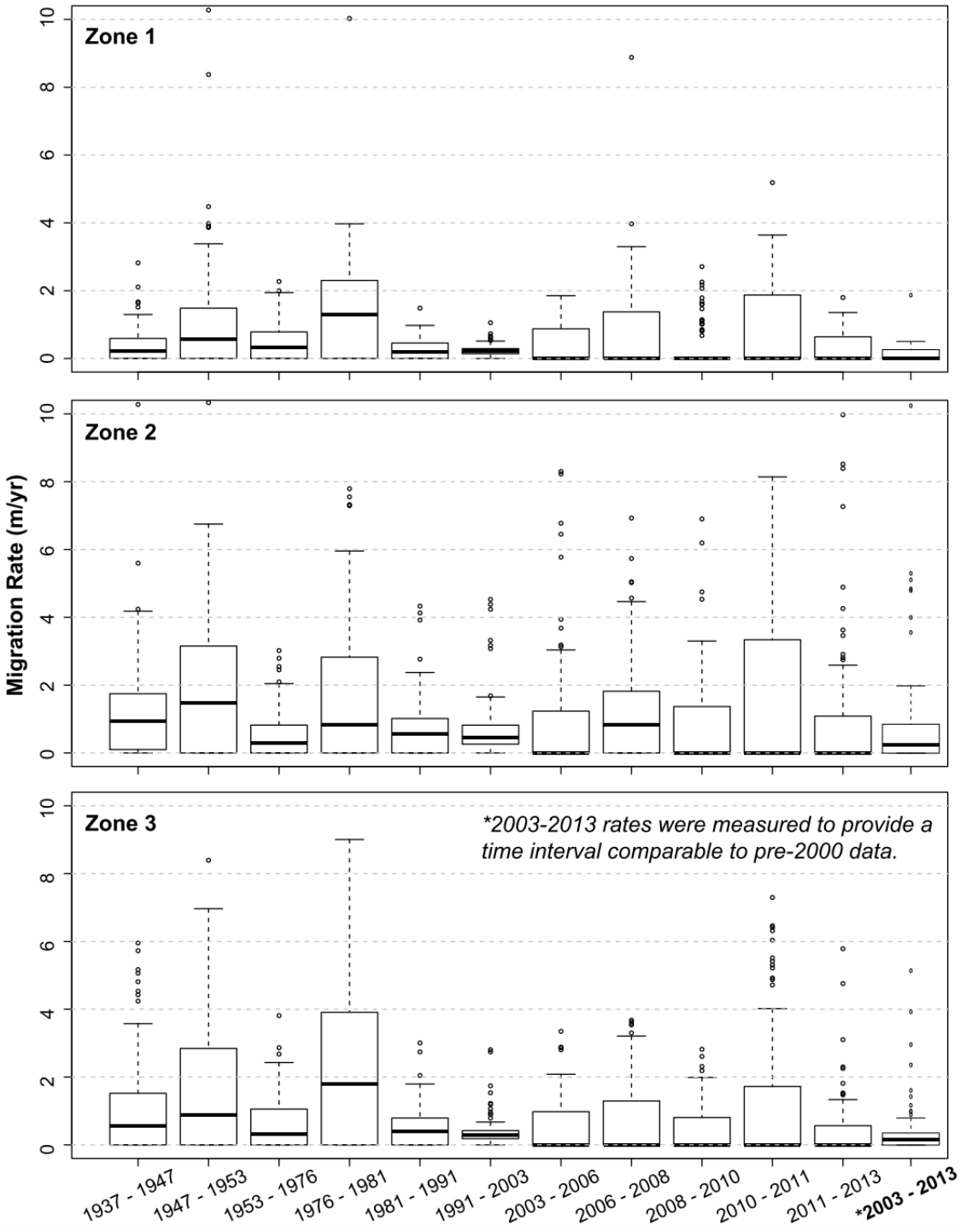

Fig. 3-9. Boxplots of migration rates for each geomorphic zone of the Root River. The farthest right boxplot shows cumulative migration from 2003 to 2013, which provided a comparable measurement interval to those from before 1991 (see text).

measurement interval. We tested the fit of four linear models to predicting bias using: reversal frequency, time interval, as well as the sum and products of the two using Akaike's Information Criterion (AICc, Burnham and Anderson, 2002). AICc measures the relative quality of multiple models using the trade-off between goodness-of-fit and model complexity. Models using reversal frequency or measurement timescale alone were both significant predictors ($p < 0.001$, $r^2 \sim 0.49$ & 0.35), but the fit was markedly improved by including both predictors in a multiple linear regression model ($\delta AICc > 500$). The final multivariate linear regression model (Eq. 3, $r^2 = 0.998$) enables one to adjust, or 'correct', for the bias with a known (or estimated) reversal frequency and measurement interval:

$$U = -0.035R \times 0.021\Delta t + 0; \quad (3)$$

where U is the percent bias/underestimate, R is the reversal frequency percent ($p < 0.001$) expressed as 0 to 100, and Δt is the measurement timescale ($p < 0.001$). While it is rare to have precise knowledge of reversal frequency, using evidence in aerial imagery or high-resolution topography to estimate a range of possibilities will improve estimates of gross sediment remobilization from channel migration by reducing bias inherent in long-term measurements.

4.5. To what degree, if any, have migration rates along the Root River changed over time?

We visually and statistically evaluated empirical migration data to determine whether the medians or distributions of migration rates exhibited any systematic changes over the period of study (Figs. 3-4a & b, Fig. 3-9). For 90 comparisons of migration rates measured before 1991 and those between 1991-2013, the medians and distributions

increased significantly in 0% (0/90) and 14% (13/90) of comparisons, respectively ($p < 0.05$, Mann-Whitney-Wilcoxon and Kolmogorov-Smirnov tests). When relaxing our level of significance to 80% ($p < 0.2$), the medians and distributions still only exhibit significant increases in 1% and 39% of comparisons (Appendix B, Tables A1 and A2). However, these results are biased to favor the conclusion that migration rates have increased based on our previous empirical and model results (Figs. 3-5 & 3-7), which indicated that measurements over longer Δt values (i.e., measurements taken prior to 1991; $\Delta t = 6–23$) are likely biased low relative to those from 2003-2013 ($\Delta t = 1$-3). Despite the predisposed results, they only suggest a minor increase in Root River migration rates over the period for which flows have increased.

One approach for alleviating timescale bias is to aggregate multiple short Δt intervals for contemporary measurements to better match the longer Δt intervals of historical measurements preceding 1991 ($\Delta t = 6–23$). The MWW and K-S tests indicated no increase in the medians or distributions of migration rates (0/18), even when using a rather high $\alpha = 0.2$ (Fig. 3-8, Appendix C, Tables A1a and A1b, **bold** rows). This provided a second line of evidence that migration rates have not systematically changed despite significant changes in flow throughout the 76-year study period. Two implications thus arise: (1) the Root River is predominately not responding to increased flows with increased migration (Figs. 3-9, 3-4a & 3-4b), and (2) comparing disparate measurement timescales can introduce sufficient bias to alter results and sway inferences of channel adjustment, as corroborated by our model results (Fig. 3-8).

The previous pair of comparisons assessed the effect of comparing measurements with similar versus dissimilar measurement intervals. However, they did not address the

commonly encountered situation in which historical measurements are inherently biased toward longer Δt values due to lower frequency of air photo acquisition. To examine the effects of this sampling bias and investigate a third line of evidence to determine whether migration rates have changed, we found seven reaches (3-29 km) with historical image pairs obtained at low-Δt intervals (Δt = 1-5, and 11 years) comparable to those from 2003-2013 measurements (n = 105 comparisons). Results from Mann-Whitney and Kolmogorov-Smirnov tests indicated that medians and distributions exhibited increased migration in only 14% and 18% of 90 comparisons with $\alpha = 0.05$ (Appendix B, Tables A2a & A2b). Furthermore, all but one of these significant increases occurred for comparisons with longer measurement intervals for the historical image pair (1962-1973). This finding is consistent with both empirical (Fig. 3-5) and model results (Fig. 3-7) that suggest longer measurement intervals will exhibit systematically lower values relative to shorter measurement intervals, potentially causing false positive results. Excluding one reach with considerably higher georeferencing uncertainty, these results were robust regardless of whether we retained or discarded measurements falling below the LoD.

Our results provided three lines of evidence that channel migration has not exhibited significant increases over the 76-year study period in response to increased flows. These results appear to contradict the physical explanation for an expected direct relation between flow and channel migration rates; increased flows tend to increase shear stresses along meanders, (Schook et al., 2017). However, sand and gravel-bed river channels adjust their geometry and slope to increase uniformity of sediment transport, and thus dampen responses to changing flow conditions (Church and Ferguson, 2015;

Phillips and Jerolmack, 2016; Call et al., 2017) so adjustments may be driven more by sediment supply and transport capacity, rather than flow (Winterbottom, 2000). Our results also affirm that the timescale dependence for Root River channel migration measurements is not an artifact of differing rates for historical and contemporary data.

5. Conclusions

Both empirical and modelled results demonstrate that migration rates are dependent upon the measurement interval. Short-term measurements (< 10 years) are dominated by high variability reflecting periodic bursts of migration. On the other hand, long-term measurements (> 25 years) converge asymptotically as measurements reach a 'characteristic timescale' where all variability has been sampled and subsequent measurements are relatively constant, barring significant long-term changes. In addition, long-term measurements of gross migration, and thus, sediment flux estimates, are underestimated as the result of channel reversals that erase portions of the erosional record. Thus, the timescale of channel migration measurements affects which question(s) they are suitable to address. Without a sufficient number of short-term measurements, extrapolations will necessarily distort long-term sediment remobilization projections, sediment budgets, sediment flux estimates, and perceptions of fluvial change. Only sufficiently long intervals (> 20-25 years) beyond the 'characteristic timescale' are capable to answer whether a channel has undergone significant long-term changes (i.e., new equilibrium) when compared with similarly long-term measurements. Multiple short-term measurements are necessary to sample the episodic nature of channel migration, thereby providing a more comprehensive understanding of channels' short-term response to changes in flow and sediment flux. These results reinforce our

conclusion that authors should use caution and similar measurement intervals when interpreting fluvial changes and causal mechanisms from aerial- based measurements of channel activity.

Empirical and modelled data both confirmed that migration rate measurements are increasingly underestimated as a function of channel reversal frequency, with insignificant effects from channel dormancy. Measurement bias favors the inference that contemporary channel migration rates have increased because of mismatched sampling intervals in contemporary and historical aerial photograph records. Furthermore, we conclude that long-term migration rates underestimate contributions from streambanks for sediment budgets or fluxes without accounting for or correcting bias using an observed or estimated frequency of reversals (Eq. 3). Before and after accounting for measurement bias in our data, we find no empirical evidence that the Root River has responded to increased flow with any significant increase or decrease in migration in subsequent decades. This reinforces the notion that no simple relationship exists between discharge and migration rates, and that a predictive understanding of migration rates may require better constraints on other factors such as sediment supply, sediment transport, and hydraulic structures in meander bends.

References

Allan JD. 2004. Landscapes and Riverscapes: The Influence of Land Use on Stream Ecosystems. Annual Review of Ecology, Evolution, and Systematics **35** : 257–284. DOI: 10.1146/annurev.ecolsys.35.120202.110122

Baker RW, Knox JC, Lively RS, Olsen BM. 1998. Evidence for early entrenchment of the Upper Mississippi Valley. Report of Investigations **49** : 113–120.

Belmont P. 2011. Large shift in source of fine sediment in the Upper Mississippi River. Environmental Science & Technology **45** : 8804–8810. DOI: 10.1021/es2019109

Belmont P, Dogwiler T, Kumarasamy K. 2016a. An integrated sediment budget for the Root River watershed, southeastern Minnesota. . Minnesota Department of Agriculture: Minnesota

Belmont P, Stevens JR, Czuba JA, Kumarasamy K, Kelly SA. 2016b. Comment on "Climate and agricultural land use change impacts on streamflow in the upper midwestern United States," by Satish C. Gupta et al. Water Resources Research **52** : 7523–7528. DOI: 10.1002/2015WR018476

Braudrick CA, Dietrich WE, Leverich GT, Sklar LS. 2009. Experimental evidence for the conditions necessary to sustain meandering in coarse-bedded rivers. Proceedings of the National Academy of Sciences **106** : 16936–16941. DOI: 10.1073/pnas.0909417106

Burnham KP, Anderson DR. 2002. Model selection and multimodel inference: a practical information-theoretic approach . 2nd ed. Springer Science & Business Media: Fort Collins, Colorado

Call BC, Belmont P, Schmidt JC, Wilcock PR. 2017. Changes in floodplain inundation under nonstationary hydrology for an adjustable, alluvial river channel. Water Resources Research **53** : 3811–3834. DOI: 10.1002/2016WR020277

Cambers G. 1976. Temporal Scales in Coastal Erosion Systems. Transactions of the Institute of British Geographers **1** : 246. DOI: 10.2307/621987

Church M, Ferguson RI. 2015. Morphodynamics: Rivers beyond steady state: Morphodynamics: rivers beyond steady state. Water Resources Research **51** : 1883–1897. DOI: 10.1002/2014WR016862

Constantine CR, Dunne T, Hanson GJ. 2009. Examining the physical meaning of the bank erosion coefficient used in meander migration modeling. Geomorphology **106** : 242–252. DOI: 10.1016/j.geomorph.2008.11.002

Crosato A. 2009. Physical explanations of variations in river meander migration rates from model comparison. Earth Surface Processes and Landforms **34** : 2078–2086. DOI: 10.1002/esp.1898

Donovan M, Miller A, Baker M, Gellis A. 2015. Sediment contributions from floodplains and legacy sediments to Piedmont streams of Baltimore County, Maryland. Geomorphology **235** : 88–105. DOI: 10.1016/j.geomorph.2015.01.025

Finnegan NJ, Dietrich WE. 2011. Episodic bedrock strath terrace formation due to meander migration and cutoff. Geology **39** : 143–146. DOI: 10.1130/G31716.1

Finnegan NJ, Schumer R, Finnegan S. 2014. A signature of transience in bedrock river incision rates over timescales of 104–107 years. Nature **505** : 391–394. DOI: 10.1038/nature12913

Gaeuman D, Schmidt JC, Wilcock PR. 2005. Complex channel responses to changes in stream flow and sediment supply on the lower Duchesne River, Utah. Geomorphology **64** : 185–206. DOI: 10.1016/j.geomorph.2004.06.007

Gallen SF, Pazzaglia FJ, Wegmann KW, Pederson JL, Gardner TW. 2015. The dynamic reference frame of rivers and apparent transience in incision rates. Geology **43** : 623–626. DOI: 10.1130/G36692.1

Ganti V, von Hagke C, Scherler D, Lamb MP, Fischer WW, Avouac J-P. 2016. Time scale bias in erosion rates of glaciated landscapes. Science Advances **2** : e1600204–e1600204. DOI: 10.1126/sciadv.1600204

Gardner TW, Jorgensen DW, Shuman C, Lemieux CR. 1987. Geomorphic and tectonic process rates: Effects of measured time interval. Geology **15** : 259–261. DOI: 10.1130/0091-7613(1987)15<259:GATPRE>2.0.CO;2

Geary RC. 1954. The Contiguity Ratio and Statistical Mapping. The Incorporated Statistician **5** : 115. DOI: 10.2307/2986645

Ghoshal S, James LA, Singer MB, Aalto R. 2010. Channel and Floodplain Change Analysis over a 100-Year Period: Lower Yuba River, California. Remote Sensing **2** : 1797–1825. DOI: 10.3390/rs2071797

Gran KB, Finnegan N, Johnson AL, Belmont P, Wittkop C, Rittenour T. 2013. Landscape evolution, valley excavation, and terrace development following abrupt postglacial base-level fall. Geological Society of America Bulletin **125** : 1851–1864. DOI: 10.1130/B30772.1

Gurnell AM, Downward SR, Jones R. 1994. Channel planform change on the river dee meanders, 1876–1992. Regulated Rivers: Research & Management **9** : 187–204. DOI: 10.1002/rrr.3450090402

Hooke JM. 1980. Magnitude and distribution of rates of river bank erosion. Earth Surface Processes **5** : 143–157. DOI: 10.1002/esp.3760050205

Johnson DH. 1999. The Insignificance of Statistical Significance Testing. The Journal of Wildlife Management **63** : 763. DOI: 10.2307/3802789

Kelly SA, Takbiri Z, Belmont P, Foufoula-Georgiou E. 2017. Human amplified changes in precipitation-runoff patterns in large river basins of the Midwestern United States. Hydrology and Earth System Sciences Discussions : 1–37. DOI: 10.5194/hess-2017-133

Kessler AC, Gupta SC, Brown MK. 2013. Assessment of river bank erosion in Southern Minnesota rivers post European settlement. Geomorphology **201** : 312–322. DOI: 10.1016/j.geomorph.2013.07.006

Kirchner JW, Finkel RC, Riebe CS, Granger DE, Clayton JL, King JG, Megahan WF. 2001. Mountain erosion over 10 yr, 10 k.y., and 10 m.y. time scales. Geology **29** : 591. DOI: 10.1130/0091-7613(2001)029<0591:MEOYKY>2.0.CO;2

Knox JC. 2006. Floodplain sedimentation in the Upper Mississippi Valley: Natural versus human accelerated. Geomorphology **79** : 286–310. DOI: 10.1016/j.geomorph.2006.06.031

Larsen EW, Fremier AK, Girvetz EH. 2006. Modeling the effects of variable annual flow on river channel meander migration patterns, Sacramento River, California, USA. Journal of the American Water Resources Association **42** : 1063–1075.

Lauer JW. 2007. Channel Planform Statistics Toolbox . National Center for Earth-Surface Dynamics: University of Minnesota [online] Available from: https://repository.nced.umn.edu/browser.php?current=keyword&keyword=7,5&dataset_id=15&folder=237802

Lauer JW, Parker G. 2008. Net local removal of floodplain sediment by river meander migration. Geomorphology **96** : 123–149. DOI: 10.1016/j.geomorph.2007.08.003

Lea DM, Legleiter CJ. 2016. Refining measurements of lateral channel movement from image time series by quantifying spatial variations in registration error. Geomorphology **258** : 11–20. DOI: 10.1016/j.geomorph.2016.01.009

Lenhart CF, Peterson H, Nieber J. 2011. Increased streamflow in agricultural watersheds of the Midwest: implications for management. Watershed Science Bulletin : 25–31.

Lindsay JB, Ashmore PE. 2002. The effects of survey frequency on estimates of scour and fill in a braided river model. Earth Surface Processes and Landforms **27** : 27–43. DOI: 10.1002/esp.282

Micheli ER, Larsen EW. 2011. River channel cutoff dynamics, Sacramento River, California, USA. River Research and Applications **27** : 328–344. DOI: 10.1002/rra.1360

Montgomery DR. 1999. Process domains and the river continuum. Journal of the American Water Resources Association **35** : 397–410. DOI: 10.1111/j.1752-1688.1999.tb03598.x

Motta D, Abad JD, Langendoen EJ, Garcia MH. 2012. A simplified 2D model for meander migration with physically-based bank evolution. Geomorphology **163**–**164** : 10–25. DOI: 10.1016/j.geomorph.2011.06.036

Nanson GC, Hickin EJ. 1983. Channel Migration and Incision on the Beatton River. Journal of Hydraulic Engineering **109** : 327–337. DOI: 10.1061/(ASCE)0733-9429(1983)109:3(327)

Parker G, Shimizu Y, Wilkerson GV, Eke EC, Abad JD, Lauer JW, Paola C, Dietrich WE, Voller VR. 2011. A new framework for modeling the migration of meandering rivers. Earth Surface Processes and Landforms **36** : 70–86. DOI: 10.1002/esp.2113

Passalacqua P et al. 2015. Analyzing high resolution topography for advancing the understanding of mass and energy transfer through landscapes: A review. Earth-Science Reviews **148** : 174–193. DOI: 10.1016/j.earscirev.2015.05.012

Penning-Rowsell EC, Townshend JRG. 1978. The Influence of Scale on the Factors Affecting Stream Channel Slope. Transactions of the Institute of British Geographers **3** : 395. DOI: 10.2307/622120

Phillips CB, Jerolmack DJ. 2016. Self-organization of river channels as a critical filter on climate signals. Science **352** : 694–697. DOI: 10.1126/science.aad3348

Reid LM, Dunne T. 2005. Sediment Budgets as an Organizing Framework in Fluvial Geomorphology. In Tools in Fluvial Geomorphology , . John Wiley & Sons, Ltd; 463–500.

Sadler PM. 1981. Sediment Accumulation Rates and the Completeness of Stratigraphic Sections. The Journal of Geology **89** : 569–584.

Sadler PM, Jerolmack DJ. 2015. Scaling laws for aggradation, denudation and progradation rates: the case for time-scale invariance at sediment sources and sinks. Geological Society, London, Special Publications **404** : 69–88. DOI: 10.1144/SP404.7

Schook DM, Rathburn SL, Friedman JM, Wolf JM. 2017. A 184-year record of river meander migration from tree rings, aerial imagery, and cross sections. Geomorphology **293** : 227–239. DOI: 10.1016/j.geomorph.2017.06.001

Simon A. 1989. A model of channel response in disturbed alluvial channels. Earth Surface Processes and Landforms **14** : 11–26.

Souffront M. 2014. Channel Adjustment and Channel-Floodplain Sediment Exchange in the Root River, Southeastern Minnesota, M.S. Thesis, Utah State University: Logan, Utah

Stout JC, Belmont P. 2013. TerEx Toolbox for semi-automated selection of fluvial terrace and floodplain features from lidar. Earth Surface Processes and Landforms **39** : 569–580. DOI: 10.1002/esp.3464

Stout JC, Belmont P, Schottler SP, Willenbring JK. 2014. Identifying Sediment Sources and Sinks in the Root River, Southeastern Minnesota. Annals of the Association of American Geographers **104** : 20–39. DOI: 10.1080/00045608.2013.843434

Swanson BJ, Meyer GA, Coonrod JE. 2011. Historical channel narrowing along the Rio Grande near Albuquerque, New Mexico in response to peak discharge reductions and engineering: magnitude and uncertainty of change from air photo measurements. Earth Surface Processes and Landforms **36** : 885–900. DOI: 10.1002/esp.2119

Syverson KM, Colgan PM. 2004. The Quaternary of Wisconsin: A review of stratigraphy and glaciation history. In Developments in Quaternary Sciences , . Elsevier; 295–311. [online] Available from: http://linkinghub.elsevier.com/retrieve/pii/S1571086604802057 (Accessed 11 June 2016)

Thorne CR. 1981. Field measurements of rates of bank erosion and bank material strength. presented at the Proceedings of the Florence Symposium. Florence, Italy. 503–512 pp.

Toone J, Rice SP, Piégay H. 2014. Spatial discontinuity and temporal evolution of channel morphology along a mixed bedrock-alluvial river, upper Drôme River, southeast France: Contingent responses to external and internal controls. Discontinuities in Fluvial Systems **205** : 5–16. DOI: 10.1016/j.geomorph.2012.05.033

Trimble SW. 1983. A sediment budget for Coon Creek basin in the Driftless Area, Wisconsin, 1853-1977. American Journal of Science **283** : 454–474. DOI: 10.2475/ajs.283.5.454

Trimble SW. 1999. Decreased rates of alluvial sediment storage in the Coon Creek Basin, Wisconsin, 1975-93. Science **285** : 1244–1246. DOI: 10.1126/science.285.5431.1244

Trimble SW. 2009. Fluvial processes, morphology and sediment budgets in the Coon Creek Basin, WI, USA, 1975–1993. Geomorphology **108** : 8–23. DOI: 10.1016/j.geomorph.2006.11.015

Vaughan AA, Belmont P, Hawkins CP, Wilcock P. 2017. Near-Channel Versus Watershed Controls on Sediment Rating Curves: Controls on Sediment Rating Curves. Journal of Geophysical Research: Earth Surface **122** : 1901–1923. DOI: 10.1002/2016JF004180

Wente S. 2000. Proximity-based measure of land use impacts to aquatic ecosystem integrity. Environmental Toxicology and Chemistry **19** : 1148–1152. DOI: 10.1897/1551-5028(2000)019<1148:PBMOLU>2.3.CO;2

Winterbottom SJ. 2000. Medium and short-term channel planform changes on the Rivers Tay and Tummel, Scotland. Geomorphology **34** : 195–208. DOI: 10.1016/S0169-555X(00)00007-6

CHAPTER 4

EVALUATING THE RELATIONSHIP BETWEEN MEANDER-BEND CURVATURE, SEDIMENT SUPPY, AND MIGRATION RATES

1. Introduction

1.1.Background- River meander migration and curvature

River meander migration is one of the most ubiquitous processes shaping and redistributing mass on Earth's surface. The forms and patterns of river meander development have fascinated scientists since the early 20th century (Davis, 1902; Brice, 1974; Leopold and Wolman, 1960; Schumm, 1965; Wolman and Leopold, 1957), perplexing even Albert Einstein, who proposed that river meandering was the result of rotational motion from the Coriolis effect (Einstein, 1926). The complexity inherent to meander migration is reflected in countless studies spanning multiple orders of spatial and temporal magnitude- from individual meander bends (Dietrich et al., 1979; Kasvi et al., 2017), to geologic-scale evolution of floodplains and valleys (Sun et al., 1996; Howard, 1996; Gran et al., 2013). Such studies improve models predicting where and when migration will occur, providing useful information for environmental and agricultural management, sediment loads for downstream habitats, stream restoration, and riparian/watershed management. Remotely-sensed imagery is commonly used to measure changes in river planform in response to changes in land use, urbanization, deforestation, and dam building or removal (Hickin and Nanson, 1984; Gurnell et al., 1994; Gaeuman et al., 2005; Lauer and Parker, 2008; Constantine et al., 2014; Donovan et al., 2015, 2016; Morais et al., 2016).

Using a combination of aerial imagery and USGS topographic maps, Brice (1974)

established seven generalized classes of meander development based on predictable and persistent patterns over broad scales, all of which reflect localized feedbacks between sediment loads and the flow of water (Constantine et al., 2014). Specifically, the helical flow patterns around meander bends establish asymmetries in centrifugal forces and shear stresses along the outer bank, which in turn drive erosion, transport, and deposition of sediment (Leopold and Wolman, 1960; Dietrich et al., 1979). Centrifugal forces and shear stresses along a meander bend increase with curvature of the bend, and thus, migration rates should vary directly with curvature (Howard and Knutson, 1984; Furbish, 1988). Curvature (C) is the degree to which a segment/surface deviates from a line/plane and is the reciprocal of the radius of curvature (R). Although centrifugal force and bank stress increase with bend curvature, empirical measurements indicate that migration rates peak at a radius of curvature that is 2 to 3 times the channel width (R/W ~2-3) when measurements are averaged over the scale of a meander bend (Fig. 4-1a; Hickin and Nanson, 1975, 1984). This relationship has been observed in many subsequent studies (Hudson and Kesel, 2000; Hooke, 2003; Güneralp and Rhoads, 2008; Nicoll and Hickin, 2010).

Bends with the same average curvature can have different degrees of asymmetry, suggesting that a single value of bend-averaged curvature may be associated with multiple patterns of shear stress (Furbish, 1988). For example, the two bends in Fig. 4-1b have the same bend-averaged curvature, but exhibit large differences in flow asymmetry and shear stress due to differing bend lengths. The longer bend experiences larger shear stresses along the outer bank, and therefore will have faster migration rates compared to the shorter bend. Migration trajectories along a bend depend not only on local curvature,

but also cumulative upstream curvature, which will vary with bend length. Thus, associating bend-averaged migration rates with bend-averaged curvature will result in a single curvature value being associated with a range of migration rates. Despite being published nearly 30 years ago, Furbish (1988) and Furbish (1991) have approximately 20% the citations of Hickin (1974), and 30% that of Hickin & Nanson (1975). Such contrasts highlight how widely-held beliefs amongst scientists can persist due to popularity, regardless of their rigor. While the results and empirical relationship established in Hickin & Nanson (1975) reflect rigorous science and a considerable breakthrough in understanding curvature-migration rate dynamics, subsequent research largely overlooked concerns outlined in Furbish (1988) in favor of an over-simplified approach associating bend-averaged radius of curvature and migration rate.

Models relating bank erosion to local curvature reproduce the peaked relation between local migration and curvature (Begin, 1981; Crosato, 2009). However, others note that using local curvature to model meander development results in bend form growth lacking the asymmetry (Carson and Lapointe, 1983) and spatial heterogeneity that is observed in complex planform adjustments (Güneralp and Rhoads, 2011) common to many meandering rivers. Comparing meander migration modelled using (a) local curvature, versus (b) local and upstream curvature weighted as a function of distance upstream, Howard and Knutson (1984) showed that only the latter successfully simulated asymmetrical development, downstream translation, and cutoffs typical of natural meandering streams.

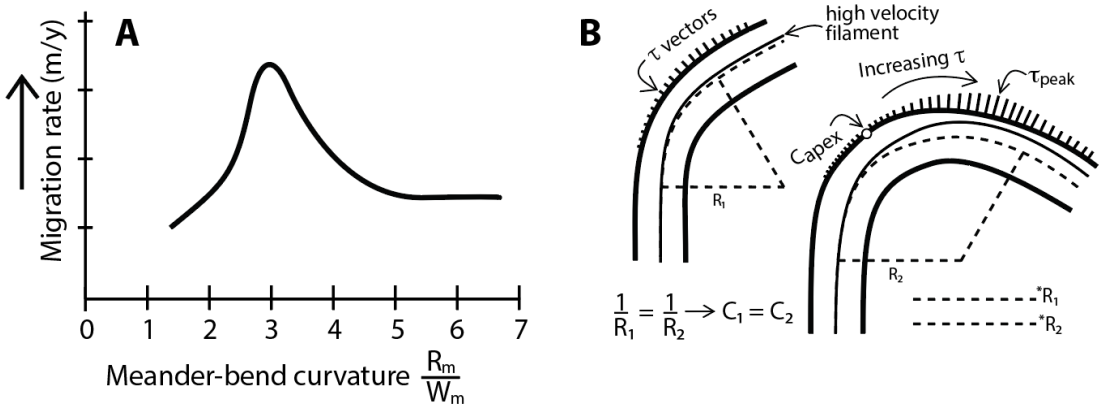

Fig. 4-1. Competing ideas regarding the relation between curvature and meander-bend migration. (Left) Meander-bend averaged migration plotted as a function of meander-bend averaged radius of curvature normalized by channel width (R/W), as reproduced from Hickin and Nanson (1975). The x-axis is the bend-averaged radius of curvature normalized by channel width, which is inversely related to curvature (see Eq. 2). (Right) Conceptual diagram, adapted from Furbish (1988), illustrating how two meander bends can have the same bend-averaged radius of curvature despite distinct differences in shear stress along the outer bank. Thus, despite having the same radius of curvature, R_2 will migrate faster due to higher shear stresses. $*R_1$ and $*R_2$ were transposed from each of the curves as evidence that the radii are equal.

Measuring migration and curvature at the scale of an entire bend also prevents the possibility of capturing sub-meander scale flow dynamics that drive heterogeneity in meander migration throughout a bend. A high velocity flow filament is directed toward the outer bank, reaching the outer bank downstream of the bend apex (Dietrich et al., 1979; Seminara, 2006, Kasvi et al., 2017), and not always within the meander bend (Leopold and Wolman, 1960). Shear stress and erosion increase along the outer bank where the highest velocities persist due to centrifugal force and acceleration of secondary flow currents (Dietrich et al., 1979; Seminara, 2006; Zhou et al., 1993). Meanwhile, inner bends have lower velocities, deposition, and point bar formation, which continue to push high velocity flow paths towards the outer bank. In this way, point bar development is causatively linked to erosion along the outer bank, and is referred to as bar push. The

spatial lag between bend apices and peak migration rates ultimately reflects the lag in acceleration of secondary flow development, and thus, peak migration should be downstream of the bend apex. The downstream length of the lag is influenced by other variables such as meander arc length, width:depth aspect ratio, friction or flow resistance, flow depth, inner-bank bar angle, and suspended sediment concentration (Furbish, 1991; Zhou et al., 1993; Seminara, 2006; Güneralp and Rhoads, 2009; Güneralp and Marston, 2012; Patnaik et al., 2014).

By measuring migration rates and channel curvature at sub-meander bend scales, Sylvester et al. (2019) provided empirical evidence to support a direct relationship between channel curvature and downstream migration rates for seven Amazonian rivers. When associating spatially lagged values of channel curvature and migration rates, migration rates did not exhibit a peak at intermediate curvature values, but rather, continually increased as curvature increased. Deviations from the general trend were attributed to reduced bank erodibility. The authors conclude that peaked curvature-migration relationships (e.g., Hickin and Nanson, 1975) result from associating bend-averaged, rather than spatially explicit and lagged, values of curvature and migration rate.

Channel migration not only reflects local patterns of shear stress, but also feedbacks between sediment loads and the flow of water (Constantine et al., 2014). When sediment supply exceeds a channel's transport capacity, deposition leads to steeper channel slope and point bar growth (Ashworth, 1996; Venditti et al., 2012; Engel & Rhoads, 2012; Kelly, 2019). As channel bars grow, the positive feedbacks associated with the asymmetry in the channel bed, flow velocities and depths, and shear stresses increase the probability of lateral migration via bar push (Eke et al., 2014). In contrast,

these dynamics are muted and typically fail to exceed bank resisting forces in reaches without sufficient sediment supply to form bars that are large enough to exert a substantial influence on the flow field. Rivers within the Amazon River exhibit some of the highest sediment transport rates in the world (Milliman and Meade, 1983; Martinelli et al., 1989), and are likely to exhibit migration rates driven by bar push feedbacks. It remains to be seen if the direct relationship between curvature and migration (Sylvester et al., 2019) holds in the absence of high sediment supply to support bar growth. Addressing the role of sediment supply and bar geometry in curvature-migration relations would provide significant advancements for this area of fluvial geomorphology. Comprehensive studies of process-form feedbacks in meander morphodynamics of natural systems are among the top research needs to be integrated into theoretical and laboratory experiments (Güneralp and Marston, 2012).

We evaluate the relation between channel curvature, migration rates, and bar geometry in the Root and Minnesota rivers, Minnesota, USA, using repeated aerial images spanning large temporal (8 and 6 sets of air photos over 76 years) and spatial scales (25 and 180 km). We first evaluate the relationship between meander-bend averaged curvature and migration and compare these results to analyses of spatially explicit and lagged values of curvature and migration rates measured at sub-meander scales. In doing so, we are able to assess if measurement lengthscale alters the form of relationship between channel curvature and migration rates (i.e., migration rates increase as a continuous function of curvature, or peak at intermediate curvature values). Specifically, we ask: What is the magnitude and variability in the spatial lag between curvature and migration rate? And, are the lag and form of the relationship between

curvature and migration rate altered for reaches with high bank erodibility and/or low sediment supply? By influencing point bar geometry and growth, sediment supply may play an important role in the relationship between curvature and migration.

2. Study Area and Data

We evaluate curvature-migration relations using channel change along centerlines derived from aerial photographs spanning approximately 25 km of the Root River, Minnesota, a single-threaded, meandering sand- and gravel-bedded river that drains into the Mississippi River (Fig. 4-2A). The 25-km reach (Fig. 4-2B) chosen for analysis contains the most active meander bends of the mainstem river, which has been studied extensively (Stout and Belmont, 2013; Stout et al., 2014; Souffront, 2014; Belmont et al., 2016). Meander bends in this reach are intermittently laterally confined by either natural or anthropogenic impingements (Fig. 4-2C). Channel confinement and variable riparian conditions provide sufficient irregularity in erosivity to test whether a simple curvature-migration model remains robust despite variable conditions. We used eight sets of images (1937, 1947, 1953, 1976, 1981, 1991, 2003, and 2013) with sufficiently similar time intervals to encompass significant channel adjustment (Donovan and Belmont, 2019).

We also include 180-km of the Minnesota River between the town of Mankato and historical Fort Snelling, near the confluence with the Mississippi River. Six sets of images (1937, 1951, 1964, 1980, 1991, and 2013) were available along this portion of the river, which has been the focus of multiple comprehensive geomorphic studies (Lenhart

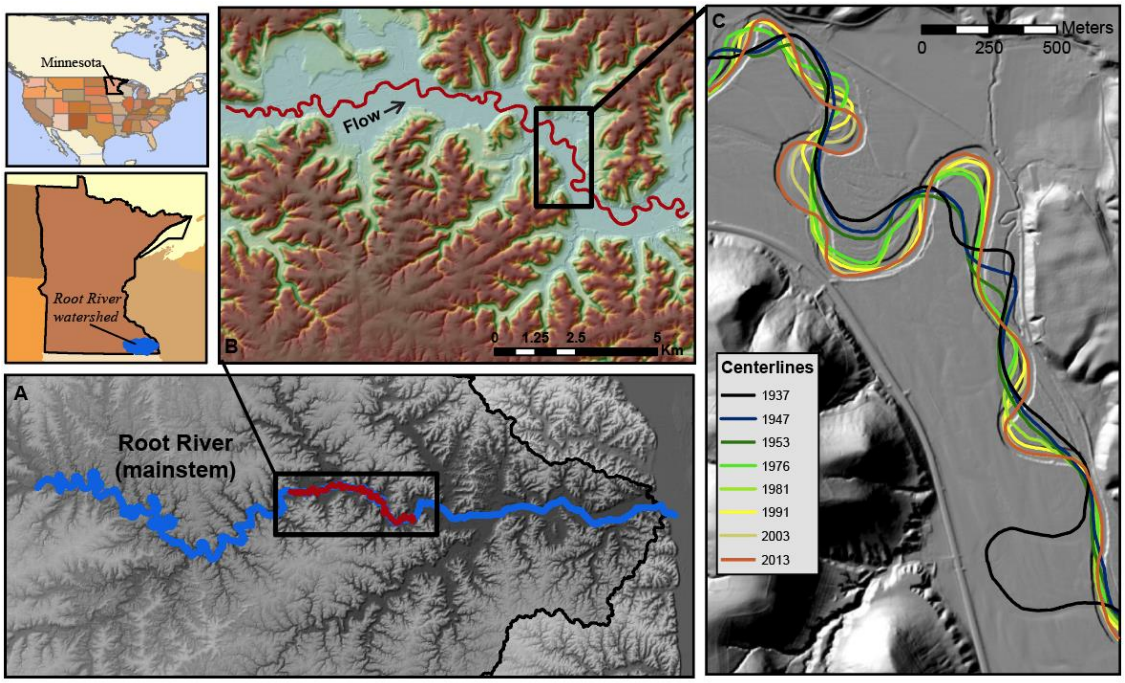

Fig. 4-2. Overview of Root River within the North American continent and state of Minnesota (top left). (A) The mainstem drains from left to right into the Mississippi River. (B) The 25-km segment of the Root River chosen for analysis. (C) An example of centerlines derived from delineations for each of the 8 sets of images spanning 1937-2013. The underlying hillshade in A, B, and C was derived from 3-meter LiDAR elevation data.

et al., 2013; Libby, 2017; Lauer et al., 2017; Kelly and Belmont, 2018) due to its unique short- and long-term geomorphic history. About 13,400 years ago, the outpouring of glacial Lake Aggasiz resulted in 70 m of incision of the mainstem Minnesota River Valley (Shay, 1967; Clayton and Moran, 1982; Matsch, 1983; Lepper et al., 2007; Gran et al., 2013). This incision has resulted in multiple knickpoints and exposure of highly-erodible glacial sediments (Belmont, 2011; Jennings, 2010). In addition, the river has been responding to contemporary land use and precipitation changes over the last 80 years, which have increased flows by 50-250% (Kelly et al., 2017; Foufoula-Georgiou et al., 2015; Novotny and Stefan, 2007; Schottler et al., 2014). The recent increases in flow

have amplified rates of lateral channel migration (Belmont et al., 2011; Libby, 2017) and notably increased channel width (Schottler et al., 2014; Lauer et al., 2017). Within the 180-km study reach, the channel experiences abrupt reductions in sediment grain size, channel-bar geometry, and slope roughly 100-km downstream near the town of Belle Plaine (Fig. 4-2b). We distinguish these reaches as the high- and low-supply reaches, and spatially, these are respectively the upper and lower portions of the study reach. Large, wide channel bars along upstream reaches promote bar-push feedbacks, while narrow and steep downstream point bars lack sediment supply to support growth. The comprehensive set of imagery and contrasts in channel-bar geometry along the Minnesota River provide an opportunity to study the role of sediment supply in the relationship between channel curvature and meander migration rates.

3. Methods

3.1. Measuring curvature and channel planform

For each year of imagery, channel banks were delineated as described in Donovan et al. (2019). Bank lines were interpolated to channel centerlines (Fig. 4-2c) and converted to coordinate points in 10-meter increments. At each increment, channel width was calculated using the Planform Statistics Toolbox (Lauer and Parker, 2008). For each sequential pair of images (n=7 for Root River, n=5 for the Minnesota River), bank migration was measured at each 10-meter increment along the channel using a dynamic time warping algorithm (DTW).

DTW was originally developed to correlate time series (e.g., Lisiecki and Lisiecki, 2002) and has been shown to greatly reduce computation time while improving

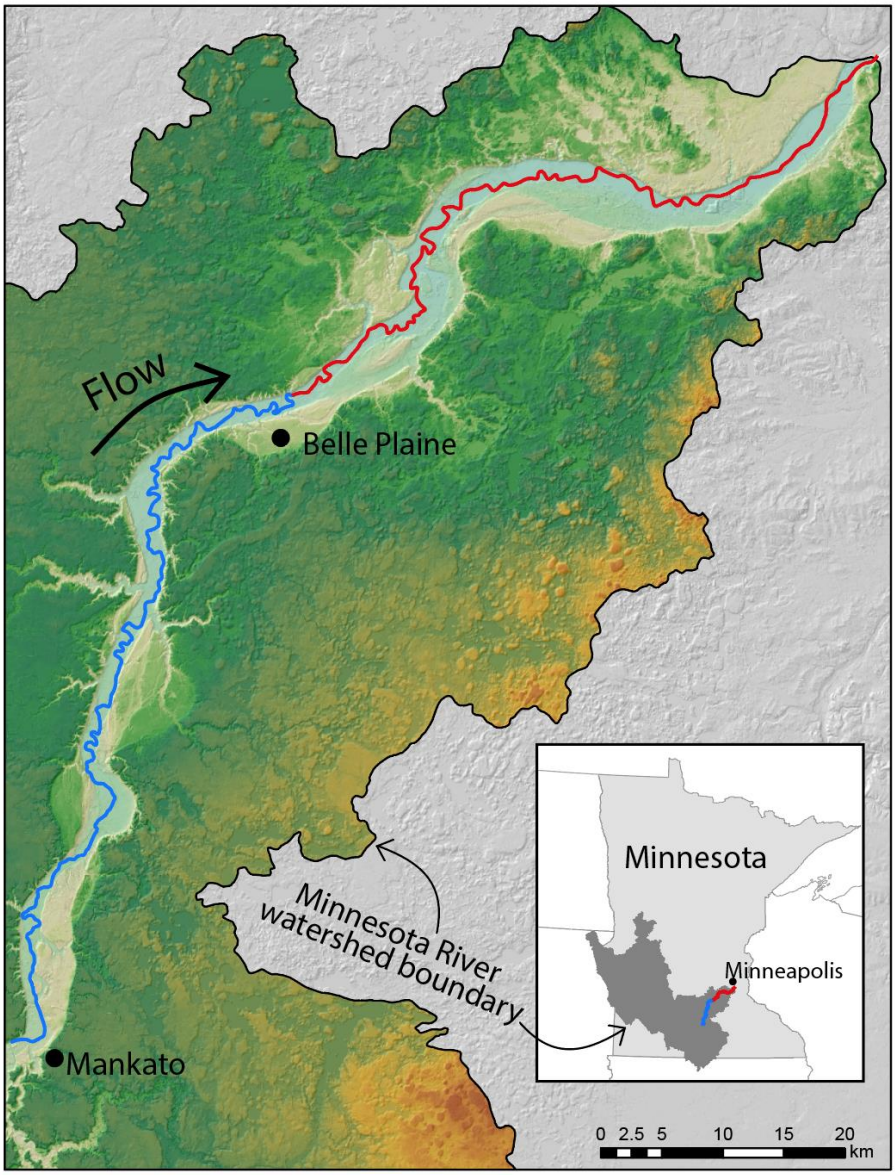

Fig. 4-3. Locator map of the study reach along the Minnesota River, which spans from the town of Mankato to Fort Snelling (center). Unique upstream and downstream reaches are highlighted in blue and red, respectively. The bed and bars of the reach north (downstream, red) of Belle Plaine contain fine sands, silts, and clays, compared to the southern (upstream, blue) reach, which consist of coarse sands and gravels.

bank migration trajectories compared to typical nearest neighbor algorithms (Sylvester et al., 2019). Unlike nearest-neighbor algorithms, DTW uses a cost matrix and 'cosine similarity' to minimize the sum of trajectories between signals, rather than minimizing

the distance of individual trajectories. Cosine similarity not only considers the magnitude (distance) between two points on a signal, but also their orientation in space relative to nearby points. Thus, the trajectories are not simply minimized Euclidean distances, but also account for the form of the local signals. Cosine similarity also helps avoid issues associated with measuring trajectories between signals of differing lengths. For example, migration inherently changes the length of the second signal relative to the first, by increasing sinuosity or reducing it via channel cutoffs. By using cosine similarity, DTW avoids bunching and/or large gaps between nodes on the terminal end of trajectories. Thus, as distance between two centerlines increases, the performance of DTW computations improves relative to nearest neighbor algorithms.

Subsequent to DTW computations, we manually identified and filtered out measurements within meander bend cutoffs before performing subsequent analyses (Fig. 4-3). Curvature (units, m^{-1}) was calculated using the x and y components of each point's Cartesian coordinates:

$$C = \frac{x'y'' - y'x''}{(x'^2 + y'^2)^{3/2}}, \quad \text{Eq. (1)}$$

where x' and x'' are the first and second-order derivatives of the x coordinate. Curvature is the reciprocal of the radius of curvature, R (Eq. 2):

$$C = \frac{1}{R}; \ \therefore \ \frac{R}{W} = \frac{1}{C \cdot W}, \quad \text{Eq. (2)}$$

and thus, is inversely related to width-normalized radius of curvature (R/W) that is commonly plotted against migration rates. Curvature and migration rates were smoothed using a Savitzky-Golay filter to reduce signal noise (Motta et al., 2012; Sylvester et al.,

2019). Savitzky-Golay filtering retains local precision without distorting the signal by fitting low-degree polynomials to successive subsets of data points (Savitzky and Golay, 1964).

3.2. Discerning spatial relationships in migration and curvature

After generating continuous profiles migration and curvature, we employed a signal processing algorithm (scipy.signal.find_peaks) in Python to find local maxima and minima (both are referred to as 'peaks'). An individual point would be defined as a peak if it was greater than adjacent (upstream or downstream) values within 40-meters (Figs. 4-3A & 4-3B). By using simple/minimal criteria to detect peaks, we eliminated false-negatives and then manually removed false-positives, retaining only curvature peaks that could be paired with peaks in migration rates. The lag distance between paired peaks in migration rates and curvature was the distance between each set of peaks, as measured along the channel centerline. Lag distances were normalized by the mean of channel widths between the peaks:

$$L^* = \frac{Loc_{Cpk} - Loc_{Mpk}}{\bar{W}_{Cpk:Mpk}} \quad \text{Eq. (3);}$$

Where L^* is dimensionless lag, Loc_{Cpk} is the location of peak curvature, Loc_{Mpk} is the location of peak migration rate, and $\bar{W}$ is the ensemble mean channel width between the two peaks.

We evaluated the magnitude and variability of these lags using summary statistics and histograms of the offsets. We computed the derivatives of curvature and migration and applied the same process to identify paired inflections in curvature and migration.

Inflections reflected where the rate of change in curvature and migration were highest along the profile, and were a distinct set of data with which to evaluate spatial lags. As before, the distances between paired inflections were normalized to average channel width between the paired inflections, thereby providing an independent test to evaluate the consistency in magnitude and variability of spatial lags.

Each peak in meander migration occurred downstream of a point at which curvature was zero, representing the initiation of the current meander bend and development of asymmetrical flow that increases shear stress along the outer bank (Furbish, 1988). While flow is not perfectly symmetrical at the location of zero curvature, it is a reasonable approximation of where the high-flow velocity path transitions from one bank to the other. We calculated cumulative upstream curvature as the sum of curvatures between the location of zero curvature (yellow points, Fig. 4-3B) and the peak in migration (e.g., green-line segment, Fig. 4-3B).

Similar to previous studies (Ikeda et al., 1981; Howard and Knutson 1984), we used an exponential decay function to weight curvature values based on distance upstream from the meander migration rate peak. We then summed these weighted values, calculating cumulative upstream curvature as:

$$CC_{us} = \sum C_i \cdot \frac{1}{e^{-\lambda d_i}}, \qquad \text{Eq. (4)}$$

where C_i is the curvature at point i, d_i is the upstream distance of point i, and λ is a weighting coefficient. The weighting coefficient, λ, was set to ensure that a weight of 0.01 was reached at a point 300 meters upstream (~6 channel widths) or at the location of zero curvature, whichever was reached first. Beyond which, there is no reason to expect nonlocal/upstream influences to continue.

We manually categorized bank erosivity at each 10-meter increment along the Root River as ‘constricted’, ‘resistance’, or ‘freely meandering’ (2, 1, and 0, respectively) based on the outer, resisting bank. Segments classified as ‘constricted’ were confined by a valley constriction, colluvium, or a human embankment/structure (e.g., bridge crossing) along the outer bank. Reaches with resistance were bounded by vegetation dense enough to mask the underlying ground or streambanks, and were presumed to be less erosive than ‘freely meandering’ reaches that lacked banks strengthened by root systems (Abeernethy and Rutherfurd, 2000; Micheli and Kirchner, 2002; Peixoto et al., 2009). With ranked values of resistance, we test whether reaches with higher cumulative resistance had greater lag distances.

We also cross-correlated series of moving windows containing a subset of the curvature and migration profiles (‘scipy.signal.correlate’) to evaluate the spatially-lagged relationship between migration and curvature signals, rather than analyzing only individual points (i.e., peaks and inflections). For each window, the two series were continually displaced relative to one another and cross-correlated at each degree of displacement. The displacement with highest signal cross-correlation was interpreted as the optimal lag/offset between curvature and migration rate signals. The lag distance (meters) was normalized to the mean channel width within the moving window. We tested window sizes spanning 2 to 20 channel widths (100-1000 meters) to encompass distances within a ‘geomorphically reasonable’ range.

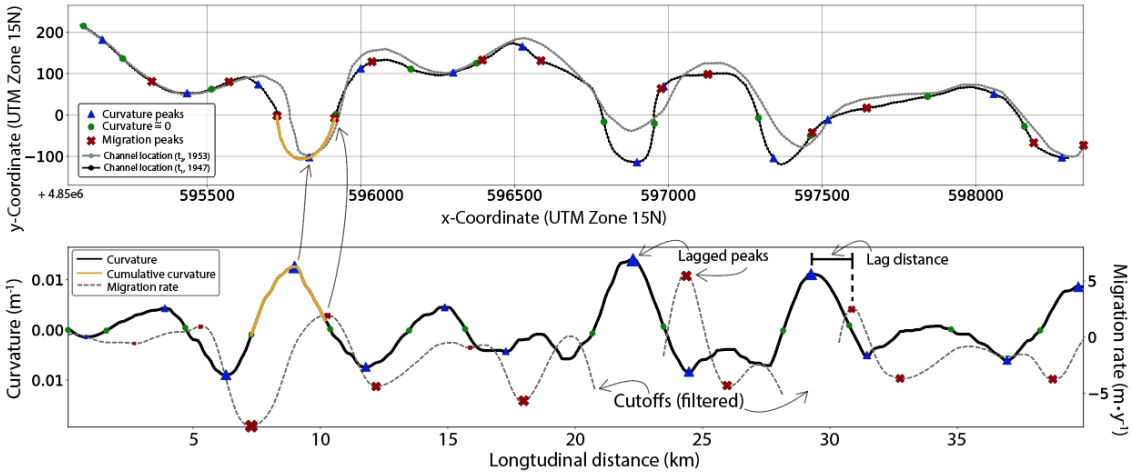

Fig. 4-4. An example of curvature and migration profiles plotted alongside their local maxima and minima (blue triangles = curvature peaks, red Xs = migration peaks). Locations of zero curvature are plotted as green points. Lag distances between peaks were calculated as the longitudinal difference, divided by the local average river width. We highlight one example (thick-golden line) to illustrate the length over which cumulative curvature was calculated as the weighted sum of curvature. Summed curvature calculations start at the nearest upstream location of zero curvature, and end at the peak meander migration rate. Channel cutoffs were manually filtered and discarded prior to the analyses.

3.3. Distinguishing the form of curvature-migration relationships

Prior literature has debated whether curvature-migration relationships are monotonic (i.e., migration continuously increases with increasing curvature), or peaked (i.e., exhibiting a maximum at low to moderate curvature values; R/W of 2-3, or W/R ~0.3-0.4). In order to frame results in the context of previous studies, we first plot bend-averaged values of R/W and migration (e.g., Hickin and Nanson, 1975; Nanson and Hickin 1983; Hudson and Kesel, 2000; Hooke, 2003; Güneralp and Rhoads, 2008; Nicoll and Hickin, 2010). Subsequently, we directly evaluate the relationship between migration and dimensionless curvature (W/R) to consider the form of the relationship between curvature and migration. We account for the phase lags in curvature and migration signals by plotting lagged local values (peaks and inflections) of curvature and migration.

In doing so, we can (1) more clearly evaluate the relationship between curvature and migration, rather than the radius of curvature (R), and (2) account for spatial lags/offsets between curvature and migration (Furbish; 1989, 1991). If plots from both approaches illustrate a peak in migration at R/W ~2-3 (equivalent to 0.3-0.4 W/R), it suggests that neither measurement scale, nor accounting for spatial lags, alter the peaked relationship found by Hickin and Nanson (1975). Conversely, if plotting the local-scale lagged values of curvature and migration illustrates a monotonic, direct trend, while the bend-averaged approach exhibits a peaked envelope curve, it provides empirical support that (1) spatial measurement scale directly influences interpretations regarding the form of the curvature-migration relationship (Furbish, 1988; Howard and Knutson, 1984; Sylvester et al., 2019) and (2) migration rates continuously increase with curvature.

4. Results

4.1. Basic data attributes and descriptions

For both the Root and Minnesota Rivers, dimensionless curvature values are normally distributed around 0, with a total range of approximately -1 to 1 (Fig. 4-4A). Migration rates follow a long-tailed right-skewed distribution (i.e., many small rates and decreasing numbers of higher rates) with median values on the order of 0.5-1.5 m/yr and maximum rates reaching approximately 15 m/y for both rivers. For the 25-km Root River study reach, mean channel width varies from 47-55 meters from year to year, with the narrowest and broadest cross-sections being 19 and 125 meters, respectively. The mean width of the Minnesota River increased from 70 meters to 102 meters throughout the period of study (1937-2013).

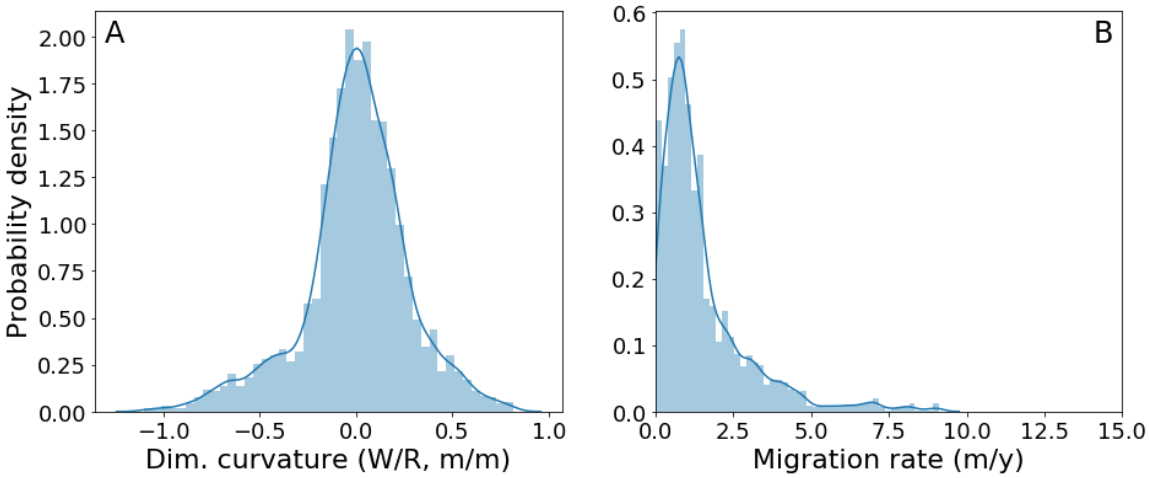

Fig. 4-5. (left) Distribution of dimensionless curvature along the Root River, derived from imagery obtained in 1981. (right) Distribution of Root River migration rates measured between 1981 and 1991.

Our final set of analyses consisted of 371 paired peaks in migration and curvature for the Root River, and 873 for the Minnesota River. These numbers are the total count after removing cutoffs and values below the level of detection. There are an additional 585 paired inflections for the Root River, and 873 along the Minnesota River, used to analyze offset between migration and curvature. Because cross-correlation analyses do not rely solely on peaks or inflections, every measurement (excluding cutoffs and measurements below the level of detection) along the study reaches is used, totaling approximately 7,200 and 86,000 for the Root and Minnesota River study reaches.

4.2. Optimizing search radius of cross-correlation analyses

For the Root River, the optimal window size for cross-correlation analysis is 600 meters (approximately 12× mean channel width), at which point, subsequent increases in window size do not change results. Narrower windows were not sufficiently wide to capture the optimized lag distance, which is evidenced by a constant lag distance

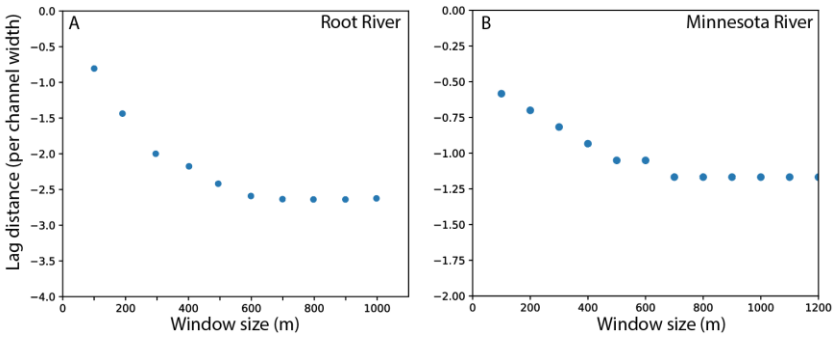

Fig. 4-6. A range of window sizes were tested as input for the cross-correlation analysis. The optimal window size was chosen as the beginning of the sill, which started at 600-meter and 800-meter search windows for the Root and Minnesota Rivers, respectively. This ensured that the window was wide enough to find the optimal lag, but was not excessively large to search beyond relevant signals.

beginning at 600 meters (Fig. 4-5a). For the Minnesota river, the optimized lag distance is 800 meters, approximately 9-12 channel widths (Fig. 4-5b). Thus, windows for the cross-correlation analysis are 600 and 800 meters, which reduces computation time (compared with larger windows) while ensuring the optimal lag distance is found. The windows are consistent with our observations of lag distances between the curvature and migration signals, made while manually matching peaks and inflections (Fig. 4-3).

4.3. Magnitude and variability of lags between signals of curvature and migration

The results of cross-correlations indicate that shifting curvature signals downstream by 2.3 (± 1.2) channel widths optimizes cross-correlation coefficients for the Root River (Figs. 4-6a, 4-6b), which was nearly identical to signal offset of 2.2 (± 1.3) for the Minnesota River (Figs. 4-6c, 4-6d). All cross-correlation coefficients with sub-optimal cross-correlation coefficients ($r<0.25$) were removed from the analysis prior to calculating the mean. Such values skew the mean value and were irrelevant for discerning an optimal phase lag, which should be based on strong correlation coefficients. For the

Minnesota River, we distinguish cross-correlation data from the downstream reach with low-sediment supply as red points (Fig. 4-6c). Partitioning the data in this way revealed that 94% of cross-correlations along the reach with low bedload sediment supply (downstream of Belle Plaine) had low signal matching (<0.25), compared to reaches with high bedload sediment supply along the upper Minnesota River study reach (70%). In the Root River, only 50% of the cross-correlations exhibited low signal matching. The reduction of signal correlation in the downstream reach (low bedload sediment supply) of the Minnesota River suggests that without significant sediment supply for point bar growth, signal similarity is greatly diminished. In other words, the relationship between migration rates and channel curvature, using bend-averaged or spatially explicit and lagged measurements, is greatly diminished in reaches where bedload sediment supply is low relative to transport capacity and therefore the channel does not establish marked asymmetry in bed morphology and flow dynamics.

The magnitude and variability for lag distances in peaks (2.6 ± 1.4) and inflections (2.8 ± 1.6) along the Root River were remarkably similar to each other (Figs. 4-7a, 4-7b), and to the phase lags in cross-correlations (2.3 ± 1.2). The results were also consistent with the lag distances for peaks (2.5 ± 1.4) and inflections (2.3 ± 1.2) along both reaches of the Minnesota River (Figs. 4-7c, 4-7d). The consistency in lag distances suggests that peak stress along the outer bank is roughly 2.5 to 3 channel widths downstream of the apex of a meander bend. Of the 873 paired peaks found along the Minnesota River, 80% (693) of the peaks were obtained along the high bedload sediment transport (upstream) reaches. The lack of paired peaks is supported by a loss in signal similarity between migration rates and channel curvature for reaches without significant

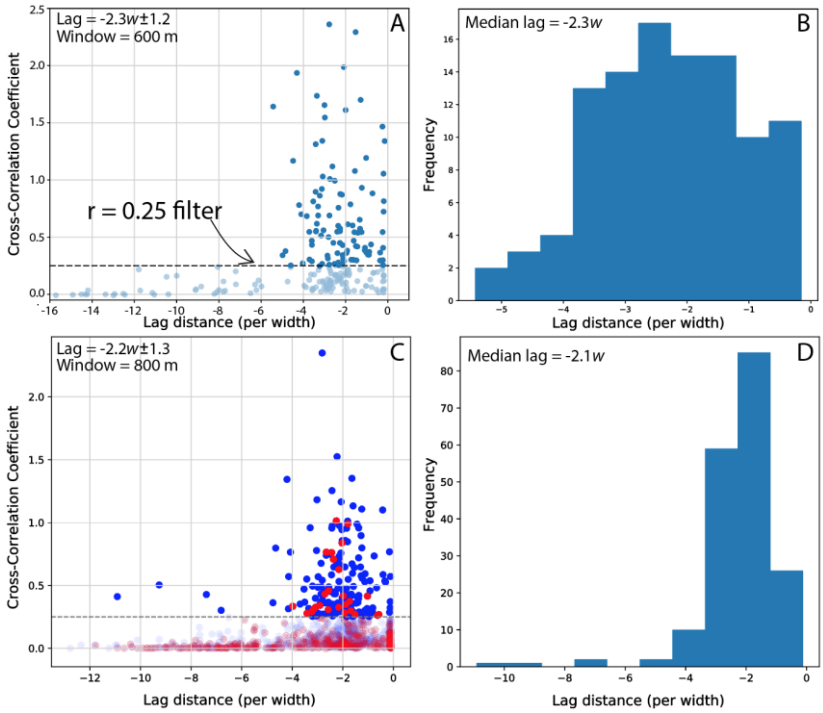

Fig. 4-7. Scatterplot and histogram showing the distribution of lag distances between curvature and migration signals for the Root (A & B) and Minnesota (C & D) River. Similar mean and median lags of -2.2 to -2.3 channel widths for both rivers indicate that the signal of migration is typically a distance of 2.3 channel widths downstream of a correlated signal in curvature (Fig. 4-3). We filtered cross-correlations below 0.25 (transparent blue points) that skewed the central tendency and reflected reaches with weak signal matching due to local conditions. The vast majority (94%) of cross-correlations in the Minnesota River reach with low sediment transport (red-points, plot C) had very low signal matching, indicated by coefficients below 0.25.

bedload sediment supply (Fig. 4-8). In reaches with excess sediment supply (top plot, Fig. 4-8), the profile of migration rates are very nearly a translated form of the channel curvature trends. However, profiles of channel curvature and migration rates exhibit no similarity in the absence of ample bedload sediment supply (bottom plot, Fig. 4-8).

4.4. Variables affecting spatial lag in the curvature-migration relation

We hypothesized that variations in the lag between channel curvature and migration rates would be a function of local curvature, upstream cumulative curvature, or

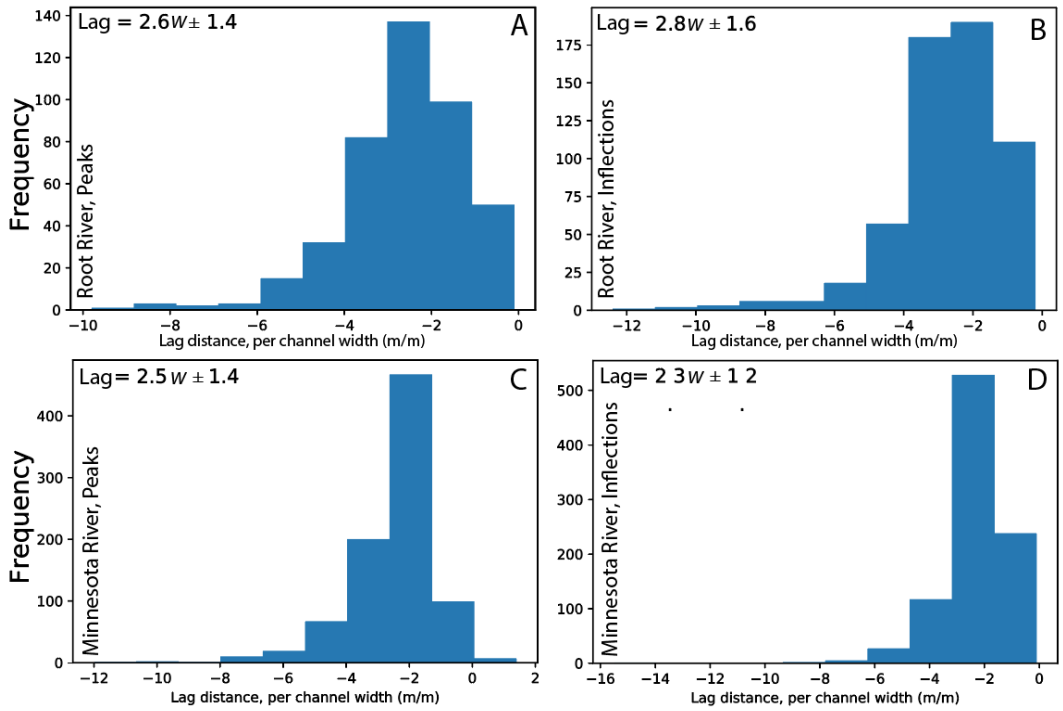

Fig. 4-8. Histograms of lag distances between peaks (A/C) and inflections (B/D) in curvature and migration for the Root (top) and Minnesota (bottom) Rivers. Lag distances (meters) were scaled to channel width for simpler interpretation and comparability with other systems. Similar to results of cross-correlations, lag distances between curvature and migration were typically 2.6x (peaks) to 2.8x (inflections) channel width.

bank erosivity. Neither curvature nor upstream cumulative curvature had any significant grass, bush/shrub, tree), bank material (e.g., floodplain, terrace, colluvium), and explanatory power in the variance of the measured lag distances. We expect that variability in lag distances is influenced in part, by differences in vegetation type (e.g., channel constrictions (valley impingements, concrete embankments). While available data did not allow for quantitative constraints on bank erosivity, the manual categorical classifications along the Root River did not suggest that erosivity increased lag distance. Observations of partially confined reaches suggest that migration trajectories are shifted farther downstream for constricted bends (Inset 1, Fig. 4-9) compared to freely meandering bends (Inset 2).

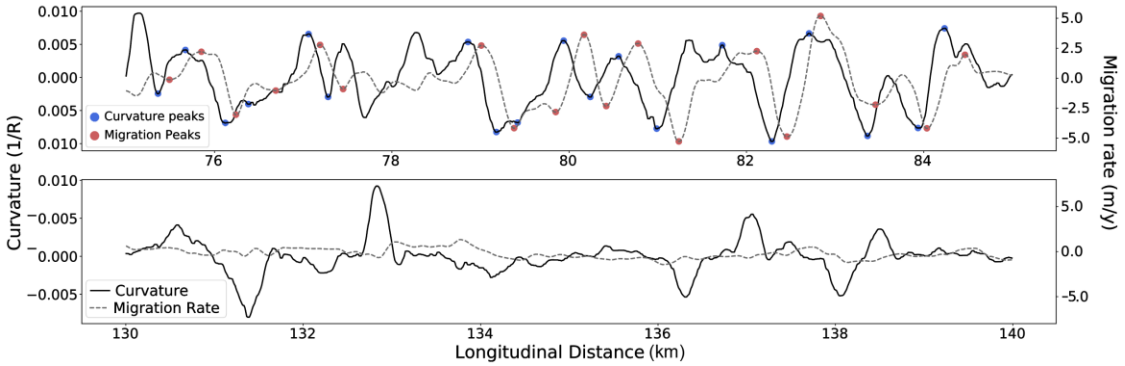

Fig. 4-9. Longitudinal profiles of migration rate (grey-dashed lines) and curvature (solid black lines) for two distinct 10-km reaches of the 180-km Minnesota River study area. The top profile is from the upstream portion of our study reach with steeper slopes and high sediment supply of coarse-grained sediments (sand and gravel). The lower profile is from the downstream reach with lower slopes and sediment supply of fine sand, silt, and clay. (Top) Curvature and migration signals show strong spatially lagged signals and have many paired peaks (red and blue points). (Bottom) Despite similar curvature values and variability as the top reach, the migration rates are nearly zero, and lack any resemblance of a lagged signal.

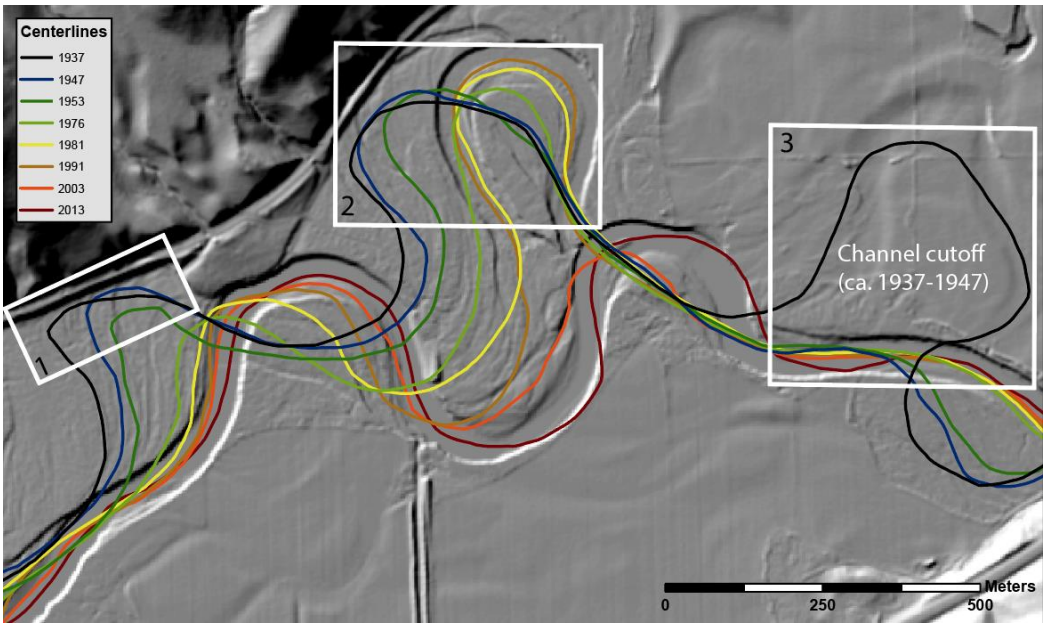

Fig. 4-10. Planform view of channel changes from 1937-2013 (black to maroon sequence). Inset areas illustrating: (1) a valley wall constriction is inhibiting river migration trajectories directly downstream of the bend apex, resulting in migration pulses downstream; (2) typical trajectory of peak migration shifted downstream of the apex in curvature, resulting in a downward shift in migration; (3) example of a channel cutoff that occurred between 1937 (black) and 1947 (blue).

4.3. The structure of the curvature-migration relation

It remains to be determined whether measurements of local-curvature and migration rates versus bend-averaged curvature and migration rates yield different relationship forms. On one hand, we expect migration rates should continually increase with curvature (Ikeda et al., 1981; Howard and Knutson, 1984; Furbish, 1988; Sylvester et al., 2019), while many empirical studies suggest and illustrate an envelope of migration rates that generally decrease at the highest bend-averaged curvatures (Hickin and Nanson 1975, 1984; Hudson and Kesel, 2000; Hooke, 2003; Güneralp and Rhoads, 2008; Nicoll and Hickin, 2010). We set out to answer whether the peaked curvature-migration curve reflects measurement scales that smooth over sub-meander bend variability and fail to consider the spatial lag between peak curvature and migration values.

We begin by plotting bend-averaged, normalized, radius of curvature (R/W) and normalized migration rates (M/W) (Figs. 4-10a, 4-10b) As in previous empirical studies (Hickin and Nanson, 1984; Hooke, 2003; Hudson and Kesel, 2000; Nicoll and Hickin, 2010), this measurement approach results in an envelope of values that are generally scattered, with some values peaking near R/W of 2-3 (Figs. 4-10a and 4-10b). Next, we consider the trends that arise when we plot spatially lagged dimensionless curvature and normalized migration rates (Fig. 4-11), similar to Sylvester et al., (2019). For both the Root and Minnesota rivers, the relationship between channel curvature and migration rates are generally direct monotonic trends, fit reasonably well with linear regressions. Thus, differences in measurement scale and spatially explicit comparisons are enough to alter the apparent relationship between channel curvature and migration rate.

Within each study site, the relationships exhibit similar positive slopes with

intercepts at or near zero. For the Root River, regression slopes ranged from 0.1-0.2, while the Minnesota River was much lower, on the order of 0.03-0.08. Differences in sediment supply and bar size between the upper and lower study reaches of the Minnesota (blue vs. red points; Fig. 4-11b) did not explain deviations from the typical trend (e.g., most notable in the first plot of Fig. 4-11), but may reflect reaches with high bank resistance (Sylvester et al., 2019).

5. Discussion

The empirical results herein support multiple studies indicating that migration rates peak downstream of bend apices (Furbish, 1988; Howard and Knutson, 1984; Seminara, 2006; Sylvester et al., 2019). For the Root and Minnesota rivers, the lag distance between signals of curvature and migration exhibit a relatively narrow range, between 2.3-2.8 channel widths. These results fall within the range of 2.1-4.7 channel widths found for Amazonian Rivers (Sylvester et al., 2019). Importantly, our results also match experimental flume results indicating peak shear stress along the outer bank occurred 2.5 channel widths downstream of the bend apex (Fig. 4-11; Hooke, 1975). The similarity in lag distances for both study sites and previous literature suggests that the spatially lagged relationship not only holds up for meander bends, but also the entire longitudinal signals of curvature and migration. The exception to these results was along the downstream portion of the Minnesota River, which has nearly negligible bedload sediment supply relative to the upstream study reach. The lack of strong signal correlations and rare occurrence of paired peaks along this reach both suggests that curvature-migration relationships are greatly diminished without excess bedload sediment supply to support bar growth (Fig. 4-8).

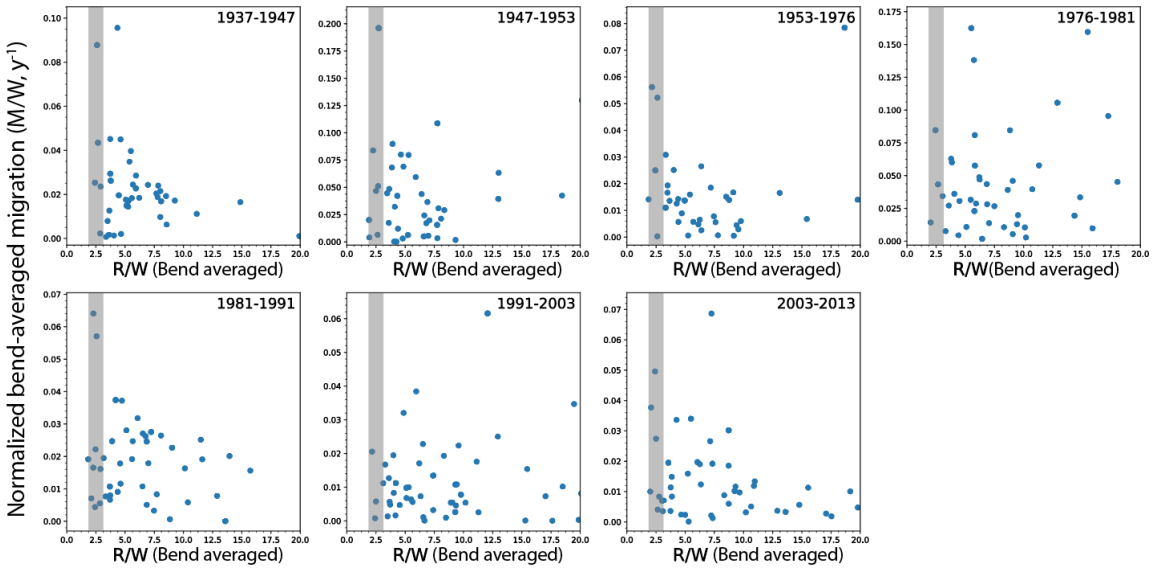

Fig. 4-11a. Bend-averaged migration and curvature plotted in accordance with Hickin and Nanson (1975) for the Root River. Few of the data peak at values near or larger than the range of R/W values (2 to 3) expected by Hickin and Nanson's envelope curve, while others are void of any strong trend. However, this approach conflates fine-scale changes in curvature by averaging over the entire bend and fails to account for lags between migration and curvature.

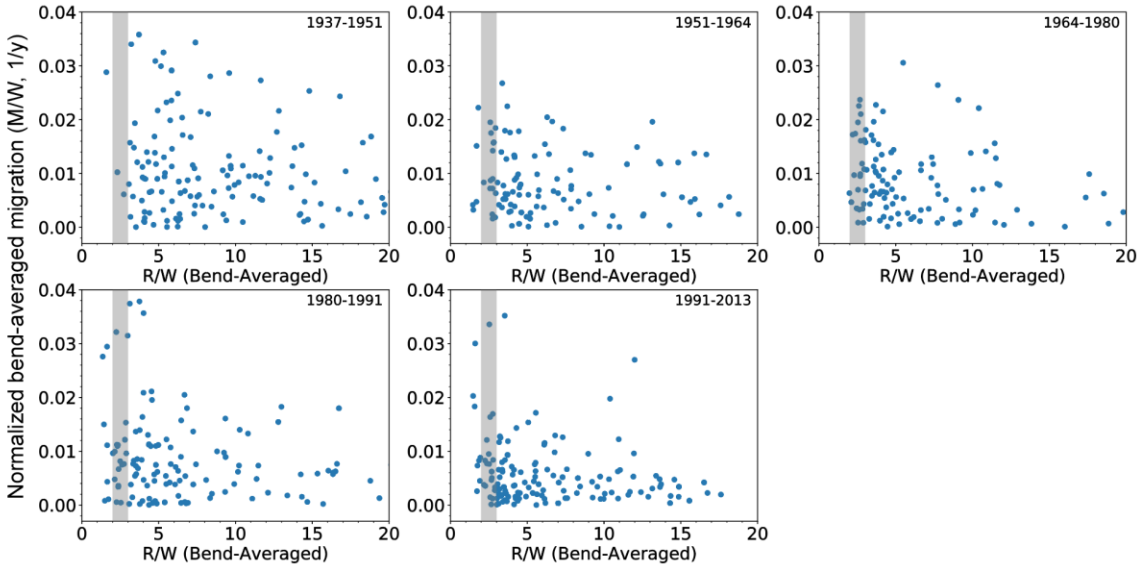

Fig. 4-11b. Bend-averaged migration and curvature plotted in accordance with Hickin and Nanson (1975) for the Minnesota River. The same description from Fig. 4-9a applies.

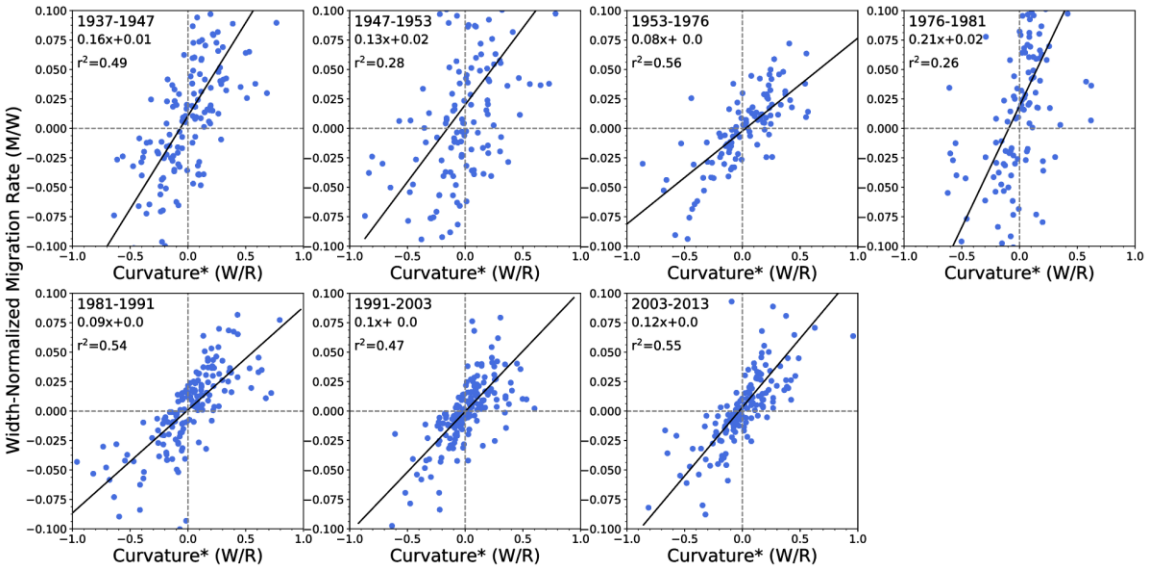

Fig. 4-12a. Relationships between dimensionless curvature (W/R) and normalized migration rates (M/W) for the Root River. All years exhibit linear trends, with similar slopes (0.1-0.2) and intercepts at or nearly 0.

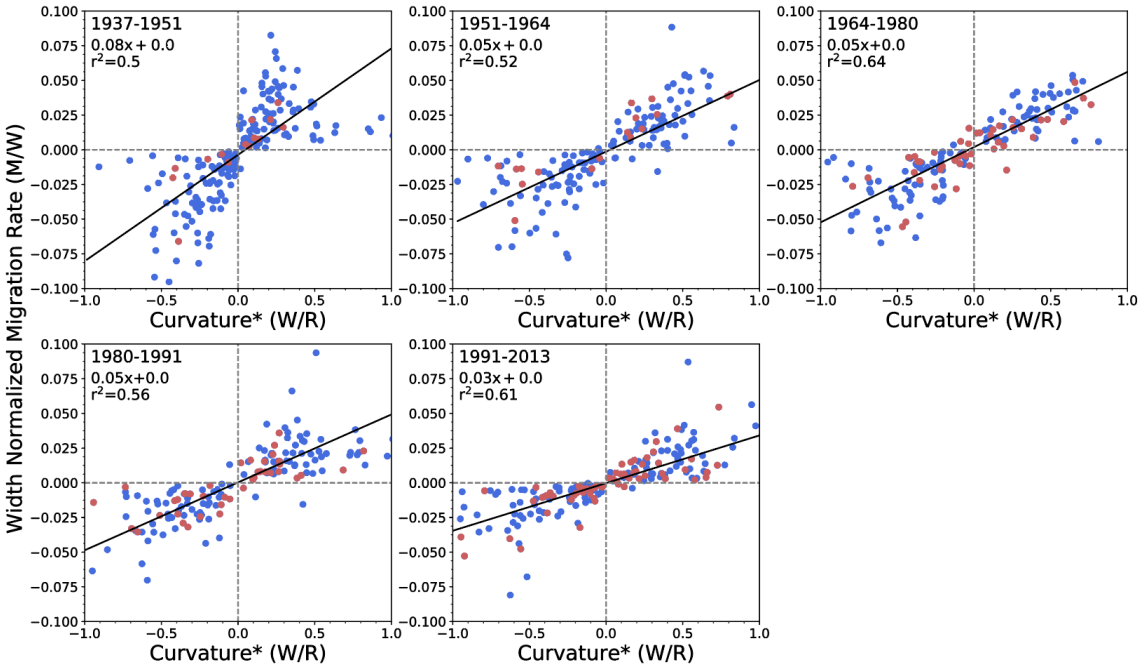

Fig. 4-12b. Relationships between dimensionless curvature (W/R) and normalized migration rates (M/W) for the Minnesota River. Most years follow linear trends, with the exception of the first plot. Red data points are for the downstream portion of the study reach where sediment transport rates were significantly lower than upstream reaches. Regressions include upstream and downstream reaches.

In this study, the use of sub-meander measurement scales shed light on the spatially lagged relation between curvature and migration. Many previous studies suggest that migration rates peak at intermediate values of meander-bend curvature (Hickin and Nanson, 1975; Nanson and Hickin 1983; Hudson and Kesel, 2000; Hooke, 2003; Güneralp and Rhoads, 2008; Nicoll and Hickin, 2010). However, these results reflect the use of bend-averaged values of curvature and migration, which smooth over variability occurring at sub-meander bend scales. Our work supports both empirical and theoretical work illustrating a direct linear relationship between curvature and migration (Furbish, 1988; Howard and Knutson, 1984; Sylvester et al., 2019) with similar slopes (0.1-0.2, Root River; and 0.03-0.08 Minnesota River) and intercepts of zero within each site. We expect that residuals in the relationship between curvature and migration rates stem from differences in bank resistance, channel bed morphology, local and upstream width-to-depth ratios, and bedload sediment supply relative to transport capacity. As channel curvature increases, the rate of increase in migration rates for the Root River are 2- to 4-fold higher than that of the Minnesota River based on the trend slopes (Figs. 4-10 and 4-11). Previous research has demonstrated the importance of migration and widening as a dominant source of sediment for the Root River (Belmont et al., 2016), which is known to have some of the steepest relationships between Q and TSS (discharge-total suspended sediment) relationships.

Lastly, this research highlights the importance of using appropriate measurement lengthscales to address questions in earth-science research. In studies of relations between channel curvature and migration rates, measurements averaged over the scale of a reach or single meander bend provide useful insights when driving mechanisms don’t

vary significantly over such scales. However, issues arise when spatial averaging obscures the spatial heterogeneity occurring at finer scales, which diminishes the opportunity to make accurate inferences of mechanisms driving migration rates. Plots comparing bend-averaged radius of curvature with migration rates contain two common features: (1) multiple migration rates can be associated with a single curvature value, and (2) migration rates fall at low radius of curvature values (e.g., Hickin and Nanson, 1984; Hooke, 1987; Hudson and Kelsel, 2000). The former arises because bend-averaged curvature smooths over variability in shear stress throughout a meander bend (Furbish, 1988, 1991). The latter reflects comparing local channel curvature and migration rate measurements, and is the result of the downstream shift of maximum migration rate relative to the bend apex (Sylvester et al., 2019). Understanding the relationship between channel curvature and migration rate will benefit from using measurement lengthscales that capture the variability in shear stress along meander bends. Analyses should compare channel curvature values with migration rates approximately 2 to 3 channel widths downstream.

The knowledge gleaned herein from studying feedbacks between channel curvature, bar geometry and sediment supply demonstrate how each plays an important role in meander migration. Our results suggest that sediment supply and bar geometry are crucial agents influencing the relationship between channel curvature and migration rates. Future work should continue to use widely-available aerial imagery and bathymetry of natural river systems to explore how the relationship between curvature and migration rates is influenced by bedload sediment supply, transport and deposition, and related factors of bar geometry and flow field dynamics. While aerial imagery has been sufficient

to highlight the differences between reaches with and without ample sediment supply, including 3-dimensional bed topography and bed-sediment sampling. In order to make mechanistic inferences and associations between these variables, measurement scales in ongoing work must be sufficiently fine to capture sub-meander scale variability in underlying physical mechanisms such as shear stress (Hooke, 1975; Dietrich et al., 1979; and Seminara, 2006).

References

Abernethy, B., Rutherfurd, I.D., 2000. The effect of riparian tree roots on the mass-stability of riverbanks. Earth Surface Processes and Landforms 25, 921–937. https://doi.org/10.1002/1096-9837(200008)25:9<921::AID-ESP93>3.0.CO;2-7

Begin, Z.B., 1981. Stream Curvature and Bank Erosion: A Model Based on the Momentum Equation. The Journal of Geology 89, 497–504. https://doi.org/10.1086/628610

Belmont, P., 2011. Floodplain width adjustments in response to rapid base level fall and knickpoint migration. Geomorphology 128, 92–102. https://doi.org/10.1016/j.geomorph.2010.12.026

Belmont, P., Dogwiler, T., Kumarasamy, K., 2016. An integrated sediment budget for the Root River watershed, southeastern Minnesota., Final Report to the Minnesota Department of Agriculture. Minnesota Department of Agriculture, Minnesota.

Belmont, P., Gran, K.B., Schottler, S.P., Wilcock, P.R., Day, S.S., Jennings, C., Lauer, J.W., Viparelli, E., Willenbring, J.K., Engstrom, D.R., Parker, G., 2011. Large shift in source of fine sediment in the Upper Mississippi River. Environmental Science & Technology 45, 8804–8810. https://doi.org/10.1021/es2019109

Brice, J., C., 1974. Evolution of Meander Loops. GSA Bulletin 85, 581–586. https://doi.org/10.1130/0016-7606(1974)85<581:EOML>2.0.CO;2

Carson, M.A., Lapointe, M.F., 1983. The Inherent Asymmetry of River Meander Planform. The Journal of Geology 91, 41–55. https://doi.org/10.1086/628743

Clayton, L., Moran, S.R., 1982. Chronology of late wisconsinan glaciation in middle North America. Quaternary Science Reviews 1, 55–82. https://doi.org/10.1016/0277-3791(82)90019-1

Constantine, J.A., Dunne, T., Ahmed, J., Legleiter, C., Lazarus, E.D., 2014. Sediment supply as a driver of river meandering and floodplain evolution in the Amazon Basin. Nature Geoscience 7, 899–903. https://doi.org/10.1038/ngeo2282

Crosato, A., 2009. Physical explanations of variations in river meander migration rates from model comparison. Earth Surface Processes and Landforms 34, 2078–2086. https://doi.org/10.1002/esp.1898

Davis, W.M., 1902. River Terraces in New England, in: Geographical Essays. Boston, Ginn, and Co., pp. 514–586.

Dietrich, W.E., Smith, J.D., Dunne, T., 1979. Flow and Sediment Transport in a Sand Bedded Meander. The Journal of Geology 87, 305–315. https://doi.org/10.1086/628419

Donovan, M., Belmont, P., 2019. Timescale Dependence in River Channel Migration Measurements. Earth Surface Processes and Landforms. https://doi.org/10.1002/esp.4590

Donovan, M., Miller, A., Baker, M., 2016. Reassessing the role of milldams in Piedmont floodplain development and remobilization. Geomorphology 268, 133–145. https://doi.org/10.1016/j.geomorph.2016.06.007

Donovan, M., Miller, A., Baker, M., Gellis, A., 2015. Sediment contributions from floodplains and legacy sediments to Piedmont streams of Baltimore County, Maryland. Geomorphology 235, 88–105. https://doi.org/10.1016/j.geomorph.2015.01.025

Einstein, A., 1926. Die Ursache der Mäanderbildung der Flußläufe und des sogenannten Baerschen Gesetzes - “The cause of the formation of meanders in the courses of rivers and of the so called Baer’s law.” Die Naturwissenschaften 14, 223–224. https://doi.org/10.1007/BF01510300

Furbish, D.J., 1991. Spatial autoregressive structure in meander evolution. GSA Bulletin 103, 1576–1589. https://doi.org/10.1130/0016-7606(1991)103<1576:SASIME>2.3.CO;2

Furbish, D.J., 1988. River-bend curvature and migration: How are they related? Geology 16, 752–755. https://doi.org/10.1130/0091-7613(1988)016<0752:RBCAMH>2.3.CO;2

Gaeuman, D., Symanzik, J., Schmidt, J.C., 2005. A Map Overlay Error Model Based on Boundary Geometry. Geographical Analysis 37, 350–369. https://doi.org/10.1111/j.1538-4632.2005.00585.x

Gran, K.B., Finnegan, N., Johnson, A.L., Belmont, P., Wittkop, C., Rittenour, T., 2013. Landscape evolution, valley excavation, and terrace development following abrupt postglacial base-level fall. Geological Society of America Bulletin 125, 1851–1864. https://doi.org/10.1130/B30772.1

Güneralp, İ., Marston, R.A., 2012. Process–form linkages in meander morphodynamics: Bridging theoretical modeling and real world complexity. Progress in Physical Geography: Earth and Environment 36, 718–746. https://doi.org/10.1177/0309133312451989

Güneralp, İ., Rhoads, B.L., 2011. Influence of floodplain erosional heterogeneity on planform complexity of meandering rivers. Geophysical Research Letters 38, n/a-n/a. https://doi.org/10.1029/2011GL048134

Güneralp, İ., Rhoads, B.L., 2009. Empirical analysis of the planform curvature-migration relation of meandering rivers. Water Resources Research 45. https://doi.org/10.1029/2008WR007533

Güneralp, İ., Rhoads, B.L., 2008. Continuous Characterization of the Planform Geometry and Curvature of Meandering Rivers: Planform Geometry and Curvature of Meandering Rivers. Geographical Analysis 40, 1–25. https://doi.org/10.1111/j.0016-7363.2007.00711.x

Gurnell, A.M., Downward, S.R., Jones, R., 1994. Channel planform change on the river dee meanders, 1876–1992. Regulated Rivers: Research & Management 9, 187–204. https://doi.org/10.1002/rrr.3450090402

Hickin, E., Nanson, G., 1984. Lateral Migration Rates of River Bends. J. Hydraul. Eng. 110, 1557–1567. https://doi.org/10.1061/(ASCE)0733-9429(1984)110:11(1557)

Hickin, E.J., Nanson, G.C., 1975. The Character of Channel Migration on the Beatton River, Northeast British Columbia, Canada. GSA Bulletin 86, 487–494. https://doi.org/10.1130/0016-7606(1975)86<487:TCOCMO>2.0.CO;2

Hooke, J., 2003. River meander behaviour and instability: a framework for analysis: River meander behaviour and instability. Transactions of the Institute of British Geographers 28, 238–253. https://doi.org/10.1111/1475-5661.00089

Hooke, R.L.B., 1975. Distribution of Sediment Transport and Shear Stress in a Meander Bend. The Journal of Geology 83, 543–565. https://doi.org/10.1086/628140

Howard, A., 1996. Modelling Channel Evolution and Floodplain Morphology, in: Floodplain Processes. pp. 15–62.

Howard, A.D., Knutson, T.R., 1984. Sufficient conditions for river meandering: A simulation approach. Water Resources Research 20, 1659–1667. https://doi.org/10.1029/WR020i011p01659

Hudson, P.F., Kesel, R.H., 2000. Channel migration and meander-bend curvature in the lower Mississippi River prior to major human modification. Geology 28, 531–534. https://doi.org/10.1130/0091-7613(2000)28<531:CMAMCI>2.0.CO;2

Ikeda, S., Parker, G., Sawai, K., 1981. Bend theory of river meanders. Part 1. Linear development. Journal of Fluid Mechanics 112, 363. https://doi.org/10.1017/S0022112081000451

Jennings, C.E., 2010. Draft Digital Reconnaissance Surficial Geology and Geomorphology of the Le Sueur River Watershed (Blue Earth, Waseca, Faribault, and Freeborn Counties in South-Central MN) (No. Open File Report 10-03), Map, Report, and Digital Files. Minnesota Geological Survey, Minnesota.

Kasvi, E., Laamanen, L., Lotsari, E., Alho, P., 2017. Flow Patterns and Morphological Changes in a Sandy Meander Bend during a Flood—Spatially and Temporally Intensive ADCP Measurement Approach. Water 9, 106. https://doi.org/10.3390/w9020106

Kelly, S., Belmont, P., 2018. High Resolution Monitoring of River Bluff Erosion Reveals Failure Mechanisms and Geomorphically Effective Flows. Water 10, 394. https://doi.org/10.3390/w10040394

Lauer, J.W., 2007. Channel Planform Statistics Toolbox. National Center for Earth-Surface Dynamics, University of Minnesota.

Lauer, J.W., Echterling, C., Lenhart, C., Belmont, P., Rausch, R., 2017. Air-photo based change in channel width in the Minnesota River basin: Modes of adjustment and implications for sediment budget. Geomorphology 297, 170–184. https://doi.org/10.1016/j.geomorph.2017.09.005

Lauer, J.W., Parker, G., 2008. Net local removal of floodplain sediment by river meander migration. Geomorphology 96, 123–149. https://doi.org/10.1016/j.geomorph.2007.08.003

Lenhart, C.F., Titov, M.L., Ulrich, J.S., Nieber, J.L., Suppes, B.J., 2013. The role of hydrologic alteration and riparian vegetation dynamics in channel evolution along the lower Minnesota River. Transactions of the American Society of Agricultural and Biological Engineers, Erosion and Landscape Evolution 56, 549–561.

Leopold, L.B., Wolman, M.G., 1960. River Meanders. GSA Bulletin 71, 769–793. https://doi.org/10.1130/0016-7606(1960)71[769:RM]2.0.CO;2

Lepper, K., Fisher, T.G., Hajdas, I., Lowell, T.V., 2007. Ages for the Big Stone Moraine and the oldest beaches of glacial Lake Agassiz: Implications for deglaciation chronology. Geology 35, 667. https://doi.org/10.1130/G23665A.1

Libby, D., J., 2017. Assessing Historical Planform Channel Change in an Altered Watershed with Quantification of Error and Uncertainty Present in a GIS/Aerial Photography-based Analysis; Case Study: Minnesota River, Minnesota, USA (Thesis). Minnesota State University, Mankato, Mankato, MN.

Lisiecki, L.E., Lisiecki, P.A., 2002. Application of dynamic programming to the correlation of paleoclimate records: DYNAMIC PROGRAMMING SIGNAL CORRELATION. Paleoceanography 17, 1-1-1–12. https://doi.org/10.1029/2001PA000733

Martinelli, LuizA., Victoria, ReynaldoL., Devol, AllanH., Richey, JeffreyE., Forsberg, BruceR., 1989. Suspended sediment load in the Amazon basin: An overview. GeoJournal 19. https://doi.org/10.1007/BF00176907

Matsch, C.L., 1983. River Warren, the southern outlet of Lake Agassiz, in: Teller, J.T., Clayton, L. (Eds.), Glacial Lake Agassiz, Special Paper. Geological Society of Canada, Canada, pp. 232–244.

Micheli, E.R., Kirchner, J.W., 2002. Effects of wet meadow riparian vegetation on streambank erosion. 1. Remote sensing measurements of streambank migration and erodibility. Earth Surface Processes and Landforms 27, 627–639. https://doi.org/10.1002/esp.338

Milliman, J.D., Meade, R.H., 1983. World-Wide Delivery of River Sediment to the Oceans. The Journal of Geology 91, 1–21. https://doi.org/10.1086/628741

Morais, E.S., Rocha, P.C., Hooke, J., 2016. Spatiotemporal variations in channel changes caused by cumulative factors in a meandering river: The lower Peixe River, Brazil. Geomorphology 273, 348–360. https://doi.org/10.1016/j.geomorph.2016.07.026

Motta, D., Abad, J.D., Langendoen, E.J., Garcia, M.H., 2012. A simplified 2D model for meander migration with physically-based bank evolution. Geomorphology 163–164, 10–25. https://doi.org/10.1016/j.geomorph.2011.06.036

Nicoll, T.J., Hickin, E.J., 2010. Planform geometry and channel migration of confined meandering rivers on the Canadian prairies. Geomorphology 116, 37–47. https://doi.org/10.1016/j.geomorph.2009.10.005

Patnaik, M., Patra, K.C., Khatua, K.K., Mohanty, L., 2014. Modelling boundary shear stress in highly sinuous meandering channels. ISH Journal of Hydraulic Engineering 20, 161–168. https://doi.org/10.1080/09715010.2013.860733

Peixoto, J.M.A., Nelson, B.W., Wittmann, F., 2009. Spatial and temporal dynamics of river channel migration and vegetation in central Amazonian white-water floodplains by remote-sensing techniques. Remote Sensing of Environment 113, 2258–2266. https://doi.org/10.1016/j.rse.2009.06.015

Savitzky, Abraham., Golay, M.J.E., 1964. Smoothing and Differentiation of Data by Simplified Least Squares Procedures. Analytical Chemistry 36, 1627–1639. https://doi.org/10.1021/ac60214a047

Schottler, S.P., Ulrich, J., Belmont, P., Moore, R., Lauer, J.W., Engstrom, D.R., Almendinger, J.E., 2014. Twentieth century agricultural drainage creates more erosive rivers. Hydrological Processes 28, 1951–1961. https://doi.org/10.1002/hyp.9738

Schumm, S.A., 1965. Patterns of alluvial rivers. Annual Review of Earth and Planetary Science 13, 5–27.

Seminara, G., 2006. Meanders. Journal of Fluid Mechanics 554, 271. https://doi.org/10.1017/S0022112006008925

Shay, C.T., 1967. Vegetation history of the southern Lake Agassiz basin during the past 12,000 years, in: Life, Land, and Water: Proceedings of the 1960 Conference on Environmental Studies of the Glacial Lake Agassiz Basin. Presented at the Conference on Environmental Studies of the Glacial Lake Agassiz Basin, University of Manitoba Press, Winnipeg, Canada, pp. 231–252.

Souffront, M., 2014. Channel Adjustment and Channel-Floodplain Sediment Exchange in the Root River, Southeastern Minnesota (M.S. Thesis). Utah State University, Logan, Utah.

Stout, J.C., Belmont, P., 2013. TerEx Toolbox for semi-automated selection of fluvial terrace and floodplain features from lidar. Earth Surface Processes and Landforms 39, 569–580. https://doi.org/10.1002/esp.3464

Stout, J.C., Belmont, P., Schottler, S.P., Willenbring, J.K., 2014. Identifying Sediment Sources and Sinks in the Root River, Southeastern Minnesota. Annals of the Association of American Geographers 104, 20–39. https://doi.org/10.1080/00045608.2013.843434

Sun, T., Meakin, P., Jøssang, T., Schwarz, K., 1996. A Simulation Model for Meandering Rivers. Water Resources Research 32, 2937–2954. https://doi.org/10.1029/96WR00998

Sylvester, Z., Durkin, P., Covault, J.A., 2019. High curvatures drive river meandering. Geology 47, 263–266. https://doi.org/10.1130/G45608.1

Wolman, M.G., Leopold, L.B., 1957. River Flood Plains: Some Observations on Their Formation (USGS Professional Paper No. 282– C). U.S. Geological Survey, Washington, DC: US Government Printing Office.

Zhou, J., Chang, H.H., Stow, D., 1993. A model for phase lag of secondary flow in river meanders. Journal of Hydrology 146, 73–88. https://doi.org/10.1016/0022-1694(93)90270-J

CHAPTER 5

CONCLUSIONS

This research has advanced our understanding of river meander migration by evaluating the how spatiotemporal measurement scales impact river migration patterns and processes, and by laying out a framework for addressing uncertainty in measurements of river planform change. In reviewing and testing best approaches to handling uncertainty (Chapter 2), we demonstrate how spatially variable levels of detection not only retain more measurements than RMSE-based levels of detection, but also improve the quality of those measurements that are retained. Investigating the impacts of temporal (Chapter 3) and spatial (Chapter 4) scales results in two main advances, amongst others. First, channel migration rate measurements depend on the timescale over which they are measured as a result of reversals in channel migration direction. Second, the widely accepted peaked-relationship between curvature and migration is an artifact of averaging rates over the length of meander bends, not considering the spatial lag in curvature and migration signals, and failing to account for cumulative upstream curvature.

The framework established for handling uncertainty in Chapter 2 includes (1) a review and evaluation of present best practices, (2) tests of new approaches to quantify and handle uncertainty, and (3) recommendations for future work using remotely-sensed measurements of river migration and width changes. While our research focuses on river systems, the principles and approaches are applicable to research delineating boundaries or using boundaries to measure other changes, including: glacier retreat or advance, erosion or deposition along coastlines and lakeshores, changes in wetland extent,

expansion or contraction of vegetation (e.g., deforestation), cliff retreat, sea level rise due to climate change, change in aeolian depositional systems, and anthropogenic/political boundary disputes. From our results, we draw the following conclusions and recommendations:

1. Planform change measurements should span spatial intervals larger than coherent units of adjustment to avoid spatial autocorrelation.

2. Uncertainty in manual riverbank delineations is dominated by arbitrary user inconsistency rather than poor image quality (i.e., resolution, color versus grayscale, year of acquisition) or environmental conditions (i.e., shadows and vegetation cover).

3. Channel delineations should follow the vegetated boundary that best approximates bankfull width, whenever possible, to avoid inconsistency along ambiguous reaches.

4. Using a spatially variable level of error detection (LoD) threshold improves the quantity and quality of retained measurements relative to a uniform LoD.

5. After applying a LoD threshold, we recommend first using expert discretion to manually classify any ‘nondetect’ measurements that qualify as ‘significant’ measurements of zero (i.e., no change actually occurred).

6. Subsequently, three methods may be used for handling the remaining nondetects; Kaplan-Meier (KM) and Maximum Likelihood Estimators (MLE). The specific approach chosen for handling nondetects is contingent upon each case, but can be guided and informed by descriptions and assumptions of each method, references to external resources, and results of our river-focused analyses.

7. Finally, we encourage a focus on improving the simplicity, generalizability,

and open-source opportunities of tools and packages used for calculating river planform change and spatially variable uncertainty, thereby enabling a common platform to measure and compare results.

In Chapter 3, we explore how temporal measurement scales impact measured, compared to actual, rates of migration. Migration rates measured from aerial photographs spanning 1 to 76 years of change are used to develop a statistical model simulating channel migration and reversals. The model allows us to explore mechanisms that may cause measurement timescale to bias comparisons of migration rates measured over different intervals. Empirical and modelled data both confirm that migration rate measurements are increasingly underestimated as a function of channel reversal frequency, with insignificant effects from channel dormancy. The reversals necessarily cause an underestimation of the actual migration distance between the photos because migration is only measured as the distance captured at the fixed times of photo acquisition. Measurement bias favors the inference that contemporary channel migration rates have increased because of differences in historical versus contemporary sampling intervals. Historical aerial photographs are much less common, and thus, have broader time intervals than contemporary imagery, which is often acquired at annual timesteps. This reinforces our conclusion that authors should use caution and similar measurement intervals when interpreting fluvial changes and causal mechanisms from aerial- based measurements of channel activity. Before and after accounting for measurement bias in our data, we find no empirical evidence that the Root River has responded to increased flow with any significant change in migration rates in subsequent decades. This reinforces the notion that without an understanding of sediment supply, no simple

relationship exists between discharge and migration rates alone. Knowing that river migration measurements are timescale dependent will improve our ability to discern how river morphology responds, and is responding, to changes in flow and sediment supply.

Empirical and modelled results also demonstrate that short-term migration rate measurements (< 10 years) are dominated by high variability reflecting periodic bursts of migration, while long-term measurements (> 25 years) converge asymptotically as measurements reach a 'characteristic timescale' over which all variability is sampled and subsequent measurements are relatively constant, barring significant long-term changes. Thus, we conclude that the timescale of channel migration measurements can influence which question(s) are suitable to address. For example, without a sufficient number of short-term measurements, extrapolations will necessarily distort long-term sediment remobilization projections, sediment budgets, sediment flux estimates, and perceptions of fluvial change. Sufficiently long intervals (> 20-25 years) beyond the 'characteristic timescale' are needed to answer whether a channel has undergone significant long-term changes (i.e., new equilibrium) when compared with similarly long-term measurements. Multiple short-term measurements are necessary to sample the episodic nature of channel migration, thereby providing a more comprehensive understanding of channels' short-term response to changes in flow and sediment flux.

Chapter 4 evaluates the empirical relationships between curvature, sediment supply to channel bars, and migration rates using a fine-scale measurement strategy derived from remotely-sensed imagery for the Root and Minnesota Rivers. We focus on evaluating the phase lag between channel curvature and migration rate, and whether the correlation between these two holds without sufficient sediment supply to support bar

growth. For both the Root and Minnesota Rivers, the lag distance between signals of curvature and migration, as well as peaks and inflections, exhibits a relatively narrow range, between 2.3-2.8 channel widths. These results match experimental flume results indicating that peak shear stress along the outer bank occurs 2.5 channel widths downstream of the bend apex (Fig. 4-11; Hooke, 1975). These results also fall within the range of 2.1-4.7 channel widths, found for Amazonian Rivers (Sylvester et al., 2019). The similarity in results from cross-correlation analyses suggest not only a persistent lag distance, but a consistent correlation between the entire longitudinal signals of curvature and migration. However, this similarity does not hold for those portions of the Minnesota River with lower slopes and nominal supply of coarse bed-material sediment. The lack of strong signal correlations and rare occurrence of paired peaks along the low-supply reach both support the conclusion that curvature-migration relationships break down without sufficient sediment supply to foster point bar growth and bar-push feedbacks.

Before accounting for the phase lag between curvature and migration, plots of bend-averaged radius of curvature (R/W) against bend-averaged migration rates (M/W) exhibited a peaked relationship similar to that in previous research (Hickin and Nanson, 1975; Nanson and Hickin 1983; Hudson and Kesel, 2000; Hooke, 2003; Güneralp and Rhoads, 2008; Nicoll and Hickin, 2010). However, after accounting for lag distances, our work supports both empirical and theoretical work illustrating a direct linear relationship between curvature and migration (Furbish, 1988; Howard and Knutson, 1984; Sylvester et al., 2019).

Future work should continue to focus on evaluating the role of sediment supply and channel-bar growth in the relationship between channel curvature and migration rates

using natural river systems. Research should explore the effects of varying aspect ratios and bank resistance on the lag between curvature and migration. Sediment transport plays a key role in aspect ratios, flow dynamics, and meander bend evolution, and is thus underlying the aforementioned variables influencing lag distances. In order to make mechanistic inferences and associations between these variables and meander migration, measurement scales must be sufficiently fine to capture variability in these physical mechanisms (i.e., shear stress). Work by Hooke, (1975), Dietrich et al., (1979), and Seminara (2006) all demonstrate sub-meander scale variability in shear stresses that drive bank erosion. Averaging measurements over the scale of a meander bend obscures the spatial heterogeneity, thus diminishing the opportunity to make accurate inferences of mechanisms driving migration rate variability. The knowledge gleaned herein from studying feedbacks between channel curvature and sediment supply to channel bars demonstrate how each plays an important role in meander migration.

APPENDICES

Appendix A. Timescale dependence in channel migration rates

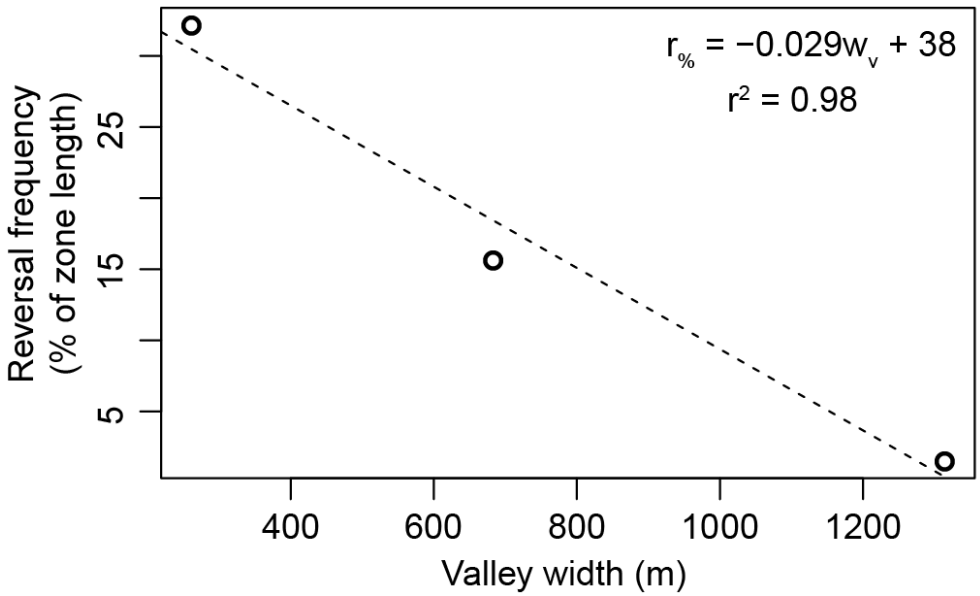

Fig. A1. A significant indirect relationship between mean valley width and the reversal frequency, expressed as both a length and percent. From left to right, each data point reflects the mean width of Zones 1, 2, and 3 (see main text, Fig. 3-1, Table 3-1).

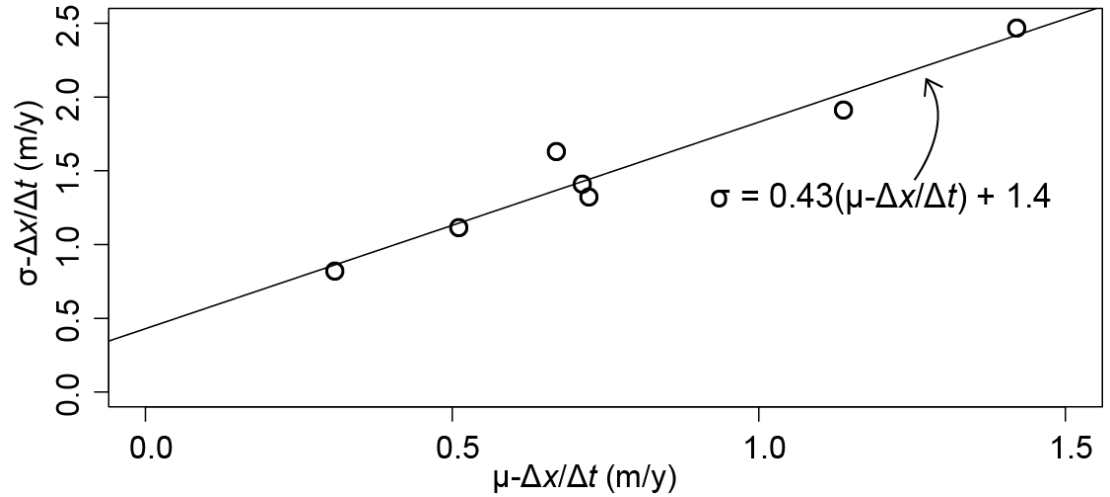

Fig. A2. Empirical relationship between the mean (μ) and variance (σ) of migration rate measurements along the Root River with $\Delta t \leq 3$. The reduced complexity model used the relation to predict variance associated with a mean value randomly selected from the range of observed means.

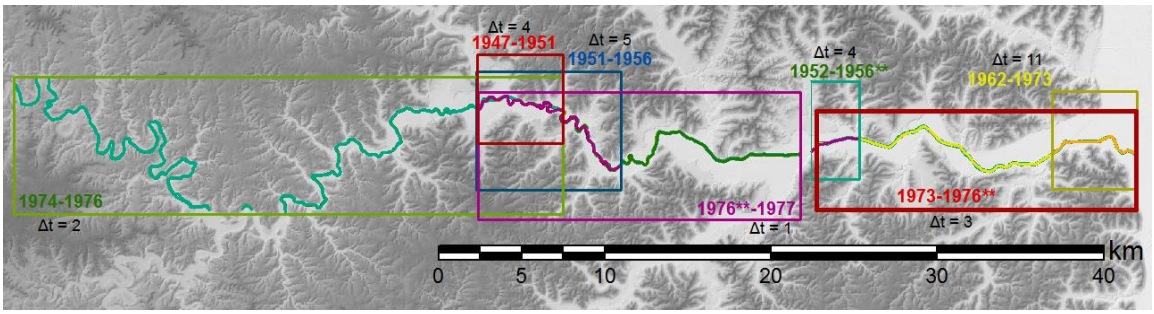

Fig. A3. Aerial view of seven reaches having historical image pairs obtained at relatively high temporal frequencies ($\Delta t \leq 5$ years and 11 years). We compared migration for these reaches with contemporary migration along the same reaches as an additional, independent line of evidence confirming whether migration had increased with time (Supporting Information Tables A3 and A4).

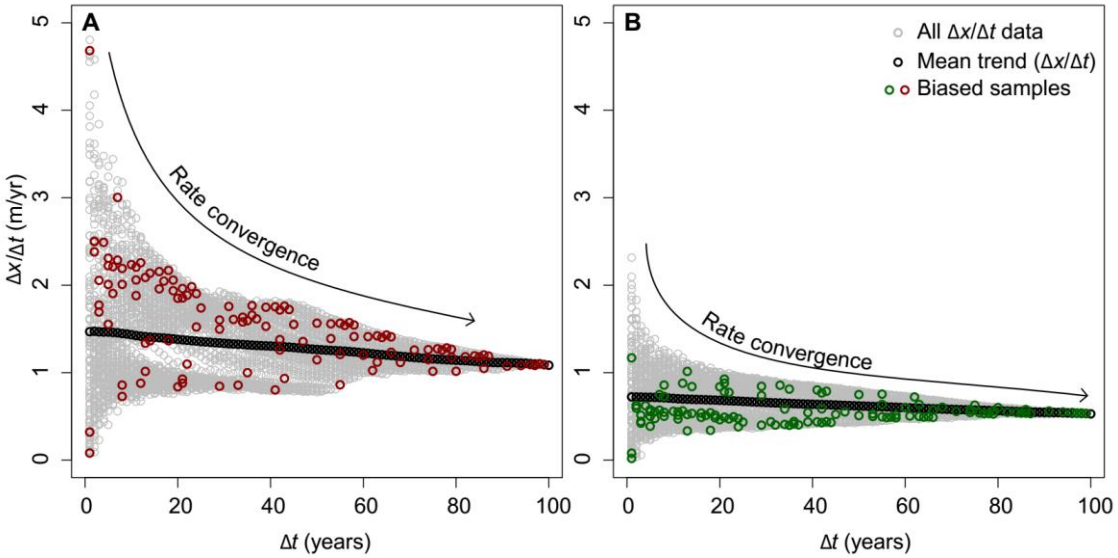

Fig. A4. Model scenarios with increased (A) and decreased (B) were subjected to biased sampling that mimicked the majority of datasets with low Δt intervals dominated by contemporary rates, while historical measurements dominate longer Δt intervals. The biased samples exhibit systematic shifts above and below (values within black boxes) the unbiased trend (black points) that reflects the mean of all Δx – Δt measurement combinations (gray points).

Table A1. Results of Mann–Whitney–Wilcoxon signed rank test. Red cells indicate significant ($p < 0.05$) increase in median migration rates during contemporary image pairs (rows) relative to historical image pairs (columns). Orange and yellow indicate the same, for α-values of 0.1 and 0.2, respectively.

A.	Image years	1937-1947	1947-1953	1953-1976	1976-1981	1981-1991
Zone 1	1991-2003	1.00	1.00	1.00	1.00	1.00
	2003-2006	1.00	1.00	1.00	1.00	1.00
	2006-2008	0.97	0.97	0.91	1.00	0.95
	2008-2010	1.00	1.00	1.00	1.00	1.00
	2010-2011	1.00	1.00	1.00	1.00	1.00
	2011-2013	1.00	1.00	1.00	1.00	1.00
	2003-2013	**1.00**	**1.00**	**1.00**	**1.00**	**1.00**
Zone 2	1991-2003	1.00	1.00	0.64	1.00	1.00
	2003-2006	1.00	1.00	0.48	1.00	0.91
	2006-2008	0.92	1.00	0.10	1.00	0.47
	2008-2010	1.00	1.00	1.00	1.00	1.00
	2010-2011	1.00	1.00	0.99	1.00	1.00
	2011-2013	1.00	1.00	1.00	1.00	1.00
	2003-2013	**1.00**	**1.00**	**0.68**	**1.00**	**0.99**
Zone 3	1991-2003	1.00	1.00	1.00	1.00	1.00
	2003-2006	1.00	1.00	1.00	1.00	1.00
	2006-2008	1.00	1.00	0.99	1.00	0.91
	2008-2010	1.00	1.00	1.00	1.00	1.00
	2010-2011	0.86	0.95	0.48	1.00	0.25
	2011-2013	1.00	1.00	1.00	1.00	1.00
	2003-2013	**1.00**	**1.00**	**1.00**	**1.00**	**1.00**

H_o: Contemporary and historical migration medians are not significantly different

H_1: Contemporary migration median is significantly greater than historical.

Table A2. Kolmogorov–Smirnov test results. Red cells indicate that the distribution of migration rates for historical image pairs (columns) are not significantly less than ($p < 0.05$) migration distributions of contemporary image pairs (rows). Orange and yellow indicate the same, for α-values of 0.1 and 0.2, respectively. Row '2003–2013' (bold typeface) demonstrates that once we compare similar rates from similar measurement intervals, there are no instances of increased migration.

B.	Image years	1937-1947	1947-1953	1953-1976	1976-1981	1981-1991
Zone 1	1991-2003	1.00	1.00	1.00	1.00	1.00
	2003-2006	0.99	1.00	0.41	1.00	0.10
	2006-2008	0.07	0.47	0.01	1.00	0.00
	2008-2010	0.83	1.00	0.47	1.00	0.13
	2010-2011	0.38	0.83	0.18	0.90	0.24
	2011-2013	0.99	1.00	0.90	1.00	0.30
	2003-2013	**1.00**	**1.00**	**1.00**	**1.00**	**0.99**
Zone 2	1991-2003	1.00	0.95	0.33	0.22	0.93
	2003-2006	0.74	0.97	0.01	0.97	0.01
	2006-2008	0.31	0.93	0.00	0.97	0.00
	2008-2010	0.99	1.00	0.48	1.00	0.38
	2010-2011	0.05	0.60	0.00	0.82	0.00
	2011-2013	0.75	0.81	0.19	0.82	0.20
	2003-2013	**0.99**	**0.99**	**0.75**	**0.99**	**0.74**
Zone 3	1991-2003	1.00	1.00	1.00	1.00	1.00
	2003-2006	1.00	1.00	0.87	1.00	0.29
	2006-2008	0.97	0.99	0.12	0.99	0.00
	2008-2010	1.00	1.00	0.93	1.00	0.14
	2010-2011	0.00	0.11	0.00	0.94	0.00
	2011-2013	0.99	1.00	0.74	1.00	0.18
	2003-2013	**1.00**	**1.00**	**0.97**	**1.00**	**0.97**

H_o: Historical migration distribution is not significantly less than contemporary

H_1: Historical migration distribution is significantly less than contemporary

Table A3. Results of Mann–Whitney–Wilcoxon signed rank test for seven reach-specific comparisons between contemporary and historical rates. The seven reaches were chosen based on availability of historical image pairs with relatively short measurement intervals (Δt). Red cells indicate significant ($p < 0.05$) increase in median migration rates during contemporary image pairs (rows) relative to historical image pairs (columns). Orange and yellow indicate the same, for α-values of 0.1 and 0.2, respectively.

2. Partial Segment Direct Comparison MWW Results

A. Image years	1947-1951	1951-1956	1952-1956	1962-1973	1973-1976	1974-1976	1976-1977
1991-2003	1.00	1.00	NA	0.07	1.00	1.00	1.00
2003-2006	1.00	1.00	NA	0.00	1.00	1.00	1.00
2003-2008	1.00	1.00	NA	0.00	1.00	1.00	1.00
2003-2010	1.00	1.00	NA	0.00	1.00	1.00	1.00
2003-2011	1.00	1.00	NA	0.13	1.00	1.00	1.00
2003-2013	1.00	1.00	NA	0.36	1.00	1.00	1.00
2006-2008	1.00	1.00	NA	0.00	1.00	1.00	1.00
2006-2010	1.00	1.00	NA	0.00	1.00	1.00	1.00
2006-2011	1.00	1.00	NA	0.00	1.00	1.00	1.00
2006-2013	1.00	1.00	NA	0.00	1.00	1.00	1.00
2008-2010	1.00	1.00	NA	0.00	1.00	1.00	1.00
2008-2011	1.00	1.00	NA	0.00	1.00	1.00	1.00
2008-2013	1.00	1.00	NA	0.00	1.00	1.00	1.00
2010-2011	1.00	0.06	NA	0.00	0.83	1.00	1.00
2010-2013	1.00	1.00	NA	0.00	1.00	1.00	1.00
2011-2013	1.00	1.00	NA	0.00	1.00	1.00	1.00

H_o: Contemporary and historical migration medians are not significantly different

H_1: Contemporary migration median is significantly greater than historical.

Table A4. Kolmogorov–Smirnov test results. Red cells indicate that the distribution of migration rates for historical image pairs (columns) are not significantly less than ($p < 0.05$) migration distributions of contemporary image pairs (rows). Orange and yellow indicate the same, for α-values of 0.1 and 0.2, respectively.

2. Partial Segment Direct Comparison KS Results

B. Image years	1947-1951	1951-1956	1952-1956	1962-1973	1973-1976	1974-1976	1976-1977
1991-2003	1.00	1.00	NA	0.01	1.00	0.84	1.00
2003-2006	1.00	1.00	NA	0.00	1.00	1.00	1.00
2003-2008	1.00	1.00	NA	0.00	1.00	1.00	1.00
2003-2010	1.00	1.00	NA	0.00	1.00	1.00	1.00
2003-2011	1.00	1.00	NA	0.00	1.00	1.00	1.00
2003-2013	1.00	1.00	NA	0.04	1.00	1.00	1.00
2006-2008	1.00	0.93	NA	0.00	0.86	1.00	1.00
2006-2010	1.00	0.99	NA	0.00	1.00	1.00	1.00
2006-2011	1.00	1.00	NA	0.00	1.00	1.00	1.00
2006-2013	1.00	1.00	NA	0.00	1.00	1.00	1.00
2008-2010	1.00	0.99	NA	0.00	1.00	1.00	1.00
2008-2011	1.00	1.00	NA	0.00	1.00	1.00	1.00
2008-2013	1.00	1.00	NA	0.00	1.00	1.00	1.00
2010-2011	1.00	0.00	NA	0.00	0.70	0.88	1.00
2010-2013	1.00	1.00	NA	0.00	1.00	1.00	1.00
2011-2013	1.00	1.00	NA	0.00	1.00	1.00	1.00

H_o: Historical migration distribution is not significantly less than contemporary

H_1: Historical migration distribution is significantly less than contemporary

CURRICULUM VITAE

EDUCATION:

+ Utah State University (Logan, UT) June 2015 – Present
Ph.D. Candidate, Natural Resources- Watershed Sciences
Committee: Drs. **Patrick Belmont**, Peter Wilcock, Sarah Null, Joel Pederson, Dave Tarboton

+ University of Turku (Turku, FI) August, 2014 – June, 2015
Fulbright Exchange Researcher, Geography and Landscape Change
Collaborators: Dr. Petteri Alho, Dr. Jukka Käyhkö

+ University of Maryland- Baltimore County [UMBC] (Baltimore, MD) – 3.80 GPA
M.S., Geography and Environmental Systems, Graduated - May 2014
Thesis: Assessing the contribution of legacy sediment and mill dam storage to sediment budgets in the Piedmont of Maryland
Committee Members: Dr. Andy Miller (Chair), Dr. Allen Gellis, and Dr. Matthew Baker.
Field: Geomorphology, GIS, Fluvial Morphology, Hydrology
Top 30 Graduating Class of 2014

+ UMBC (Baltimore, MD) – 3.56 GPA
B.S., Geography and Environmental Science, Graduated - May 2011
Certificate in Geographic Information Systems
Cum Laude and Top 30 Graduating Class of 2011

PUBLICATIONS:

Donovan, M., Belmont, P., Notebaert, B., Coombs, T., Souffront, M., Larsen, P., *(Accepted)*. Accounting for uncertainty in measurements derived from remotely sensed aerial photographs. Earth-Science Reviews.

Donovan, M., Belmont, P., *In Press*. Timescale Dependence in River Channel Migration Measurements. Earth Surface Processes and Landforms.

Belmont, P., **Donovan, M.,** Brahney, J., Capito, L., Burgert, Z. (2018). Sediment Dynamics in the Bear River-Mud Lake-Bear Lake System. Sedimentology Commons.

Donovan, M., Miller, A., Baker, M., 2016. Reassessing the role of milldams in Piedmont floodplain development and remobilization. Geomorphology 268, 133–145. doi:10.1016/j.geomorph.2016.06.007

Donovan, M., Miller, A., Baker, M., Gellis, A., 2015. Sediment contributions from floodplains and legacy sediments to Piedmont streams of Baltimore County, Maryland. Geomorphology 235, 88–105. doi:10.1016/j.geomorph.2015.01.025

Harpold, A. A., Marshall, J. A., Lyon, S. W., Barnhart, T. B., Fisher, B. A., **Donovan, M.**, Brubaker, K. M., Crosby, C. J., Glenn, N. F., Glennie, C. L., Kirchner, P. B., Lam, N., Mankoff, K. D., McCreight, J. L., Molotch, N. P., Musselman, K. N., Pelletier, J., Russo, T., Sangireddy, H., Sjöberg, Y., Swetnam, T., and West, N. (2015): Laser vision: lidar as a transformative tool to advance critical zone science. *Hydrol. Earth Syst. Sci., 19, 2881-2897.* doi:10.5194/hess-19-2881-2015

RESEARCH EXPERIENCE:

Utah State University, Logan, Utah
Ph.D. Candidate 07/2015 – Present
We evaluate the roles of human intervention, land-use, and hydrologic change as drivers of change along the Root River, a single threaded meandering sand- and gravel-bedded river in southeastern Minnesota, USA. We use spatial data (i.e., lidar, aerial imagery) in order to document planform change across 120 river-km and 76 years of drastic land use change and altered flow. We developed a statistical model based on empirical measurements to further test factors influencing measurement bias.

Universidade Fedural Rural do Semi-árido, Mossoró, Brazil
Team Research 04/2017 – Present
Working with a team of researchers from São Paulo, Brazil, to understand how the establishment of Furna Feia National Park has impacted land use and cultural perceptions in the region. My role of the project was to use machine learning algorithms (e.g., supervised classification using maximum likelihood estimators) within GIS to calculate the area of multiple land uses for images obtained before and after park establishment (2001, 2002, 2014, 2017). Using the differences in semi-automated landuse area surveys, I projected landuse scenarios and their impacts on local residents. These quantified changes were used in conjunction with local interviews, conducted by the Brazilian researchers, in order to evaluate actual versus perceived changes.

University of Turku, Turku, Finland
Fulbright Research 08/2014- 06/2015
- Quantifying Geomorphic Change Along the Pulmanki River, Northern Finland
Used 3 sets of high-resolution remote sensed aerial images, obtained from airplanes and UAVs, to quantify spatial and temporal patterns of river width change for the Pulmanki River. Because the Pulmanki River lies in the remote Northern Finland (Lapland), and thus lacks significant impacts from human land use, we were able to survey the watersheds response to climate change.

UMBC, Baltimore, MD
M.Sc. Thesis Research, 08/2011 – 05/2014
Thesis research uses aerial images, contemporary lidar, and historical topographic survey maps to quantify streambank erosion and riverine response to agricultural land use, deforestation, and the widespread use of mill dams throughout European colonization. I used multiple geospatial data types and software (ArcGIS, R, and Matlab) to measure linear rates, area of change, and volume of bank erosion over multi-decadal timescales. Data included aerial imagery spanning multiple decades, high-resolution (1:2400 scale) historic topographic maps, and a 1-meter LiDAR dataset. Used ArcMap software on a daily basis for multiple hours to develop my own tools and methods of measuring stream response to landuse change.

U.S. Geological Survey, Baltimore, MD, 07/2011 – 08/2014
Job-related research- varied based on working group. Included geomorphic, water quality, hydrologic, and landuse research (overviewed in ‘Professional Experience’).

PRESENTATIONS:

Summer Institute of Earth Surface Dynamics, "Coupled hydro-eco-geomorphologic processes in human dominated landscapes: cascade of changes and the use of modeling for management and decision making", 2016. Minneapolis, MN.
- Poster; *Temporal trends and timescale bias in measuring migration rates*
- Oral; *Distinguishing landuse impacts on critical flows driving morphologic change within the Le Sueur Basin*
American Geophysical Union (AGU) Fall Meetings 2016 & 2013. San Francisco, CA
- *Assessing the contribution of legacy sediment and mill dam storage to sediment budgets in the Piedmont of MD – The influence of measurement scale on temporal changes in channel migration*
European Geophysical Union (EGU) Spring Meeting 2015. Vienna, Austria
- Oral; *Patterns and contributions of floodplain and legacy sediments remobilized from Piedmont streams of the mid-Atlantic U.S.*
Community Surface Dynamics Modeling System (CSDMS) Annual Meeting 2016, 2017
- *Temporal changes in channel migration and the influence of temporal measurement scale*
Maantiede (Geography) Seminar Series 2014. Turku, Finland
- *The role of streambank erosion, legacy sediments and mill dam storage in Piedmont streams of Maryland.*
USGS MD-DE-DC Water Science Seminar Series; June 2014.
Title: Assessing the contribution of legacy sediment and mill dam storage to sediment budgets of the Maryland Piedmont
Chesapeake Bay Program Scientific and Technical Advisory Committee, 2014. Maryland
- ****Invited Speaker**: *Stream bank erosion as a sediment source from the Piedmont region*.
Critical Zone Exploration Network (CZEN) NSF LiDAR Workshop; 2014, Colorado
- Oral; *Quantifying long-term streambank erosion using a single Lidar DEM*
International NSF EarthCube Fluvial Sedimentology Conference; 2013, Colorado
- Oral; *Processes governing storage and remobilization of historical 'legacy' sediments*
AMTRAK Club, 2013- Baltimore, MD; 2015- Philadelphia, PA
- Poster; *Quantifying remobilization rates of legacy sediment from MD Piedmont Floodplains*
- ****Invited Speaker**; *Assessing the contribution of legacy sediment and mill dam storage to sediment budgets in the Piedmont of Maryland.*
American Voices Seminar 11/2014. Turku, Finland.
- Oral Presentation; *American Culture; Childhood lessons through television*

GRANTS AND SCHOLARSHIPS:

- **Fulbright CIMO Research Scholarship**, 2014-2015 ($18,000)
- **Utah State University 4-year Quinney Fellowship**
- **Blue Goes Green Grant**; 2017 $1,500
- **Maryland Sea Grant,** MD Water Resources Research Center ($30,000) 2012 – 2013
- **CSDMS-Sediment Experimentalist Network Grant**; (Twice) Fully funded conference travel and lodging (2016 & 2017)
- **CZEN/NSF Travel Grant**, Awarded a grant from NSF to participate in the CZR LiDAR Workshop- "The Next Generation of LiDAR Analysis for Critical Zone Research" 05/2014.
- **NSF EarthCube Travel Grant**, 04/2013, Awarded travel and lodging expenses by an NSF-funded organization to travel to Colorado and attend a Biogeochemistry and Fluvial

Sedimentology Workshop.
- GSA 2015 Northeastern Travel Grant
- Travel grants (3), UMBC Graduate Student Association, 2012 – 2013
Top 30 Graduating Class of 2014, President's Selection, 2014
Top 30 Graduating Class of 2011, President's Selection, 2011
Undergraduate Dean's Scholar
Undergraduate Athletic Scholarship

CONFERENCES:

Patterns and contributions of floodplain and legacy sediments remobilized from Piedmont streams of the mid-Atlantic U.S. **European Geophysical Union** (**EGU**). Vienna, Austria 05/2015

Quantifying geomorphic change along the Pulmanki River, Northern Finland. Fulbright Research Forum. **Session chair****: Monitoring Biological Communities and Physical Environments of Finland. Jyvaskyla, Finland 03/2015.

Assessing the contribution of legacy sediment and mill dam storage to sediment budgets in the Piedmont of Maryland, ****Invited Speaker**; **AMTRAK Club**, 2015. Philadelphia, PA

The role of streambank erosion, legacy sediments and mill dam storage in Piedmont streams of Maryland. **Maantiede Seminar Series**. Turku, Finland 09/2014

American Culture; Childhood lessons through television. Oral Presentation; **American Voices Seminar**. Turku, Finland 11/2014

Quantifying long-term stream bank erosion using a single LiDAR DEM. Oral presentation; Workshop- **LiDAR Analysis for Critical Zone Research**. 05/2014.

Stream bank erosion as a sediment source from the Piedmont region. ****Invited speaker**; Chesapeake Bay Program Workshop- **Scientific and Technical Advisory Committee**. 04/2014.

Assessing the contribution of legacy sediment and mill dam storage to sediment budgets in the Piedmont of Maryland. Poster presentation; American Geophysical Union Meeting. Fall 2013.

Quantifying remobilization rates of legacy storage across Piedmont streams of Baltimore County. Poster and oral presentations, Amtrak Club- Soil to Sea Geomorphology Conference. Johns Hopkins University. 05/2013.

Processes governing storage and remobilization of historic 'legacy' sediments. Oral presentation- Earth Cube Biogeochemistry and Fluvial Sedimentology Workshop. 04/2013.

Processes governing storage and remobilization of historic 'legacy' sediments. Oral presentation- Graduate Research Conference, UMBC. 02/2013.

FIELD EXPERIENCE:

Finland: 08/2014 – 06/2015; Fulbright Research Scholarship at the University of Turku
- Terrestrial lidar surveys, boat-based lidar surveys, streambed sediment sampling using Russian streambed sampler technique, meander bar sediment core survey, drone-based aerial image acquisition, remote-controlled ADCP bathymetric surveys
Minnesota: - 07/2014, 06/2015; 07/2016 Root River and Minnesota River field work

- Boat-based ADCP bathymetric surveys, Structure from Motion camera maintenance
New Zealand: 06/2010 – 07/2010; Leadership Course and Team Development
(Multiple sites) U.S. Geological Survey Monitoring: 05/2009 – 07/2015 Patuxent R., Potomac, Patapsco R., Susquehanna R., Choptank R., Mattawoman Cr., Rock Cr., and Sligo Cr. sampling for **River Input Management** (RIM) and **NAWQA Water Quality Programs**
Baltimore: 10/2012 – 09/2013 (thesis field research),
- ****Piedmont Legacy Sediment Field Trip Coordinator and Leader**; Led a team of leading USGS and University geomorphologists and geologists through field sites used in M.S. research.
Virginia: 07/2012 U.S. Geological Survey field measurements. Surveyed channel cross sections and established sites suited for measuring bank erosion using bank pins and floodplain deposition using cemented clay tiles.
Baisman Run: 05/2013, Field trip through Department of Geology and Environmental Engineering, Johns Hopkins University

TEACHING AND VOLUNTEER EXPERIENCE
- Invited Lecturer: Remote Sensing of the Land Surface, Department of Plant, Soils, and Climate Graduate Course 6003. Presentation: *"A birds-eye view: Evaluating river responses to landcover change and landuse intensification"*.
- Class lecture: Tectonic Geomorphology - GEOL6120,
Topic: '*Using LiDAR and DEMs in Geomorphologic Analyses*' (Spring 2017)
- Teaching Assistant & Laboratory Proctor: Small Watershed Hydrology WATS6490, (Academic Year, 2016)
- Undergraduate Mentor; Instructed multiple undergraduates seeking research experience and advanced degrees. Panel speaker on skills needed for graduate school, application materials, and balancing research with classwork and life.
- Utah State University Sustainability Programs; Food Recovery Network
Volunteer Board Member, Grant Writer, and Collector (October, 2015 – Present)
Spend 4-5 hours per week recovering food from cafes to be distributed to students in need. Also wrote grants to improve infrastructure and planned future directions. Worked with a team of volunteers and USU employees to expand partnerships with community food pantries, restaurants, and farmers. Attended regional meetings to teach and learn from other food recovery networks across the state of Utah.
- Scientific writing/revision teacher; (2015-Present), 4 hr/week
See: http://emarde.wixsite.com/revise
- Provide revision and editing services for researchers and graduate students, largely for those who do not have English as their first/primary language. Beyond revisions, I explain how writers can improve their personal and scientific writing.
- Field Course Instructor; Research Methods in Geography (MAAN 7141)
University of Turku; Finland
Instructed B.S. and M.S. students on appropriate techniques and sampling locations for field measurements of water quality, discharge, and floodplain and streambed sediments.
- Guest Lecturer, Geomorphology – GES611. **UMBC,** Baltimore, MD
Lectured on the evolution of floodplains in the Piedmont of the U.S. and incorporated my thesis research as it relates to fundamental fluvial processes.
- Teaching Assistant & Instructor, Physical Geography, 08/2013 – 01/2014
Developed course material, digital-visual learning material; lead lectures and discussions, and evaluate the performance of 160+ students in Physical Geography.
- Research Supervisor, (Baltimore, MD) 11/2012 - 07/2013
Through funding, I organized a team of paid and volunteer undergraduate students seeking to

gain field experience, GIS skills, and an understanding of laboratory equipment/procedures. I trained and educated students on how to conduct research, along with specific tasks oriented towards their future academic and career goals.

- Assistant Field Coordinator, Difficult Run Sedimentation Assessment, 07/2012
U.S. Geological Survey, Fairfax, Virginia
Helped instruct students and co-workers to establish sites along Difficult Run suitable for measuring deposition and erosion for a multi-year mass balance study.